UC San Diego
UC San Diego Electronic Theses and Dissertations

Title

Luminescent organosilicon polymers and sol-gel synthesis of nano-structured silica

Permalink

Author

Martinez, H. Paul

Publication Date

2011

Peer reviewed|Thesis/dissertation

UNIVERSITY OF CALIFORNIA, SAN DIEGO

Luminescent organosilicon polymers and sol-gel synthesis of nano-structured

silica

A dissertation submitted in partial satisfaction of the requirements for the degree

of Doctor of Philosophy

in

Chemistry

by

H. Paul Martinez

Committee in charge:

      Professor William C. Trogler, Chair
      Professor Seth M. Cohen
      Professor Andrew Dickson
      Professor Clifford P. Kubiak
      Professor Michael Tauber

2011

The dissertation of H. Paul Martinez is approved, and it is acceptable in quality and form for publication on microfilm and electronically:

_____

_____

_____

_____

_____
Chair

University of California, San Diego

2011

DEDICATION

This thesis is dedicated to Lynne, for all of love, support, and encouragement that let

smile though the good days and pick myself up after the bad ones, this one is for

you.

EPIGRAPH

You win some, you lose some.

TABLE OF CONTENTS

LIST OF FIGURES

LIST OF SCHEMES

LIST OF EQUATIONS

LIST OF TABLES

LIST OF SYMBOLS AND ABBREVIATIONS

Å Ångstrøm

[A] Analyte concentration

ACE acetone

ACN acetonitrile

AFM Atomic Force Microscopy

$AgIO_3$ silver iodate

AIBN 2,2'-Azobisisobutyronitrile

AIE aggregated induced emission

AN ammonium nitrate

$AgNO_3$ silver nitrate

a.u. arbitrary units

br broad

BQ benzoquinone

C carbon

°C degree Celsius

calcd calculated

CCDC Cambridge Crystallographic Data Centre

$CDCl_3$ deuterated chloroform

CDI color Doppler imaging

cm centimeter

cm^{-1} wavenumber

cm^{-2} per centimeter squared

cm^{-3} per centimeter cubed

° degree

Δ delta, heat, or change

δ chemical shift; ppm

CL-20 2,4,6,8,10,12-hexanitro-2,4,6,8,10,12- hexaazaisowurtzitane

C-4 plastic explosive composition using RDX as its main explosive component

D diameter

d doublet or days

DAN 2,3-diaminonaphthalene

DC peroxide dicumyl peroxide

dd doublet of doublets

DDNP diazodinitrophenol

DEB diethynylbenzene

Δ delta

decomp decomposition DFT density functional theory

DMSO dimethylsulfoxide

DNB dinitrobenzene

DNT dinitrotoluene

e^- electron

ε molar extinction coefficient; M^{-1} cm^{-1}

ε_{max} molar extinction coefficient at wavelength of maximum absorption; $M^{-1} cm^{-1}$

η viscosity (cP)

EGDN dinitroethylene glycol

EPA Environmental Protection Agency

eq equivalents

EtOH ethanol

Et_2O diethyl ether

eV Electron-Volt (1 eV = $1.6 \cdot 10^{-19}$ Joules)

Φ fluorescence quantum yield

Φ_{rel} relative fluorescence quantum yield

fg femtogram

g gram

GPC gel permeation chromatography

h hour

H hydrogen

H_2O water

H_2O_2 hydrogen peroxide

H_2PtCl_6 chloroplatinic acid

HMTD hexamethylene triperoxide diamine

HMX cyclotetramethylene-tetranitramine

HOMO highest occupied molecular orbital

Hz hertz, s^{-1}

I fluorescence intensity

I_0 initial fluorescence intensity

IED improvised explosive device

IMS ion mobility spectrometry, ion

mobility spectrometer

∞ infinity

INEPT insensitive nuclei enhanced by polarization transfer

IR infrared (spectroscopy or radiation)

J coupling constant; Hz

k reaction rate constant; s^{1} K Kelvin

K_a association constant

K_{SV} Stern-Volmer constant

kHz kilohertz

kJ kilojoules

KOH potassium hydroxide

λ wavelength, lambda

λ_{abs} wavelength of absorption, lambda

λ_{em} wavelength of emission, lambda

λ_{ex} wavelength of excitation, lambda

λ_{flu} wavelength of fluorescence, lambda

L liter

LED light emitting diode

ln natural log

LUMO lowest unoccupied molecular orbital

M molar; mol L^{-1}

M_w weight-averaged molecular weight

M_N number-averaged molecular weight

m multiplet

m^3 cubic meter

MCL maximum contaminant level

MeOH methanol

mg milligram

μg microgram

μs microsecond

MHz megahertz

min minutes

MIP molecularly imprinted polymer

μL microliter

mL milliliter

μm micrometer

μM micromolar

mM millimolar

μmol micromole

mmol millimole

MP micro-particle

mol mole, $6.022 \cdot 10^{23}$

MP melting point

ms millisecond

n degree of polymerization

NaOH sodium hydroxide

NB nitrobenzene

ng nanogram

nm nanometer

NP nano-particle

NM nitromethane

NMR nuclear magnetic resonance

ns nanosecond

OLED organic light emitting diode

ONC octanitrocubane

OSHA Occupational Safety and Health Administration

PA picric acid

PDI polydispersity index

π pi; bond or orbital

π^* pi-star; anti-bonding π orbital

PETN pentaerythritol tetranitrate

pg picogram

$pH = -\log[H^+]$

Ph phenyl

PL photoluminescence

PLED polymer light emitting diode

ppb parts per billion

PPE poly(*p*-phenylenethynlene)

ppm parts per million

PN potassium nitrate

ppt parts per trillion

ppth parts per thousand

PPV poly(*p*-phenylenevinylene)

P_{vap} vapor pressure (Torr)

[Q] concentration of quencher

R^2 coefficient of determination

RDX cyclotrimethylene-trinitramine

ROS reactive oxygen species

rt room temperature

ρ density (g cm^{-3})

σ sigma; bond or orbital

σ^* sigma-star; anti-bonding σ orbital

s singlet or seconds

Si silicon

SN sodium nitrate

SOMO singly occupied molecular orbital

spnmr single pulse delay NMR

t time

T Tesla

T_1 spin-lattice relaxation time

TATB 1,3,5-triamino-2,4,6-trinitrobenzene

TATP triacetone triperoxide

Tetryl 2,4,6-trinitrophenyl-N-methylnitramine

THF tetrahydrofuran

TLC thin-line chromatography

TMS trimethylsilyl or trimethylsilane

TNB trinitrobenzene

TNG trinitroglycerin

TNT trinitrotoluene

TTT tris-(trinitromethyl)triazine

UV ultra-violet

UV-A ultra-violet (254 nm)

UV-B ultra-violet (302 nm)

UV-C ultra-violet (360 nm)

UV-vis ultra-violet – visible radiation

v wave number, cm^{-1}

w:v weight:volume; g solute per 100 mL solvent

ACKNOWLEDGEMENTS

I find myself at the end of a journey that I can say that I would have never predicted. I can't tell you how I got on this ride, but through the ups and downs, it has been one crazy adventure. I guess you can say that I was always curious and wanted to know how things worked. I have to thank my dad for that and for giving me my first set of tools and not being too mad when I took everything apart to "fix it". When all I really wanted was to see what was inside, no matter what I always seemed to have extra "unnecessary" parts, and I did take apart everything. My dad who had work and live out of town, always found time to call and ask a million questions that made me feel like I never left. My baby brother, Lenny who was always riding shotgun with me for all of those "builds," his drive, ingenuity, and relentlessness inspires me. Words can describe how much my mom supported, nurtured, and pushed me. She has always known just how to push me and let me find my own way all at the same time, without this I would never have ended up here. Thank you so much mom for sitting up with me, helping me with homework, driving me all over, picking me up, never missing a parent teacher conference, taking out the bully who punched me and working so hard to give us all the things you never had.

My first experience with chemistry came in high school where Mr. Mier always seemed to make chemistry so fun, I always remember not being able to wait until our next experiment. When I got to Glendale Community College via

the University of New Mexico, yeah I know, it's the wrong order, but what can I say I do things a special way. Here I met Dr Larry Byrd, who for some reason just kept encouraging me, no matter how bad I did on his tests. He is the one who came up to me one day with a flyer in hand and said, " have you seen this program? It's a summer research program, I think you'd be really good at it." Before I knew it I was accepted and working in the lab of Dr. Carlos Gutierrez. Dr. G is very interesting and brilliant man, no matter how bad things are he has a way of pumping you up that you're ready to conqueror the world. It was here is his lab that I learned a ridiculous amount of useful chemistry, not the cool stuff in books, but trial by fire, and there were a couple of fires, but in front of a fume hood is where it happened. As much as Dr Gutierrez helped me figure out my way around a lab, it was Lisa Bautista who helped keep me in school, she always helped get me extra money, jobs and did my taxes a few times. And of course I can't mention Lisa without talking about Maria Manzanares, the friend who helped me see the art in everything.

Once I got to UCSD and I still have no idea how I got in, I don't think I could have ever found a better lab or PI. You can always count on Bill to walk in and talking about the Chargers or to ask you about the new "break throughs," sometimes at 30-minute intervals. Anyone who has ever been in a lab knows it like a dysfunctional family, ours was no different, but I'd never trade it. Sarah Toal, Forest Boher and Jason Sanchez helped me find my place in the lab. Jian, Sharaya, Alex, Pauline and Sergio have made all of my nano experience so fun and

taught me more about biology and engineering than I ever wanted to know. I have to say that with out Dr. Sara Blair, Dr. Yuko, and Dr. Robert Mattrey, the got me into an operating room, taught me how to run an ultrasound. Then there are my partners in crime Kristina (with her "sidekick" Salim) and Katie who I have probably wasted more time with then anyone. Everyday was an adventure and more than that it was way too fun. Mr. John Geoltz, one of the smartest men I've ever met, yet who somehow always found a way to make me feel smart.

I have saved the best for last, Lynne, the woman who without a thought uprooted herself to new city for the chance that I might succeed. Without you I know I would never been able to handle the trials and tribulations of grad school, for this, for just being there, for helping with detection limits, for always being for anything and so much more I can't tell enough, thank you.

SPECIFIC CHAPTER ACKNOWLEDGMENTS

VITA

2003   Bachelor of Arts, California State University Los Angeles

2007   Master of Science, University of California San Diego

2011   Doctor of Philosophy, University of California San Diego

AWARDS

1999   NSF-REU Fellowship
1999 - 2003   NIH-MBRS-RISE Undergraduate Fellowship
2003 - 2004   NIH-MBRS-RISE Bridges to the Ph.D Fellowship
2004 - 2005   NSF-LSAMP Bridges to the Ph.D Fellowship
2005 - 2006   NSF-AGEP Fellowship
2007 –2008   San Diego Match Fellowship
2008--2010   NCI-ET Cure Fellowship

PUBLICATIONS

Martinez, H.P.; Kono, Y.; Blair, S.L.; Sandoval, S.; Wang-Rodriguez, J.; Mattrey, R.F.; Kummel, A.C.; and Trogler, W.C. "Hard shell gas-filled contrast enhancement particles for colour Doppler ultrasound imaging of tumors," *Med. Chem. Commun.*, **2010**, 1, 266–270.

Yang, J.; Ashmeyer, S.; Martinez, H.P.;Trogler, W.C. "Hollow silica nanosheres containing a silafluorene-fluorene conjugated polymer for aqueous TNT and RDX detection," *Chem. Commun.,* **2010,** *46,* 6804-6804.

Martinez, H.P. Front cover. *Med. Chem. Commun.*, **2010**, 1, (*4*) .

PATENTS

Martinez, H. P.; Trogler, W.C. "Thin Layer High Explosive Fluorescence and Chromatographic Sensing Methods, Sensors and Kits" provisional patent filed **2011** (No. SD61/454,620).

ABSTRACT OF THE DISSERTATION

Luminescent organosilicon polymers and

sol-gel synthesis of nano-structured silica

by

H. Paul Martinez

Doctor of Philosophy in Chemistry

University of California San Diego, 2011

Professor William C. Trogler, Chair

There remains a demand for inexpensive and reliable explosive sensors to be used in a field setting for identifying specific explosives. High explosives are considered to be organic and oxidizing, a relatively rare combination that makes them tractable for molecular recognition event. For this reason, fluorescent polymers have had favorable success in their use as sensors for high explosive. Here we report the use of fluorescent, silicon based copolymers, covalently linked to a silica TLC support. A thin layer of the polymer allows for a more efficient interaction with an analyte, thus yielding enhanced detection sensitivity. The attachment of the sensing polymers onto a chromatographic support allows for

the separation of a mixture, as well as the identification of multiple explosives through the use of multiple sensing polymers.

Hollow hard shell particles of 200 nm and 2 micron diameter with a 10 nm thick porous silica shell have also been synthesized using polystyrene templates and a sol–gel process. The template ensures that the hollow particles are monodisperse, while the charged silica surface ensures that they remain suspended in solution for weeks. When filled with perfluorocarbon gas, the particles behave as an efficient contrast agent for color Doppler ultrasound imaging in human breast tissue. The silica shell provides unique properties compared to conventional soft shell particles employed as ultrasound contrast agents: uniform size control, strong adsorption to tissue and cells immobilizing particles at the tissue injection site, a long imaging lifetime, and a silica surface that can be easily modified with biotargeting ligands or small molecules to adjust the surface charge and polarity.

Chapter 1

A Brief Introduction on Sensors

General Introduction

Improvement of existing sensor platforms along with development of new chemical sensors are always needed.[1]   As with all physical characterization techniques, there are compromises which must be taken into account such as, resolution versus time or portability versus sensitivity: for sensors, this is very evident. An increase in portability most often leads to a decrease in sensitivity. This is the constant struggle for sensors, to achieve reliable and low detection limits while remaining cost effective and portable. There are a variety of types or classes of chemosensors such as: colorimetric, ampiometric, and fluorometric just to name few types being utilized today.

Ampiometric sensors have a large reach into our everyday lives; one example would be the ionizing smoke detector. These work by using their battery to charge plates in the ionizing chamber, where a small piece of
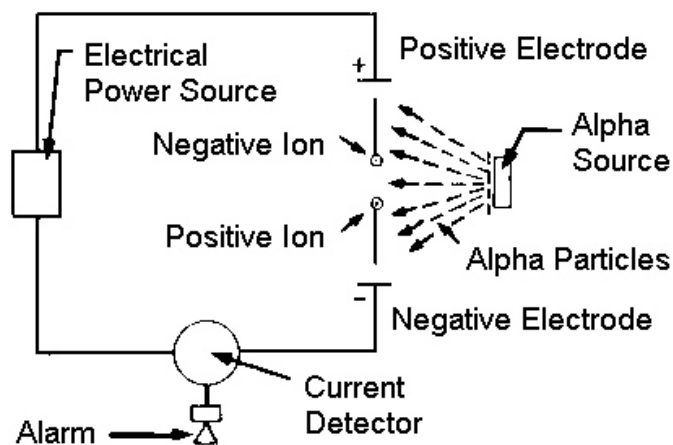
Figure **1** shows a schematic representation of an ionizing smoke detector

Americium-241 resides. The alpha particles emitted by the americium-241 ionize the air, thus creating a stream of charged particles which complete a circuit and allows current to flow.[2] When smoke enters the chamber, it neutralizes the ionized gas, thus breaking the circuit, and setting off an alarm (shown in Fig. **1**). Another form of ampiometric sensors are resistive sensors, such as the ones developed by Bohrer *et al.*[3] Here a device composed of metal and metal free phthalocyanines interact with gases that coordinate to the phthalocyanine. An example can be seen below in Fig. **2**. The most common commercial example of resistive gas sensors are household carbon monoxide sensors, which employ a semiconducting metal oxide film.
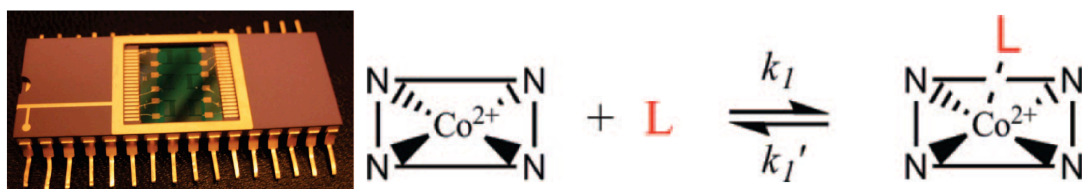
Figure **2** shows an example of a finished device and a schematic of a ligand coordinating to the phthalocyanine.[3d]

The majority of colorimetric sensors function by undergoing a chemical reaction in order to produce a distinguishable color change. At times, this process can be slow depending on the reaction kinetics, and may not produce trace level detection limits.[4] When optimized, these sensor platforms can be reliable, portable, require minimal training, and are cost effective enough to be

used in disposable detection systems. Some examples of optimized systems would include field detection kits for cocaine, gunshot residue, or explosives. A number of colorimetric field detection kits are commercially available. For example, the field detection kit for cocaine uses a solution of cobalt thiocyanate in water and glycerine, which upon reaction with the cocaine turns an easily distinguishable, blue colored precipitate, which is the result of the amine of cocaine displacing the thiocyanate ligands. For conformation, a few drops of acid are added which reforms the pink, cobalt thiocyanate. Last, chloroform is forming a blue organic layer of the cocaine base (shown in Fig. **3**).[5]
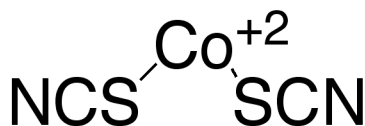
Figure **3** shows (left) cobalt (II) thiocyanate and an example of the Co solution described being used to test cocaine.

Another example would be the E.L.I.T.E. explosives detection kit. This kit functions by treating the nitrate analyte with tetrabutylammonium hydroxide in ethanol, reagent A, forming a colored Meisenheimer complex. This reagent works best for the detection of nitroaromatic compounds, such as: trinitrotoluene (TNT), tetryl, or trinitrobenzene (shown in Fig. **4**). [4a, 6] In addition to the reagent

Figure **4** shows the E.L.I.T.E. field explosives test kit pre (left) and post (right). In this case, pink color would indicate a positive test for the presence of nitro groups.

A, the kit also includes two other reagents, one being diphenylamine in sulfuric acid (H_2SO_4) allows for the detection of nitroamines, nitro-esters, or triacetonetriperoxide (TATP). Another reagent included is Nessler's reagent, which consists of aqueous mercury iodide, and potassium hydroxide iodide, which is specific for ammonium nitrate (AN). This colorimetric system reliably detects a variety of explosives at a nanogram level. Fig. **5** shows the reaction that must take place to form a Meisenheimer complex, all of which is in the E.L.I.T.E. field kit.

A

B
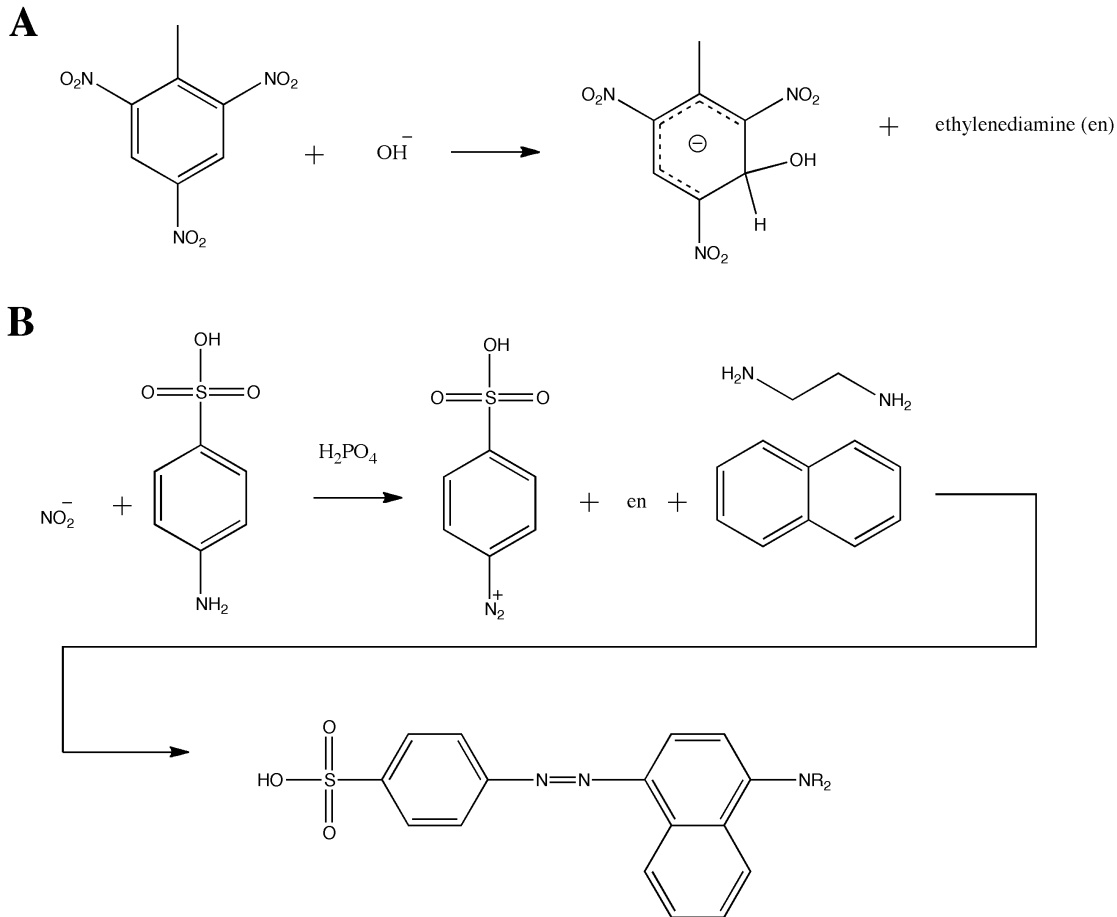
Figure **5** shows the chemical reaction needed to form a Meisenheimer complex (**A**) and also produce a positive result (**B**) with NO_2^- liberated by base reacting with nitrate explosives, such as RDX and PETN, using the E.L.I.T.E field test. [6b, c]

Colorimetric sensor platforms have been shown to be reliable, robust field sensors, but they can, at times, lack sensitivity for lower, trace level detection. For these instances, it has been shown that fluorometric based sensors can achieve the necessary sensitivity. Fluorometric sensors can be generally broken into two groups: fluorescent vapor sensor and fluorescent particulate sensors.

This improved detection occurs because the fluorometric sensor ("turn off") do not depend upon reaction kinetics, but rather on electron transfer which is on average an order of magnitude faster. It should be noted that the majority of
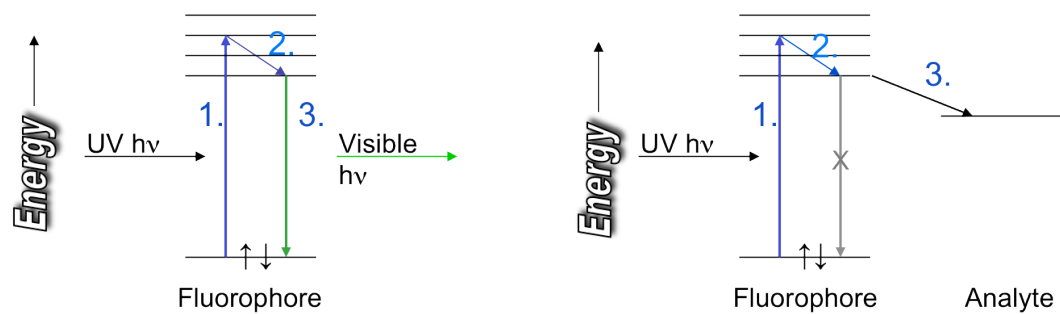
No quencher present

1. UV light excites an electron
2. Non-radiative decay
3. Electron relaxes to original energy, emitting excess energy as visible light (Fluorescence)

Quencher present

1. UV light excites an electron
2. Non-radiative decay
3. Excited electron transfers to LUMO of electron-deficient analyte (Quenching)

Figure **6** is the modified Jablonski diagram to illustrate the fluorescence and quenching process.[7]

 fluorescent "turn-on" sensors require a fluorophore to be formed either by chemical or conformational change.[8] These types of changes occur on a similar time scale with that of a colorimetric sensor. The "turn-off" process occurs when a fluorophore, excited by some UV/vis radiation, promotes an electron into a higher energy state. In the absence of an analyte quencher, upon relaxation back to the ground state a photon is ejected, resulting in the emission of light. When an analyte with similar HOMO-LUMO energy levels is present, the relaxing

electron can be transferred to the analyte, thus ceasing the flux of photons and halting emission of the fluorophore.[9] The process described is illustrated above in Fig. **6**, a modified Jablonski diagram. This mechanism holds true for both vapor sensors and particulate sensors.

Vapor sensors have been shown to be extremely reliable and detect most target analytes at low levels. Their effectiveness can sometimes be reduced when attempting to detect analytes with low vapor pressures. This specifically applies to the detection of high explosives. The low vapor pressure of nitro-based explosives makes them difficult to detect with gas sensors.   In fact, it has been proposed that sensors which detect TNT are actually detecting DNT, a byproduct always present in TNT, which has a lower vapor pressure and similar reactivity of TNT. Fig. **7** shows a few commonly used high explosives and the amounts that
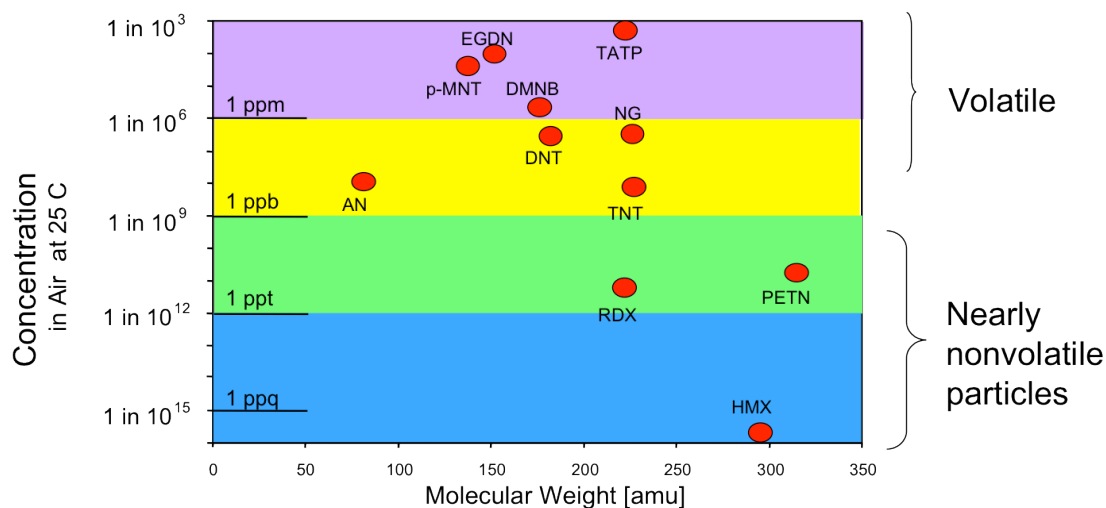
Figure **7** is graphical plot of the vapor pressures and molecular weights of many common explosives. Courtesy of Dr. John Parmeter, Sandia National Laboratory

would be present in the vapor phase at 25°C. If we look at TNT, one of the more ubiquitous explosives used, we see that at room temperature there is approximately 1ppb in the vapor phase. The values drop even more for PETN, RDX, or HMX whose vapor concentration would be in the parts per trillion and parts per quadrillion ranges. The situation is further exacerbated by the fact that most explosives are produced as mixtures such as: Semtex which is a mixture of PETN and RDX, Pentolite a mixture of TNT and PETN, or H6 which is a mixture of RDX and TNT, just to name a few. There are many explosives, which contain a single energetic compound such as C-4, but in order to increase the stability of the munitions used in the field plasticizers, waxes, and oils are all used as fillers and stabilizers. A summary of some of the common mixtures of production explosives can be seen on the next page in Table **1**.

Table **1** is list of the mixtures used to make up some commercially produced high explosives.[10]

Mixture	Explosive components
Composition A	RDX, plasticizer
Composition B	RDX, TNT, wax
H-6	RDX, TNT, aluminum, wax
Pentolites	PETN, TNT
Picratol	Picric Acid, TNT
PTX-1	RDX, Tetryl, TNT
PTX-2	RDX, PETN, TNT
Tetrytols	Tetryl, TNT
Torpex	RDX, TNT, aluminum
C-2	RDX, TNT, DNT, NC, MNT
C-3	RDX, TNT, DNT, Tetryl, NC
C-4	RDX, Fuel Oil
DBX	TNT, RDX, AN, aluminum
HTA-3	HMX, TNT, aluminum
Dynamite 3	TNG, NC, SN
Semtex-H	PETN, RDX, plasticizer
Red Diamond	TNG, EGDN, SN, AN, Chalk

While the detection of explosives in the vapor phase can be a difficult task, it must be said that there are some very good, reliable sensors that operate by vapor phase detection. The iptycene based polymer sensor developed by the Swager group is an example of a very sensitive vapor phase sensor.[11] The system has been commercialized into the Fido® portable explosive sensor (seen in Fig.

8).[12] The heart of the Fido® is an iptycene polymer, which is a highly conjugated,

extremely bright fluorophore. Its low level detection is a result of amplified

fluorescent quenching using a sensitive waveguide. The main, if any detractor of

this system is the difficulty required in synthesizing the fluorescent polymer.

Because it requires a multi-step synthetic process, the polymer must be used in

conjunction with an electronic system that allows the polymer to be reusable.

Along with the aforementioned associated difficulties that come with the

detection of compounds with low vapor pressures, a closer look at the Fig. **7**

illustrates the extremely low amounts of explosives present in the vapor phase,

Figure **8** (left) shows a general representation of iptycene polymers that are utilized as the primary fluorescent sensors that powers the amplified fluorescent quenching of the Fido portable explosive sensor (right).[11-12]

at room temperature. If we look at PETN, RDX, or HMX which are some of the more common high explosives, the amount present in the vapor phase at room temperature are in the ranges of parts per trillion (ppt) and parts per quadrillion (ppq). This assumes equilibrium between the vapor phase and the particulates, but in most practical cases the environmental surfaces present will further trap vapor when collisions occur. As previously stated, the fact remains that most explosives are produced as mixtures such as: Semtex which is a mixture of PETN and RDX, Pentolite a mixture of TNT and PETN, or H6 which is a mixture of RDX and TNT just to name a few. There are many explosives, which contain a single energetic compound such as C-4, but in order to increase the stability of the munitions used in the field plasticizers, waxes, and oils are all used as fillers and stabilizers. [10b]

This brings us to particulate fluorescent sensors; for the most part, this has been accomplished through the use of the polysilole homo- and co-polymers. The silole belongs to a general group called metalloles. A metallole is composed of a cyclopentadienyl fragment with any element from group 14 at the 1 position (seen in Fig. **9**). This accounts for siloles, germoles, and stanoles.[13] The advantage of using a silole over a cyclopentadiene is that the low lying σ^* orbitals of the silicon atom have a favorable overlap with that of the π^* orbital of the cyclopentadienyl organic framework, as seen in Fig. **9**. This favorable interaction produces fluorescence with relatively low energy excitement. It is this fluorescence that makes the silole group an attractive moiety to use for sensing

applications. The method of sensing utilized is fluorescence quenching; the process described in detail earlier, occurs first by the excitement of the fluorophore, which promotes an electron into the lowest unoccupied molecular orbital (LUMO) of the fluorophore. In the presence of a quencher, rather than
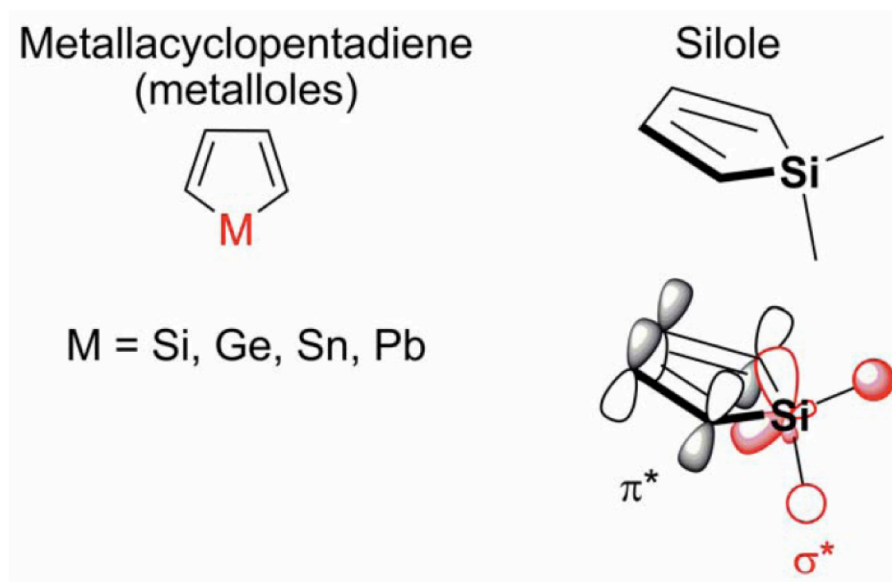
Figure **9** is a structural representation of a metallole (left) and more specifically a silole and its ability to interact with organic framework.[14]

producing a photon, the electron is transferred to the quencher, thereby "turning-off" the fluorescence. In order for this process to occur the quencher must have a high affinity for or be in close proximity to the fluorophore.
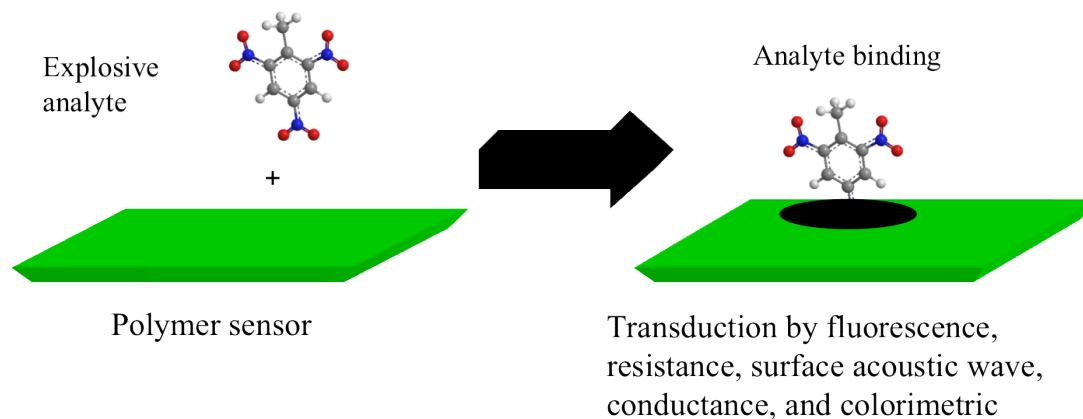
Figure **10** shows the sensing transduction mechanism for fluorescence, as well as for other molecular recognition event sensors.[15]

As seen in Fig. **10**, the mechanism for any detection, whether it is by fluorescence, colorimetry, or conductance, requires the analyte to have some interaction with the sensor and as discussed earlier, the detection of the targeted analytes or explosives can be challenging in the vapor phase. The advantage of their detection as a particulate or in the solid state is that the affinity for the sensor can be eliminated. Sohn *et al* first demonstrated this; a polysilole solution was made up and the solution was delivered as an aerosol directly to the analyte. [7, 13-16] Specifically, the polymeric solution was sprayed onto different substrates with analyte previously deposited in the same site. Once the solvent evaporated, what was left behind was a thin layer of the polysilole, which was in direct contact with the analyte. The substrates could then be visualized using an ultraviolet lamp and an impartial observer could easily distinguish the quenched area from the region unaffected.
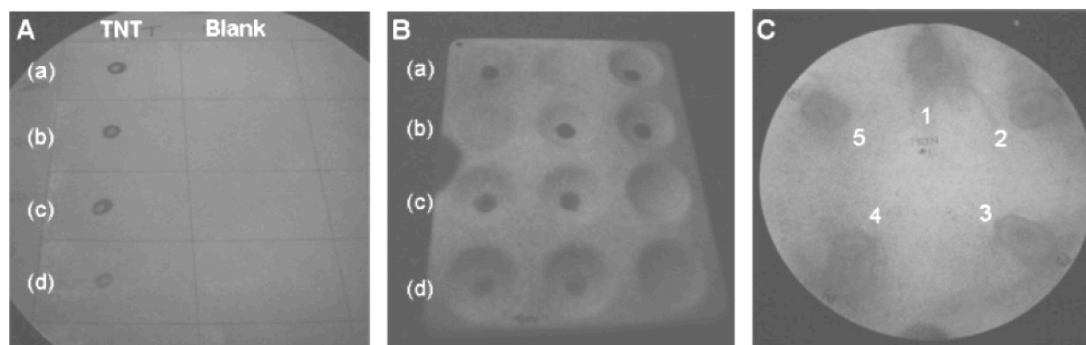
Figure **11** shows examples of fluorescence quenching of a thin film of polymer 5 by solid particulates of various explosives. (A) Detection of TNT particulates (a) 64, (b) 32, (c) 16, and (d) 3 ng cm-2 on filter paper. A toluene blank was spotted as a control. (B) Detection of tetryl particulates (a) 64, (b) 32, (c) 16, and (d) 3 ng cm-2 on a porcelain tray. The analyte was randomly place in 2 of 3 wells, and observed quenching was confirmed by an independent observer. (C) Detection of five successive thumbprints on filter paper contaminated with production-line PETN particulates. Successive prints were placed in succession without further handling of the explosive material.[10, 17]

This improved method has negated the vapor pressure issue and allowed for the detection of high explosives that were previously not attainable. Some examples of this method can be seen in Fig. **11**, where various amount of TNT (**A**) were deposited onto filter paper, tetryl (**B**) was deposited in ceramic wells, and PETN (**C**) successive thumbprints were all visible after a polysilole solution was applied. Newer generations have incorporated diethynylbenzene (DEB), 2,7-diethynylfluorene, and 2,7-diethynyl-9,9'-spirobi[fluorene]. The addition of these organic co-monomers has primarily accomplished two things. First, the addition of a co-monomer has added a vinyl linkage that allows the co-polymer to be less sterically hindered. Second, their incorporation, along with the use of fused silacycle, silafluorene has increased the quantum efficiency of the co-polymers.

The outcome of the both of these effects has been an improved detection limit for all of the nitro-based high explosives.[18]

The latest innovation in this sensor platform is the attachment of these silole co-polymers onto a chromatographic support, specifically a thin layer chromatography plate. The incorporation of a chromatographic support has improved detection limits, due to a thinner layer of sensory material being applied. This reduces the amount of polymer-polymer self quenching and improved the efficiency of the interaction between the polymer and the analyte. Furthermore, the use of a chromatographic support allows for the separation of explosive mixtures. More information about the polymeric attachment to chromatographic support is detailed in chapter 2.

References

1.   (a) Basabe-Desmonts, L.; Reinhoudt, D. N.; Crego-Calama, M., Design of fluorescent materials for chemical sensing. *Chem. Soc. Rev.* **2007,** *36* (6), 993-1017; (b) Smith, R. G.; D'Souza, N.; Nicklin, S., A review of biosensors and biologically-inspired systems for explosives detection. *Analyst* **2008,** *133* (5), 571-584.

2.   (a) IONIZATION SMOKE DETECTOR. 1972; (b) Sasaki, K. T., JA), Kobayashi, Akihiro (Fujisawa, JA), Takahashi, Naoki (Yokohama, JA) IONIZATION SMOKE DETECTOR. 1973.

3.   (a) Bohrer, F. I.; Colesniuc, C. N.; Park, J.; Ruidiaz, M. E.; Schuller, I. K.; Trogler, W. C.; Kummel, A. C., Comparative Gas Sensing in Cobalt, Nickel, Copper, Zinc, and Metal-Free Phthalocyanine Chemiresistors. *J. Am. Chem. Soc.* **2009,** *131*, 478; (b) Bohrer, F. I.; Colesniuc, C. N.; Park, J.; Schuller, I. K.; Kummel, A. C.; Trogler, W. C., Selective Detection of Vapor Phase Hydrogen Peroxide with Phthalocyanine Chemiresistors. *J. Am. Chem. Soc.* **2008,** *130*, 3712; (c) Bohrer, F. I.; Kummel, A. C.; Trogler, W. C., Chemiresistive detection of peroxides using metallophthalocyanines. *(patent disclosure)* **2007**; (d) Bohrer, F. I.; Sharoni, A.; Colesniuc, C. N.; Park, J.; Schuller, I. K.; Kummel, A. C.; Trogler, W. C., Gas Sensing Mechanism in Chemiresistive Cobalt and Metal-Free Phthalocyanine Thin Films. *J. Am. Chem. Soc.* **2007,** *129*, 5640.

4.   (a) Chen, H.; Chen, H.; Cooks, R., Meisenheimer complexes bonded at carbon and at oxygen. *Journal of The American Society for Mass Spectrometry* **2004,** *15* (7), 998-1004-1004-998-1004-1004; (b) Terrier, F., Rate and equilibrium studies in Jackson-Meisenheimer complexes. *Chemical Reviews* **1982,** *82* (2), 77-152.

5.   (a) Glattstein, B. J., IL) Process and test kit for cocaine detection. 2000; (b) L.J. Scott, J., *DEA Lab Notes* **1973,** (68), 179-81.

6.   (a) Fox, J. B., Kinetics and mechanisms of the Griess reaction. *Analytical Chemistry* **1979,** *51* (9), 1493-1502; (b) Nunes, P. J. D., CA, US), Andresen, Brian D. (Livermore, CA, US) Solid phase microextraction field kit. 2005; (c) Nunes, P. J. D., CA, US), Eckels, Joel Del (Livermore, CA, US), Reynolds, John G. (San Ramon, CA, US), Pagoria, Philip F. (Livermore, CA, US), Simpson, Randall L. (Livermore, CA, US) Colorimetric chemical analysis sampler for the presence of explosives. 2007.

7.   Toal, S. J.; Trogler, W. C., Polymer sensors for nitroaromatic explosives detection. *Journal of Materials Chemistry* **2006,** *16* (28), 2871-2883.

8.   (a) Germain, M. E.; Knapp, M. J., Turn-on Fluorescence Detection of H2O2 and TATP. *Inorganic Chemistry* **2008,** *47* (21), 9748-9750; (b) Sanchez, J. C.; Trogler, W. C., Polymerization of a boronate-functionalized fluorophore by double transesterification: applications to fluorescence detection of hydrogen peroxide vapor. *J. Mater. Chem.* **2008,** *18* (42), 5134-5141.

9.   Lakowicz, J. R., *Principles of fluorescence spectroscopy*. Springer: New York, 2004.

10.   (a) Sanchez, J. C.; Trogler, W. C., Efficient blue-emitting silafluorene-fluorene-conjugated copolymers: selective turn-off/turn-on detection of explosives. *Journal of Materials Chemistry* **2008,** *18* (26), 3143-3156; (b) Sanchez, J. C.; DiPasquale, A. G.; Rheingold, A. L.; Trogler, W. C., Synthesis, Luminescence Properties, and Explosives Sensing with 1,1-Tetraphenylsilole- and 1,1-Silafluorene-vinylene Polymers. *Chemistry of Materials* **2007,** *19* (26), 6459-6470.

11.   Narayanan, A.; Varnavski, O. P.; Swager, T. M.; Goodson, T., Multiphoton Fluorescence Quenching of Conjugated Polymers for TNT Detection. *The Journal of Physical Chemistry C* **2008,** *112* (4), 881-884.

12.   Swager, T. M. N., MA, US), Yang, Jye-shane (Ping-Chen, TW), Williams, Vance (Somerville, MA, US), Miao, Yi-jun (Chester, VA, US), Lugmair, Claus G. (San Jose, CA, US), Levitsky, Igor A. (Fall River, MA, US), Kim, Jinsang (Cambridge, MA, US), Deans, Robert (Cambridge, MA, US) Emissive polymers and devices incorporating these polymers. 2007.

13.   (a) Sohn, H.; Calhoun, R. M.; Sailor, M. J.; Trogler, W. C., Detection of TNT and Picric Acid on Surfaces and in Seawater by Using Photoluminescent Polysiloles. *Angewandte Chemie* **2001,** *113* (11), 2162-2163; (b) Sohn, H.; Sailor, M. J.; Magde, D.; Trogler, W. C., Detection of Nitroaromatic Explosives Based on Photoluminescent Polymers Containing Metalloles. *Journal of the American Chemical Society* **2003,** *125* (13), 3821-3830.

14.   Toal, S. J.; Jones, K. A.; Magde, D.; Trogler, W. C., Luminescent Silole Nanoparticles as Chemoselective Sensors for Cr(VI). *Journal of the American Chemical Society* **2005,** *127* (33), 11661-11665.

15.   Toal, S. J.; Sanchez, J. C.; Dugan, R. E.; Trogler, W. C., Visual Detection of Trace Nitroaromatic Explosive Residue Using Photoluminescent Metallole-Containing Polymers. *Journal of Forensic Sciences* **2007,** *52* (1), 79-83.

16.   (a) Toal, S. J.; Magde, D.; Trogler, W. C., Luminescent oligo(tetraphenyl)silole nanoparticles as chemical sensors for aqueous TNT.

Chemical Communications **2005,** (43), 5465-5467; (b) Toal, S. J.; Sohn, H.; Zakarov, L. N.; Kassel, W. S.; Golen, J. A.; Rheingold, A. L.; Trogler, W. C., Syntheses of Oligometalloles by Catalytic Dehydrocoupling. *Organometallics* **2005,** *24* (13), 3081-3087; (c) Toal, S. J.; Trogler, W. C., Polymer sensors for nitroaromatic explosives detection. *J. Mater. Chem.* **2006,** *16* (28), 2871-2883.

17.   (a) Sanchez, J. C.; Toal, S. J.; Wang, Z.; Dugan, R. E.; Trogler, W. C., Selective Detection of Trace Nitroaromatic, Nitramine, and Nitrate Ester Explosive Residues Using a Three-Step Fluorimetric Sensing Process: A Tandem Turn-off, Turn-on Sensor*. *Journal of Forensic Sciences* **2007,** *52* (6), 1308-1313; (b) Sanchez, J. C.; Trogler, W. C., Hydrosilylation of Diynes as a Route to Functional Polymers Delocalized Through Silicon. *Macromolecular Chemistry and Physics* **2008,** *209* (15), 1527-1540; (c) Sanchez, J. C.; Urbas, S. A.; Toal, S. J.; DiPasquale, A. G.; Rheingold, A. L.; Trogler, W. C., Catalytic Hydrosilylation Routes to Divinylbenzene Bridged Silole and Silafluorene Polymers. Applications to Surface Imaging of Explosive Particulates. *Macromolecules* **2008,** *41* (4), 1237-1245.

18.   (a) Trogler, W. C. D. M., CA, US), Sanchez, Jason (San Diego, CA, US), Toal, Sara (Mission Viejo, CA, US), Wang, Zheng (La Jolla, CA, US), Dugan, Regina E. (Rockville, MD, US) DETECTION OF NITRO- AND NITRATE-CONTAINING COMPOUNDS. 2010; (b) Trogler, W. C. D. M., CA, US), Sanchez, Jason (San Diego, CA, US) FLUORESCENCE DETECTION OF NITROGEN-CONTAINING EXPLOSIVES AND BLUE ORGANIC LED. 2010; (c) Trogler, W. C. D. M., CA, US), Sanchez, Jason (San Diego, CA, US) FLUORESCENCE DETECTION OF NITROGEN-CONTAINING EXPLOSIVES AND BLUE ORGANIC LED. 2011.

Chapter 2

Surface Anchored Organosilicon Fluorescent Polymers for Explosives Detection

Introduction

There remains a demand for inexpensive and reliable explosive sensors to be used in a field setting for identifying specific explosives. Explosives detection in diverse field settings such as military facilities, minefields, remediation sites, as well as mass transit areas has become a necessity for personal safety in many parts of the world.

Many chemical sensors are based on small synthetic molecules that produce a measurable colorimetric signal by reaction or interaction with a specific analyte.[1] Chemosensors can offer a cost effective and portable sensor system for high explosives. For example, modern explosives and munitions are encased in plastic and can be easily missed by metal detectors. Furthermore, many explosives are mixed with filler, such as waxes, oils, and platsticizers.[2] Trained explosive sniffing dogs are effective, but require extensive, expensive training and can be difficult to maintain.[3] Other detection methods, such as gas chromatography coupled with mass spectrometry, surface-enhanced Raman, nuclear quadrupole resonance, energy-dispersive X-ray diffraction, neutron activation analysis, and electron capture detection are highly selective, but are expensive and require trained operators and maintenance staff.[4] They also must be ruggedized for use in a field setting.

Commercially available chemical sensors function very well under many circumstances; however, all have limitations in scope. For instance, the detection of TNT (2,4,6-trinitrotoluene) and picric acid in groundwater or seawater can be

critical for the detection of unearthed, undetonated ordnances or in locating underwater mines. This poses problems since the majority of chemical sensing detection methods are optimized for air samples and struggle with interference problems in complex aqueous media. Conventional fluorometric chemical sensors, such as highly π-conjugated, porous organic polymers, can be used to detect vapors of electron deficient chemicals with high sensitivity, but the high sensitivity leads to a limited lifetime.[5] Vapor detection is problematic for explosives detection using ambient air, since many explosives have very low vapor pressures (TNT 10^{-6} torr, RDX 10^{-9} torr, HMX 10^{-11} torr, etc.) and most are compounded with waxes, fillers, and plasticizers. All these aspects make the reliable detection of explosives in the field difficult and thus, the need for alternative detection methods is needed.

Organic and silicon metallole hybrid polymers have shown the ability to detect a broad range of explosives by way of fluorescent quenching.[6] Most high explosives are organic nitrates, nitroamines, and nitro-based compounds.[7] These explosives may be sensed using a molecular recognition-binding event involving hydrophobic interactions, followed by electron transfer quenching of a fluorophore.[8] The Lewis acidity of the Si atom also permits coordination of oxygen lone pairs from the analyte, providing an efficient electron transfer pathway between fluorophore and analyte.[8a, 9] For this reason, fluorescent silole hybrid polymers have potential as high explosive sensors. Here we report the use of fluorescent, silicon-based copolymers, covalently linked to a silica thin

layer chromatographic plate (TLC) support. A thin layer of the fluorescent polymer covalently bonded to the silica surface allows for a more efficient interaction with an analyte, thus yielding enhanced detection sensitivity. Thin surface coatings permit more complete quenching of the fluorophore with small amounts of explosive analyte.[10] Another benefit of the chromatographic support is the ability to separate a mixture and allow identification of multiple explosives through the use of multiple sensing polymers. Previously, we have used this of class polymers to detect explosive particulates at nanogram levels by spraying polymer solutions with the use of an air-brush.[8a, 9, 11] The present work explores using near monolayer amounts of polymer covalently attached to the porous surface of the silica gel, which should minimize self-quenching from polymer-polymer interactions, thereby allowing for better analyte interaction, which in turn should lead to lower detection limits. Furthermore, since the silica gel is a chromatographic support, mixtures of explosives can be separated into their individual components. The polysilole copolymer can be made in fewer than seven steps and can be easily produced. The result is a sensor platform that can be considered disposable and since the sensor needs very little equipment, it lends itself to being useful as a portable field sensor.

Results and Discussion

The polymers are prepared according to modified literature procedures,[6a, b, 12] but rather than capping the end with dimethylphenylsilane, the polymers are capped by hydrosilation with trimethoxysilane. This allows the polymers to be covalently attached to a silica surface. The polymers are characterized as the dimethylphenylsilane capped polymer, since the reactive trimethoxysilane cap could easily react with glass in an NMR tube or silica in a GPC column.

Scheme 1 A general scheme for dihydrosilole and dihydrosilafluroene polymerization.
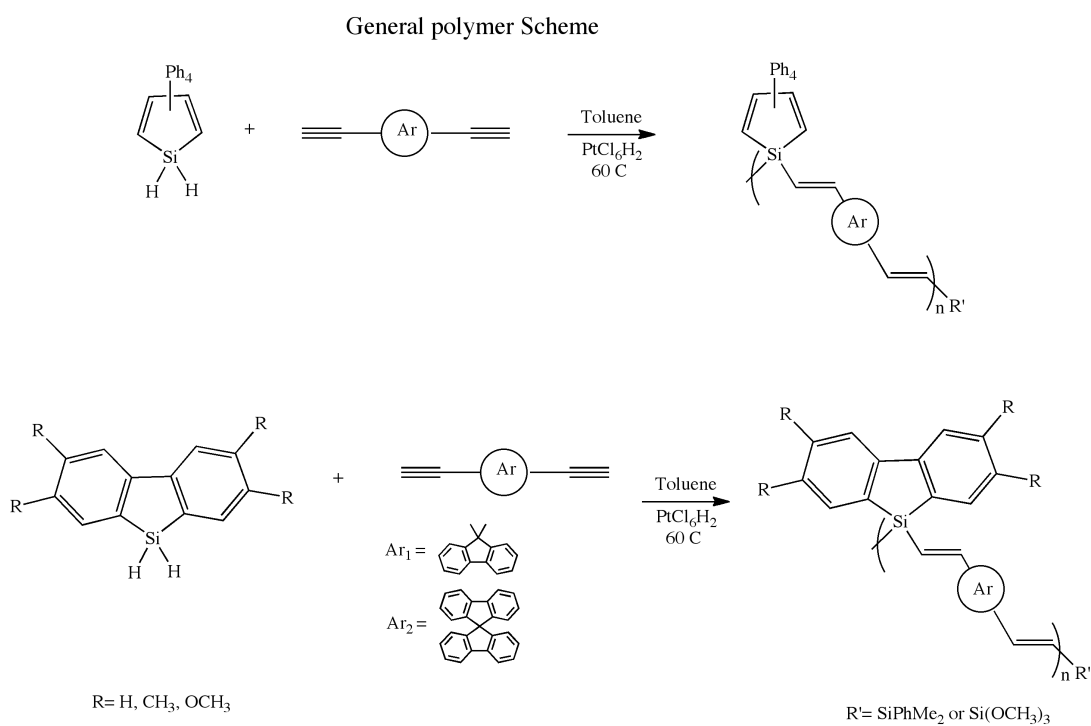
The solution and solid-state luminescence of the polysilafluorenyldiethynylspirobifluorenyl and polysilafluorenyldiethynylfluorenyl copolymers (PSFS &PSFF) are unchanged from the previous reported values. [11b] The polysilolediethynylspirobifluorenyl (PSS) polymer is a new polymer. It emits at 470nm in solution and 485nm in the solid state (Fig. **1**).
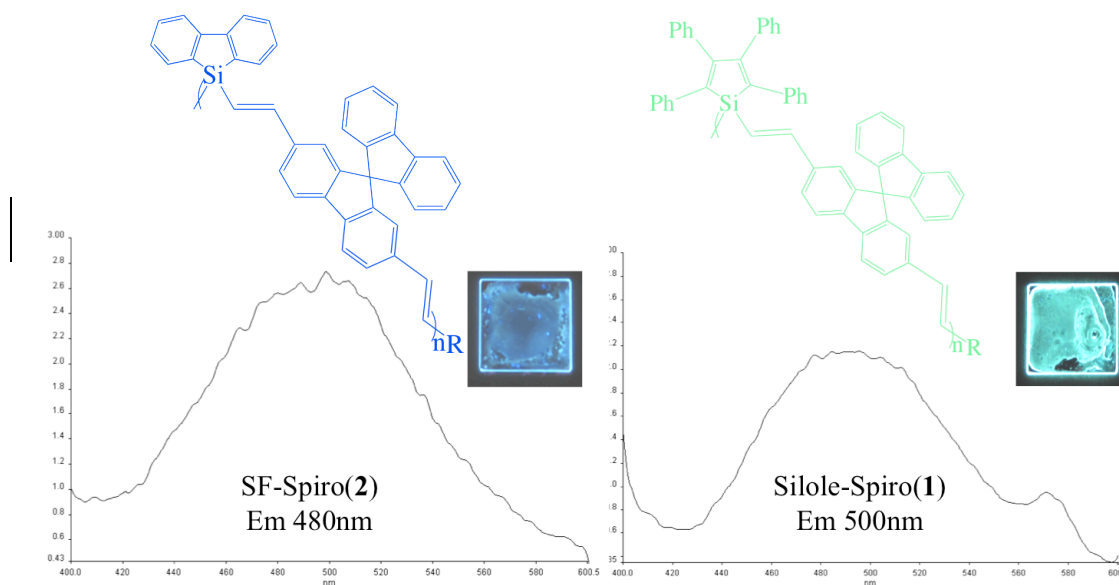
Figure **1** shows solid-state photoluminescence spectra of polymers. Spectra were taken of drop cast films on quartz slides.

The molecular weight (MW) by gel permeation chromatography (GPC) is 26kDa, with a polydispersity index (PDI) of 1.3. It exhibits an aggregation enhanced emission as expected for compounds that contain the tetraphenylsilole moiety.[13] This is attributed to freezing out rotation of the phenyl rings in the solid state, since this motion is postulated to result in the greatly decreased photoluminescence observed in fluid solutions.

For this reason, the solution quantum yield of 12% observed for PSS is deceptive. Although there is no simple way to quantify the solid-state (SS) emission, it is significantly brighter than the solution emission would indicate. For this reason, these silole polymers are excellent candidates for solid-state polymeric chemosensors. The polymers shown below in Fig. **2** were all used in their solid-state form in order to take advantage of the enhanced aggregation-

= PSFF

= PSFS

= PSS

Cap= SiMe$_2$Ph or Si(OCH$_3$)$_3$
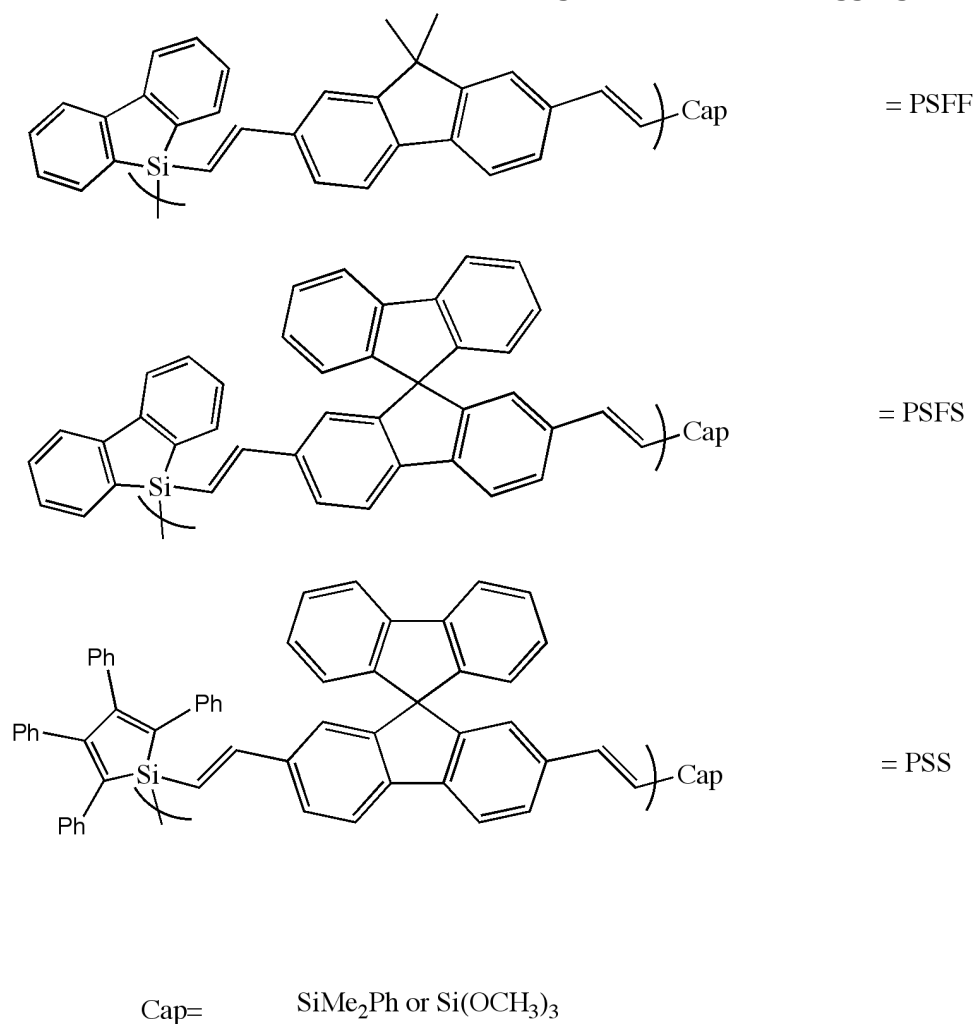
Figure **2** shows structural representation of the polymers used and the corresponding end caps used.

induced emission.

Both PSFS and PSS were covalently linked onto non-fluorescent silica TLC plates; this was done by first capping the silole polymer with trimethoxysilane and then using the condensation reaction of the surface hydroxides of the silica to the trimethoxysilane cap of the polymer (Fig. **3**). The use of a silica TLC plate as a support affords the sensor the ability to not only detect explosives at a low level, but to also be able to separate mixtures. Nitroaromatic compounds were easily separated into individual components on the treated TLC plates using common organic solvent mixtures.

Fluorescent Sensors
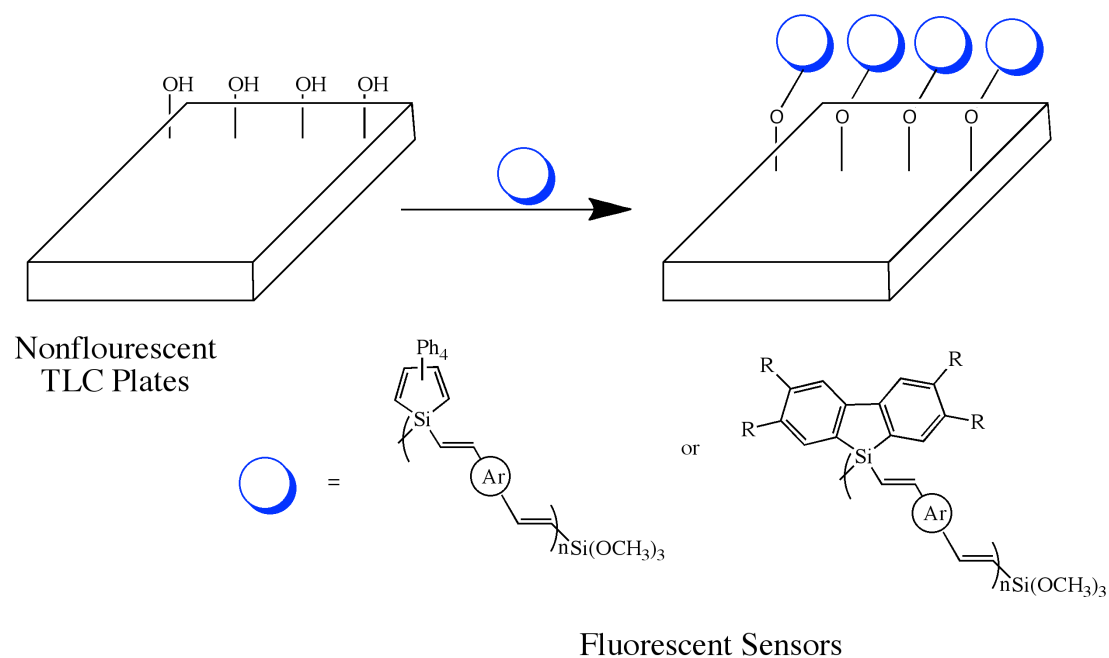
Figure **3** shows a schematic of the two general types of polymers that were used to functionalize TLC plates.

Surface attachment was done by taking a solution of the trimethoxysilane capped polymers (98%THF: 1% methanol: 1% toluene) and fully submerging the TLC plate into the solution. This was followed by washing the unreacted or unattached polymers by submerging the TLC plate into a solution of 50:50 THF/methanol. The process was repeated three times, the TLC plates were then stored in a dessiccator or an amber bottle until their use. The surface coating is uniform and yields an even, bright surface (Fig. **4**).
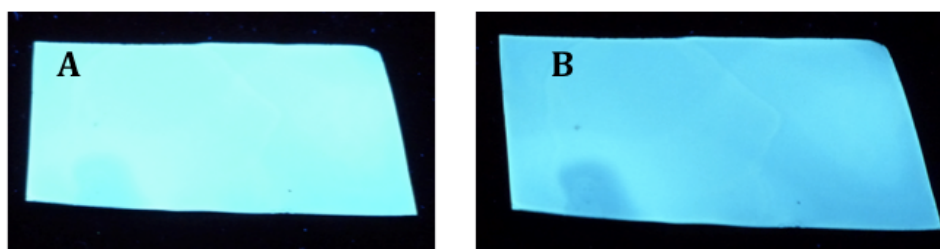
Figure **4** is (**A**) PSS coated TLC plate and (**B**) PSFS coated TLC plate (the dark edge region is due to handling with a forceps).

Due to the manner in which the polymers are attached to the support, we hypothesized that a monolayer of polymers was being anchored to the TLC surface. Initially, a direct measurement of the coated silica was attempted. This was done by coating ten 1.9cm x 4.5cm TLC plates, followed by the removal a 1cm x 1cm section of the coated silica. The silica was weighed and suspended in 2ml of toluene. UV/vis spectra were taken of all the samples. Due to scattering and a small increase of solid-state absorbance this method did not provide any

reliable data. The method that did yield useful results was accomplished by coating twenty TLC plates in a 0.025mg/ml polymer solution in toluene. Every four TLC coatings, a 1ml aliquot was removed and analyzed by UV/vis absorbance. The spectra shown in Fig. **5** shows that there is barely a detectable difference in the absorbances of the aliquots measured between each group of coatings.
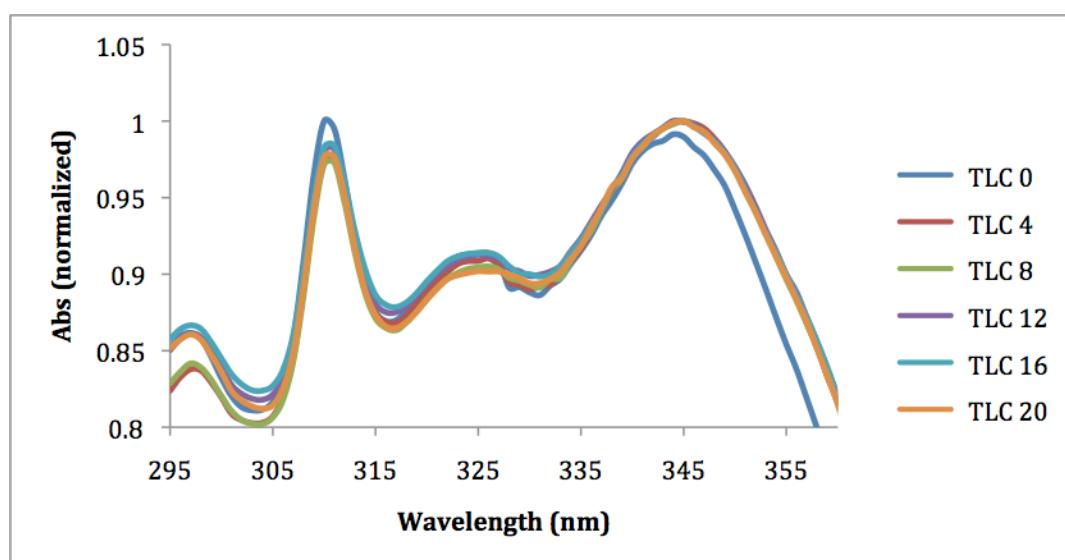
Figure **5** shows a magnified view of the UV/vis spectra taken of the aliquots taken during the coating process.

The slight difference between the non-coated TLC solution and the aliquot of the twentieth TLC group was used to estimate an upper limit on the surface coating. Using the average difference in absorbance at 311 and 325nm a concentration for the amount of polymer removed during the coating of the twenty TLC plates could be calculated. The values are shown in Table **1**. From

these calculated values it was remarkable that such small amount of polymer was sufficient to coat the entire plate and provide significant fluorescence emission that was seen in the detection studies.

Table **1** is a summary of the polymer loading for twenty and a single TLC plate.

	Average Concentration For 20 TLC plates	**Average Concentration For 1 TLC plate**
Concentration of Si atoms	6.71×10^{-7} M of Si atoms	3.36×10^{-8} M of Si atoms
Moles of Si	1.22×10^{-8} moles of Si atoms	6.1×10^{-10} moles of Si atoms
Moles of polymer	5.42×10^{-10} moles of polymer	2.71×10^{-11} moles of polymer
Mass of polymer	7.05×10^{-6} g/20 plates	3.53×10^{-7} g/ plate
Number of polymers	3.26×10^{14} molecules/20 plates	1.63×10^{13} molecules/plate
Number of polymers/area	6.88×10^{-6} polymers/nm^2	3.44×10^{-7} polymers/nm^2

In order to test whether the calculated 353ng of polymer would produce adequate fluorescence emission, a solution of 100μl was made up so that a similar mass of polymer could be delivered onto a TLC plate by multiple spotting. This solution was then spotted onto a TLC plate in an attempt to coat the entire plate. The results are shown below in Fig. **5**, which indeed indicates that the polymer mass loading calculated from the absorbance change is qualitatively reasonable since a similar mass loaded onto a TLC is easily visible. The reason that a TLC was not coated using the same method that was used to generate the uniformly coated TLCs used in the explosives detections study, was that a significantly diluted solution (due to slow kinetics of surface coating) needed to have the appropriate mass did not yield a uniformly coated plate without a considerable amount of agitation, which caused the removal of silica from the plate.
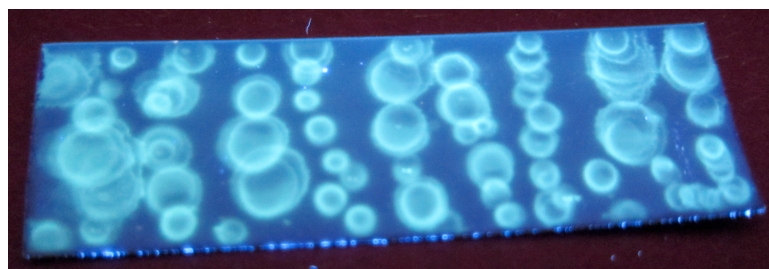
Figure **6** is 350ng of polytetraphenylsilole-diethynylspirobifluoene dissolved in 100μl of solvent, which was then pipetted in numerous 5μl aliquots onto a TLC plate.
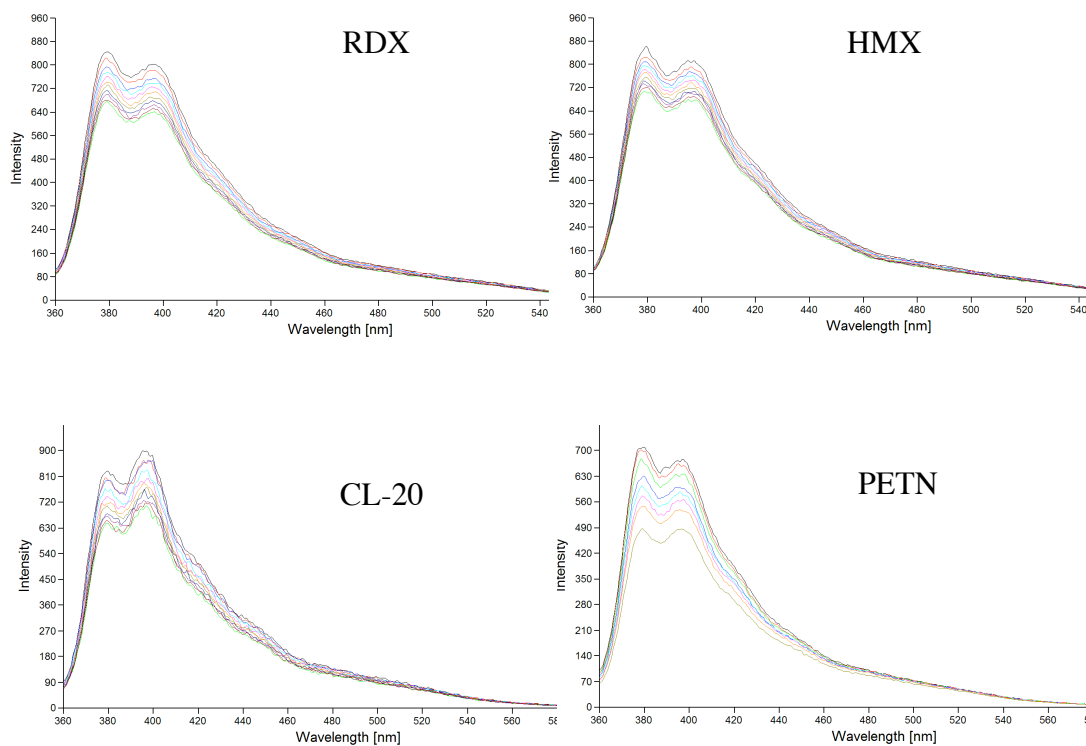
Figure **7** are the fluorescent quenching spectra of p-silafluorenyl-diethynylspirobifluorene with added: RDX, HMX, CL-20, and PETN.

It was shown by Sanchez *et.al*[8a, 9, 11] that in solution there is weak coordination to the silicon atom of the metallole fragment with that of the nitro group on the explosive. Further evidence of this can be seen in the fluorescent quenching spectra seen in Fig. **7**. The amount of quenching seen in solution for the additions of RDX, HMX, CL-20, and PETN to p-silafluoreneyl-diethnylspirobifluoren was minimal. This is further shown when plotting out the Stern-Volmer fits for these curves, as seen below in Fig. **8**.

RDX Stern-Volmer at 379 nm
$y = 11.206x + 1.0015$
$R^2 = 0.99543$

HMX Stern-Volmer at 379 nm
$y = 12.067x + 1.009$
$R^2 = 0.99147$

CL20 Stern-Volmer at 379nm
$y = 81.595x + 0.9679$
$R^2 = 0.99198$

PETN Stern-volmer at 379 nm
$y = 32.3x + 0.9167$
$R^2 = 0.94153$
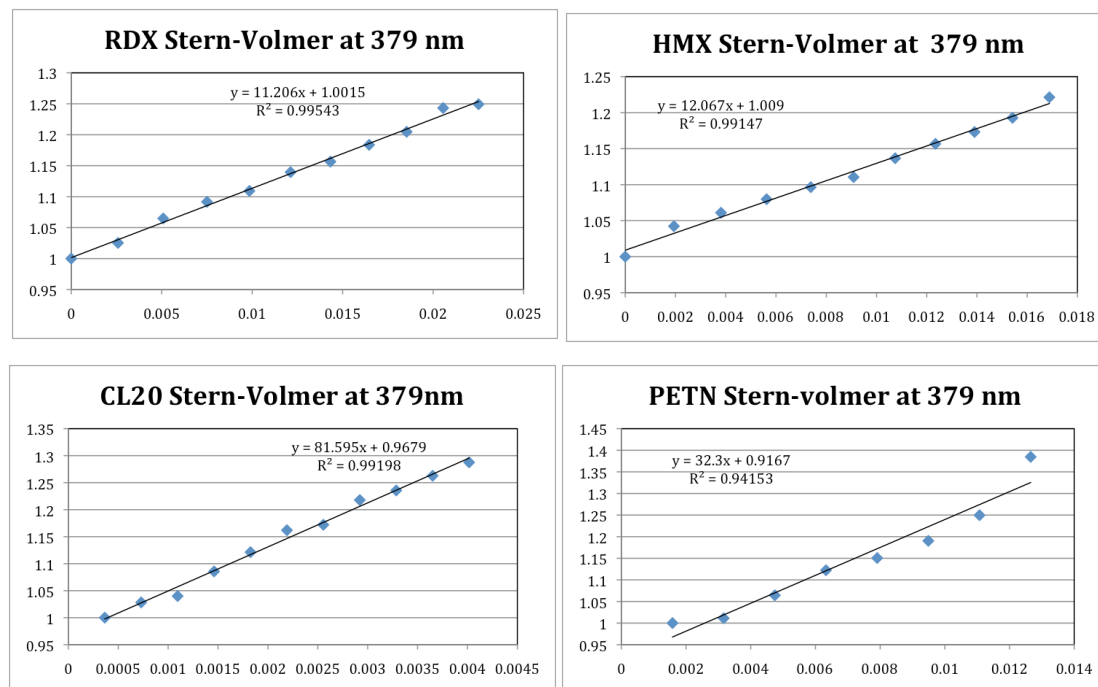
Figure **8** shows the Stern-volmer quenching plots with the explosives: RDX, HMX, CL-20, and PETN done in cyclohexanone and acetone respectively.

Using the fluorescence data from Fig. **7** and the Stern-Volmer equation the plots in Fig. **8** were generated. The K_{SV} constants calculated are listed in Table **2** along with some K_{SV} constants from the literature[9] for comparison. Furthermore, it should be noted that concentrated solutions of these analytes needed to be made up in order to observe quenching. All the experimentally determined Stern-Volmer quenching constants are orders of magnitude lower than the values for TNT, DNT, and PA reported by Sanchez *et.al.*[8a, 9, 11] Explosive testing was done in two ways: first, for the nitroaromatic compounds, which are mobile on the TLC

Table **2** is a summary of K_{SV} constants from Stern-Volmer plots.

Explosives	K_{sv}(M^{-1})
RDX	11.2
HMX	12.1
PETN	32.3
CL-20	81.6
TNT[9]	10,300
DNT[9]	4,300
Picric Acid[9]	16,400

substrate (i.e. temporary quenching), can be spotted at the bottom of the plate in a similar manner as standard thin layer chromatographic separation.

The plate is then developed using common organic solvents; the result is the separation of the mixture. As seen in Fig. **9**, a mixture of nitroaromatics can be separated to reveal the individual components. In Fig. **9A** & **B**, DNT a common by product of the manufacturing of TNT, is separated from TNT along with picric acid and tetryl using a mixture of dichloromethane: hexanes. In **9C** the TLC from **9B** is shown without UV illumination and in **9D** the separation of RDX from HMX

is performed using a mixture of 15:1, toluene to isopropanol. Both compounds are nitroamine high explosives used in compound explosives.
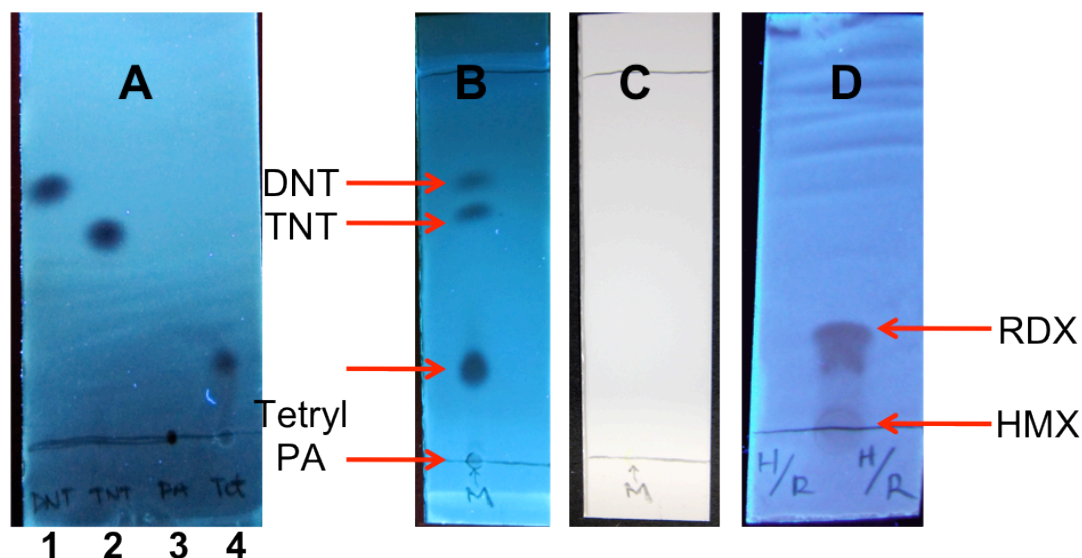
Figure **9** shows in **A** is a multi-lane separation of DNT (**1**), TNT (**2**), picric acid (**3**), and tetryl (**4**) using a 7:3 mixture of CH_2Cl_2: hexanes. **B** shows the same components as **A**, but in a single lane. **C** is a photo of **B** without UV illumination. **D** illustrates separation of RDX and HMX – separation used a 15:1 mixture of toluene: isopropanol.

Due to the mobility of the analyte on the substrate, and the use of a volatile organic solvent, it is reasonable that analytes in low concentrations will appear fainter upon development. Other explosives tested, RDX, HMX, and PETN, do not undergo this process. This is due to permanent fluorescence quenching that occurs with these explosives rendering them immobile on the TLC substrate. As seen in Fig. **10A**, permanent quenching is easily seen at levels of 50 μg for RDX, HMX, PETN, and tetryl. Furthermore, all explosives tests were detectable in

the picogram range, as shown in Fig. **10B**, where decreasing amounts of tetryl

was laid down, beginning at 50 μg and ending at 50 pg.

50 ng/mm²   500 ng/mm²   50 pg/mm²
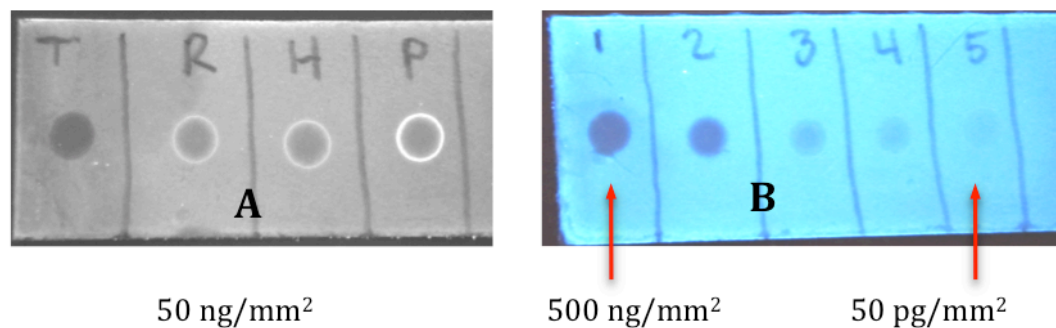
Figure **10 A** is a photograph of quenching by 50 ng aliquots of tetryl (T), RDX (R), HMX (H), and PETN (P). **B** is a photograph of quenching by aliquots in descending order of PETN, starting from 500 ng to 50pg.

It should be noted that although some spots are difficult to capture

accurately photographically, all visual detection limits were obtained using a

double blind, unbiased observer after random spotting on a substrate by a second

person. Table **3** shows a summary of the detection limits observed using both

PSS and PSFS coated TLC plates. As seen in previous applications of polysilole

polymers, the nitroaromatics are detected at the lowest levels. Nitroamines and

nitroester detection limits are often an order of magnitude less sensitive (Table

3).

Table 3 is a summary of the explosives detection limits achieved for the each of the two polymers used in this study.

PSS TLC plate detection limit

Explosive	(Mass/area)
TNT	4.5 pg/mm^2
DNT	4.5 pg/mm^2
PA	4 pg/mm^2
Tetryl	45 pg/mm^2
HMX	25 pg/mm^2
RDX	45 pg/mm^2
PETN	450 pg/mm^2
CL-20	750 pg/mm^2

PSFS TLC plate detection limit

Explosive	(Mass/area)
TNT	4.5 pg/mm^2
DNT	4.5 pg/mm^2
PA	4 pg/mm^2
Tetryl	450 pg/mm^2
HMX	45 pg/mm^2
RDX	450 pg/mm^2
PETN	450 pg/mm^2
CL-20	1500 pg/mm^2

While the differences in the detection limits between the PSS and PSFS are similar for the nitroaromatic class, they can differ by an order of magnitude for the nitroamines. This is more likely due to PSS being a more efficient green emitter, which is more easily seen by a human observer when compared to the PSFS blue emitter. As a whole, the use of silica TLC plates as a substrate has proved to be an efficient method that has improved detection limits by at least an order of magnitude over spray applications.

Conclusions

The use of silica thin layer chromatography plates as a substrate has allowed for the development of a sensitive system for detection and identification of trace explosive residues. This platform allows for the separation and detection of nitroaromatics, as well as the detection of nitroamines and nitroesters at low levels. The major benefit of this platform is improved detection limits. Less of

the polymeric sensor material is needed, the method can separate mixtures, and it is a simple inexpensive test.

Experimental

General *Caution: TNT and picric acid are high explosives and should be handled only in small quantities. Picric acid also forms shock sensitive compounds with heavy metals. Purchased explosive standards were handled as dilute solutions to eliminate their explosion hazard.* All synthetic manipulations were carried out under an atmosphere of dry argon gas using standard Schlenk techniques. Dry solvents were purchased from Aldrich Chemical Co. Inc. and used after purification with an MBraun MB Auto Solvent Purification System. Spectroscopic grade THF from Fisher Scientific was used for the fluorescence measurements. All other reagents were purchased from Aldrich Chemical Co. and used as received. Picric acid and DNT were purchased from Aldrich Chemical Co. and recrystallized from ethanol and methanol, respectively. TNT was prepared from DNT[14] and recrystallized from toluene. RDX, HMX, Tetryl, TNG and PETN were purchased as 1 mg/mL analytical standards in acetonitrile from Cerilliant®.

NMR data were collected with Varian Unity 400 or 500 MHz spectrometers (400 MHz for ^{1}H, 100 MHz for ^{13}C, and 99.4 MHz for ^{29}Si NMR).   GPC-RI data were obtained with the use of a Viscotek GPCmax VE 2001 GPC and a Viscotek VE 3580 refractive index detector calibrated with polystyrene standards. Fluorescence emission and excitation spectra were recorded with the use of a Perkin-Elmer

Luminescence Spectrometer LS 45. UV-vis spectra were obtained with the use of a Perkin-Elmer Lamda35 UV/Vis spectrometer.

Synthesis of **5H-dibenzo[b,d]silole** - 3.00g (9.62mmol) of 2,2'-dibromobiphenyl was dissolved in 35 ml of freshly distilled THF. The reaction temp was reduced to -52°C at which point 13.25 ml of 1.6 M n-butyl lithium in hexanes was added dropwise and slowly warmed to room temperature, while stirring overnight under Ar. The reaction was cooled again to -52°C and 12.l ml (28.8 mmol) of a 25%(V/V) solution of dichlorosilane in xylene was added dropwise. The reaction was allowed to stir for 1 hr, then warmed to room temperature and stirred an additional hr under Ar. The reaction was quenched with 25 ml of 10% ammonium chloride and extracted with diethyl ether. Purification was accomplished by vacuum distillation at 100 C at 10^{-3} torr. If further purification is needed, distillation can be repeated. This yielded a clear, colorless liquid (1.1g 63%). ^{1}H NMR (400 MHz, CDCl3): δ7.85d (2H), δ7.30d (2H), δ7.46-21m (4H), δ4.72s (2H).

Synthesis of **2,3,4,5-tetraphenyl-1H-silole** -9.00g (50.5 mmol) of diphenylacetylene was dissolved in 75 ml of freshly distilled diethyl ether. To this was added 0.88 g (126.2 mmol) of Li wire, cut into 2-3 mm pieces and stirred under Ar for 4 hr, or until the reaction had turned a reddish/brown color with a significant amount of precipitate. Under a heavy Ar flow the unreacted pieces of

lithium were removed using a spatula. The reaction was then frozen in a liquid N_2 bath for 30 mins. At this point 21 ml (50.5 mmol) of a 25%(V/V) solution of dichlorosilane in xylene was added dropwise. The reaction was slowly warmed to room temperature and stirred under an argon atmosphere for 3 hrs. The solvent was removed and the mixture taken up into toluene and extracted three times with brine. The combined organic layers were dried over $MgSO_4$ and the total volume reduced and left to crystallize.   This yielded bright, yellow crystals (5.9g 59%). Mp: 205-206 °C (lit. 209-210 °C34). 1H NMR (400 MHz, CDCl3): δ 6.80-6.85 and 7.00-7.24 (br m, 20H, Ph), 4.90 (s, 2H, SiH2). 13C{H} NMR (100 MHz, CDCl3): δ 157.50, 138.74, 135.20, 131.63, 129.62,129.36, 128.09, 127.72, 126.63, 126.23. IR (KBr): Si-H 2140cm-1

Synthesis of **Polysilafluorenyldiethynylspirobifluorene** -
29mg(0.16mmol) 5*H*-dibenzo[*b,d*]silole and 58mg(0.16mmol) 2,7-diethynyl-9,9'-spirobi[fluorene] were put into a clean, dry round bottom flask equipped with a condenser. To these solids a catalytic amount of $PtCl_6 \bullet H_2$ was added under Ar. To this mixture 1.5ml of dry toluene was add. The reaction was stirred under Ar at 60°C for 36hr. Then the temperature was reduced to 35°C and an excess (50 μL) of dimethylphenylsilane was added under Ar and stirring continued for 2hr. The $PtCl_6 \bullet H_2$ was removed by filtration using filter paper and the toluene was removed by vacuum. The yielded a brownish/yellow oil. The oil was taken up in 1ml of tetrahydrofuran and added to 10 ml of stirring methanol to precipitate

polymer. This process was repeated two times and gave a faintly yellow solid. GPC: 13kDa, PDI 1.3.

Synthesis of **Polytetraphenylsilolediethynylspirobifluorene** - 50mg(0.13mmol) 2,3,4,5-tetraphenyl-1*H*-silole and 48mg(0.13mmol) 2,7-diethynyl-9,9'-spirobi[fluorene] were put into a clean, dry flask equipped with a condenser. To these solids a catalytic amount of $PtCl_6 \bullet H_2$ was added under Ar. To this mixture 1.5 ml of dry toluene was added. The reaction was stirred under Ar at 60°C for 36 hr. Then the temperature was reduced to 35°C and an excess (50μL) of dimethylphenylsilane was added and stirred under Ar for 2 hr. The $PtCl_6 \bullet H_2$ was removed by filtration and the toluene was removed under vacuum. The yielded a brownish/yellow oil. The oil was taken up in 1 ml of tetrahydrofuran and added to 10ml of stirring methanol to precipitate polymer. This was repeated two times and yielded a faintly yellow solid. GPC: 26kDa, PDI 1.2.

Preparation of Trimethoxysilane capped PSS and PSFS

Trimethoxysilane capped polymers were is made in the same fashion as the dimethylphenylsilyl capped polymers. Trimethoxysilane was used in place of the dimethylphenylsilane in the hydrosilation steps above, and the polymers were precipitated using a 1:10 chloroform:hexanes, this was done to preserve the

reactive end group from possibly being partly hydrolyzed when the THF: methanol procedure was used due to trace moisture.

TLC surface functionalization

Standard TLC silica gel 60 plates on aluminum backing were used. Large plates were cut into slides approximately 5cm(H) x 1.5cm(W). The TLC plates were soaked in the polymer solution for approximately 2mins. The slides were then put into a 50/50 solution of THF/methanol to remove the non-covalently adsorbed polymer. This process was repeated two more times. After the last washing step the TLC plates were let to dry in a dessiccator. The TLC plates were stored a desiccator, where they were protected from oxygen and light until use.

Explosive testing

Explosive testing was accomplished using an observer independent from the random spotter in order to have a double blind study. Known amount of analyte deposited onto the TLC plate in multiple lanes using a standard micropipette. Once the deposition area was free of solvent, the TLC plates were illuminated using a 360nm handheld UV lamp. An observer was asked to determine the presence of any fluorescence quenching. Detection limits are the last clearly distinguishable spot, as viewed by the observer. All tests were run in triplicate.

References

1.   (a) Chen, H.; Chen, H.; Cooks, R., Meisenheimer complexes bonded at carbon and at oxygen. *Journal of The American Society for Mass Spectrometry* **2004,** *15* (7), 998-1004-1004-998-1004-1004; (b) Fox, J. B., Kinetics and mechanisms of the Griess reaction. *Analytical Chemistry* **1979,** *51* (9), 1493-1502; (c) Germain, M. E.; Knapp, M. J., Turn-on Fluorescence Detection of H2O2 and TATP. *Inorganic Chemistry* **2008,** *47* (21), 9748-9750; (d) Nunes, P. J. D., CA, US), Eckels, Joel Del (Livermore, CA, US), Reynolds, John G. (San Ramon, CA, US), Pagoria, Philip F. (Livermore, CA, US), Simpson, Randall L. (Livermore, CA, US) Colorimetric chemical analysis sampler for the presence of explosives. 2007; (e) Sanchez, J. C.; Trogler, W. C., Polymerization of a boronate-functionalized fluorophore by double transesterification: applications to fluorescence detection of hydrogen peroxide vapor. *J. Mater. Chem.* **2008,** *18* (42), 5134-5141.

2.   (a) Doane, S. R., R. India PM: Pakistan ties threatened. cnn.com (accessed July 14); (b) GlobalSecurity.org Military Explosives. http://www.globalsecurity.org/military/systems/munitions/explosives.htm.

3.   (a) Barbour, B.; Ombudsman, N. S. W., *Review of the Police Powers (Drug Detection Dogs) Act 2001*. NSW Ombudsman: Sydney, 2006; (b) Finnstrom, C. C. a. K. Are dogs the key to bomb detection at airports? http://articles.cnn.com/2009-12-30/travel/bomb.sniffing.dogs_1_bomb-sniffing-dogs-explosives-handler?_s=PM:TRAVEL (accessed Dec 30, 2009); (c) McCulloch, M.; Jezierski, T.; Broffman, M.; Hubbard, A.; Turner, K.; Janecki, T., Diagnostic Accuracy of Canine Scent Detection in Early- and Late-Stage Lung and Breast Cancers. *Integrative Cancer Therapies* **2006,** *5* (1), 30-39.

4.   (a) Agency, U. E. P., Nitroaromatics and nitramines—HPLC-Method 8330. *Standard Analysis Methods* **2004**; (b) Agency, U. E. P., Nitroaromatics and nitramines by GC/ECD-Method 8095. *Standard Analysis Methods* **2004**; (c) Armitt, D.; Zimmermann, P.; Ellis-Steinborner, S., Gas chromatography/mass spectrometry analysis of triacetone triperoxide (TATP) degradation products. *Rapid Communications in Mass Spectrometry* **2008,** *22* (7), 950-958; (d) Bohrer, F. I.; Colesniuc, C. N.; Park, J.; Schuller, I. K.; Kummel, A. C.; Trogler, W. C., Selective Detection of Vapor Phase Hydrogen Peroxide with Phthalocyanine Chemiresistors. *J. Am. Chem. Soc.* **2008,** *130*, 3712; (e) Chaloosi, M.; Nejad-Darzi, S.; Ghoulipour, V., Separation and Determination of PETN and TNT by HPTLC. *Propellants, Explosives, Pyrotechnics* **2009,** *34* (1), 50-52; (f) Ly, S.-Y.; Kim, D.-H.; Kim, M.-H., Square-wave cathodic stripping voltammetric analysis of RDX using mercury-film plated glassy carbon electrode. *Talanta* **2002,** *58* (5), 919-926; (g) Moore, D. S., Instrumentation for trace detection of high explosives. *Review of*

Scientific Instruments **2004,** *75* (8), 2499-2512; (h) Wang, J., Electrochemical Sensing of Explosives. *Electroanalysis* **2007,** *19* (4), 415-423.

5.   (a) Narayanan, A.; Varnavski, O. P.; Swager, T. M.; Goodson, T., Multiphoton Fluorescence Quenching of Conjugated Polymers for TNT Detection. *The Journal of Physical Chemistry C* **2008,** *112* (4), 881-884; (b) Swager, T. M. N., MA, US), Yang, Jye-shane (Ping-Chen, TW), Williams, Vance (Somerville, MA, US), Miao, Yi-jun (Chester, VA, US), Lugmair, Claus G. (San Jose, CA, US), Levitsky, Igor A. (Fall River, MA, US), Kim, Jinsang (Cambridge, MA, US), Deans, Robert (Cambridge, MA, US) Emissive polymers and devices incorporating these polymers. 2007; (c) Yang, J.-S.; Swager, T. M., Fluorescent Porous Polymer Films as TNT Chemosensors:‚Ää Electronic and Structural Effects. *Journal of the American Chemical Society* **1998,** *120* (46), 11864-11873.

6.   (a) Sohn, H.; Calhoun, R. M.; Sailor, M. J.; Trogler, W. C., Detection of TNT and Picric Acid on Surfaces and in Seawater by Using Photoluminescent Polysiloles. *Angewandte Chemie* **2001,** *113* (11), 2162-2163; (b) Sohn, H.; Sailor, M. J.; Magde, D.; Trogler, W. C., Detection of Nitroaromatic Explosives Based on Photoluminescent Polymers Containing Metalloles. *Journal of the American Chemical Society* **2003,** *125* (13), 3821-3830; (c) Toal, S. J.; Trogler, W. C., Polymer sensors for nitroaromatic explosives detection. *Journal of Materials Chemistry* **2006,** *16* (28), 2871-2883; (d) Toal, S. J.; Trogler, W. C., Polymer sensors for nitroaromatic explosives detection. *J. Mater. Chem.* **2006,** *16* (28), 2871-2883.

7.   (a) Fried, L. E.; Manaa, M. R.; Pagoria, P. F.; Simpson, R. L., DESIGN AND SYNTHESIS OF ENERGETIC MATERIALS1. *Annu. Rev. Mater. Res.* **2011,** *31* (1), 291-321; (b) Keshavarz, M. H., Detonation velocity of pure and mixed CHNO explosives at maximum nominal density. *Journal of Hazardous Materials* **2007,** *141* (3), 536-539; (c) Klap√∂tke, T. M. High energy density materials. http://www.myilibrary.com?id=93792; (d) Olah, G. A.; Malhotra, R.; Narang, S. C., *Nitration : methods and mechanisms*. VCH Publishers: New York, N.Y., 1989.

8.   (a) Sanchez, J. C.; Toal, S. J.; Wang, Z.; Dugan, R. E.; Trogler, W. C., Selective Detection of Trace Nitroaromatic, Nitramine, and Nitrate Ester Explosive Residues Using a Three-Step Fluorimetric Sensing Process: A Tandem Turn-off, Turn-on Sensor*. *Journal of Forensic Sciences* **2007,** *52* (6), 1308-1313; (b) Toal, S. J.; Sanchez, J. C.; Dugan, R. E.; Trogler, W. C., Visual Detection of Trace Nitroaromatic Explosive Residue Using Photoluminescent Metallole-Containing Polymers. *Journal of Forensic Sciences* **2007,** *52* (1), 79-83.

9.   Sanchez, J. C.; DiPasquale, A. G.; Rheingold, A. L.; Trogler, W. C., Synthesis, Luminescence Properties, and Explosives Sensing with 1,1-Tetraphenylsilole-

and 1,1-Silafluorene-vinylene Polymers. *Chemistry of Materials* **2007,** *19* (26), 6459-6470.

10.   Amro, K.; Clement, S.; Dejardin, P.; Douglas, W. E.; Gerbier, P.; Janot, J.-M.; Thami, T., Supported thin flexible polymethylhydrosiloxane permeable films functionalised with silole groups: new approach for detection of nitroaromatics. *Journal of Materials Chemistry* **2010,** *20* (34), 7100-7103.

11.   (a) Sanchez, J. C.; Trogler, W. C., Hydrosilylation of Diynes as a Route to Functional Polymers Delocalized Through Silicon. *Macromolecular Chemistry and Physics* **2008,** *209* (15), 1527-1540; (b) Sanchez, J. C.; Trogler, W. C., Efficient blue-emitting silafluorene-fluorene-conjugated copolymers: selective turn-off/turn-on detection of explosives. *Journal of Materials Chemistry* **2008,** *18* (26), 3143-3156; (c) Sanchez, J. C.; Urbas, S. A.; Toal, S. J.; DiPasquale, A. G.; Rheingold, A. L.; Trogler, W. C., Catalytic Hydrosilylation Routes to Divinylbenzene Bridged Silole and Silafluorene Polymers. Applications to Surface Imaging of Explosive Particulates. *Macromolecules* **2008,** *41* (4), 1237-1245.

12.   (a) Toal, S. J.; Jones, K. A.; Magde, D.; Trogler, W. C., Luminescent Silole Nanoparticles as Chemoselective Sensors for Cr(VI). *Journal of the American Chemical Society* **2005,** *127* (33), 11661-11665; (b) Toal, S. J.; Magde, D.; Trogler, W. C., Luminescent oligo(tetraphenyl)silole nanoparticles as chemical sensors for aqueous TNT. *Chemical Communications* **2005,** (43), 5465-5467.

13.   Chen, J.; Law, C. C. W.; Lam, J. W. Y.; Dong, Y.; Lo, S. M. F.; Williams, I. D.; Zhu, D.; Tang, B. Z., Synthesis, Light Emission, Nanoaggregation, and Restricted Intramolecular Rotation of 1,1-Substituted 2,3,4,5-Tetraphenylsiloles. *Chemistry of Materials* **2003,** *15* (7), 1535-1546.

14.   Dennis, W. H.; Rosenblatt, D. H.; Blucher, W. G.; Coon, C. L., Improved synthesis of TNT isomers. *Journal of Chemical & Engineering Data* **1975,** *20* (2), 202-203.

Chapter 3

Organosilicon Fluorescent Polymers Grafted onto Hollow Silica Nanoparticles for Explosives Detection

Introduction

Polysiloles and polysilole copolymers have successfully been used in explosives detection utilizing fluorescence quenching.[1] Silole and silafluorene containing polymers exhibit strong fluorescence due to favorable overlap between the σ^* of the Silicon atom and the π^* of the cyclopentadieneyl fragment. This leads to an orbital energy match between the fluorophore's excited-state [1]SOMO (singlet singly occupied excited donor molecular orbital) and the acceptor LUMO of explosive analytes.[2] Although polysiloles and other organic fluorescent materials, such as pentiptycene polymers,[3] show excellent sensitivity toward quenching of their fluorescence by TNT in organic solution or solid-state, their poor water solubility hampers their use for the detection of explosives in aqueous environments. Fluorescent anti-TNT antibodies have been shown to detect aqueous TNT at limits as low as 0.5 ppb. While this method detects TNT efficiently at low levels, it requires monoclonal antibodies which can be costly to purchase and require controlled low temperature storage.[4]

An additional benefit to polysiloles is the enhanced fluorescence in the solid state, which is attributed to aggregate-induced emission (AIE). The absence of solvent causes restricted intramolecular rotation (RIR).[5] AIE emitting siloles have been broadly adapted in biosensing and chemosensing.[6] Siloles and their derivatives are excellent candidates for the detection of explosives in aqueous media. This would fill an important void in fluorescence quenching, explosives based detection due to the current demand of detecting explosives in

groundwater or seawater as a result of undetonated ordnances or military facilities.[7] Moreover oligo(tetraphenyl)silole nanoparticles, produced by the precipitation of THF solutions of the oligomer with water, were shown to detect aqueous TNT.[8] Suspensions of siloleamine nanoparticles prepared by the same precipitation method have demonstrated the ability to be used as a chemosensor for CrO_4^{2-} in water.[9] The size, stability, and sensitivity of the nanoparticles sensor depends on the polarity of the fluorescent compounds and the ratio of organic solvent and water.[10] The soft nanoparticles produced by this precipitation method remain stable for several hours in solution before succumbing to coagulation and settling. The organic fluorophore, 9,10-bis(phenylethynyl)-anthracene, has been encapsulated in cyclodextrins and has shown recently to be a promising candidate for the detection of aqueous nitroaromatics at micromolar concentrations; unfortunately, nitroamines, such as RDX, are not detectable using this method.[11] Thus far, electrochemical methods have proved to be the most convenient general method for the simultaneous detection TNT and RDX explosives in aqueous environments,[12] but improved fluorescent methods offer an orthogonal detection method with potentially higher sensitivity.

Results and Discussion

This study describes the use of a blue emitting silafluorene-fluorene co-polymer, poly(silafluorene-(9,9-dimethyl-9H-fluorene) divinylene) (PSFF, 1), coated on hollow silica Nanoparticles (Nps) for use as a chemosensor for the

detection of aqueous solutions of TNT and RDX. PSFF is an alternating silafluorene-fluorene co-polymer conjugated through divinylphenylene bridges. The PSFF was prepared via the literature procedure.[23] Solid-state emission of PSFF exhibits a high solution relative quantum yield (0.22), when compared to 9,10-diphenylanthracene, and blue fluorescence at 446 nm. It has been shown to detect a range of explosive analytes (TNT, tetryl, RDX, HMX, and PETN) in the solid-state with detection limits as low as 1 pg cm^{-2}.[13] Hollow silica NPs with a diameter of 100 nm were fabricated by the sol-gel reaction using polystyrene microspheres as templates, which were then removed by calcination.[14] The uniform hollow silica Nanoparticles produced have a diameter of 85 nm diameter and have a porous wall about 10 nm thick, which exhibits a large surface area (400 m^2/g by BET measurement). These Nanoparticles provide an excellent mesoporous support for a thin layer of PSFF.

Three methods were used to coat PSFF (**1**) onto the silica Nps. The first method utilized was accomplished by stirring the Nps in a toluene solution of PSFF and allowing the polymer to adsorb to the mesoporous silica surface. Detailed procedures for surface modification of the silica NPs are provided in experimental section. Two other methods were used to alter surface properties of the NS. In the second method PSFF was covalently attached to the surface of the silica NS. This was accomplished by the utilization of a trimethoxysilyl-capped PSFF (**2**) and silica Nanoparticles in toluene. The trimethoxysilyl group
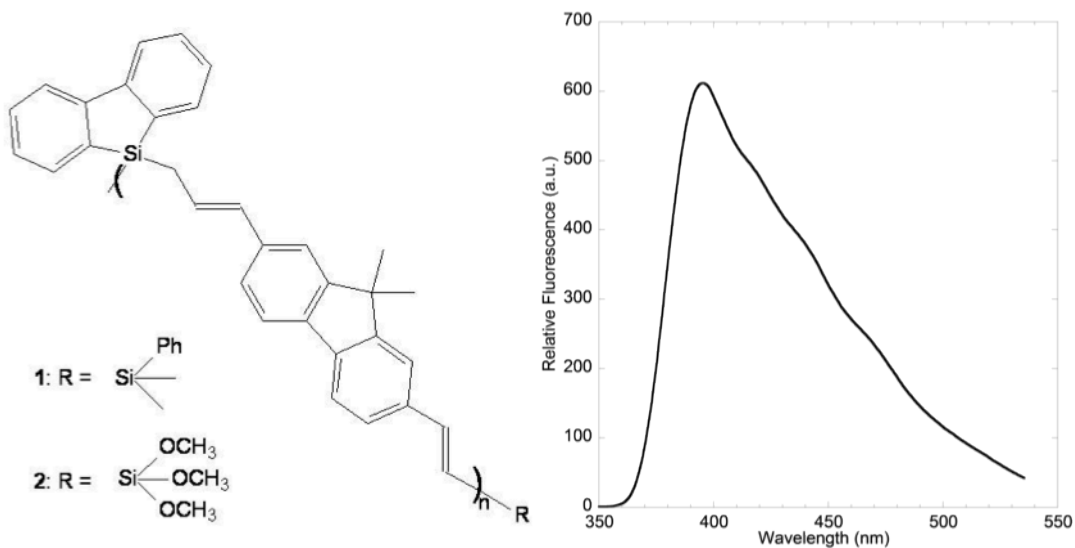
Figure **1** is Poly(silafluorene-(9,9-dimethyl-9H-fluorene)divinylene) (PSFF, left) and the emission spectrum of PSFF in toluene (right).

was used as a capping group at the end of the polymer chains by the same

catalytic hydrosilation in which the polymer was synthesized. The final method

of NS functionalization employed octadecyl modified silica Nps as the support for

adsorbed PSFF. Octadecyl groups were grafted on silica Nps by reacting

octadecyl(triethoxy)silane and the hollow silica Nps in toluene solution. Then

PSFF was adsorbed to the C_{18} modified silica Nps in toluene. The PSFF coated

silica Nps from the three coating methods were isolated by centrifugation,

washed with ethanol, dried under vacuum, and resuspended in pH 7.4 PBS with

mild sonication. The loading efficiency of PSFF on the silica Nps was determined

from the UV/vis absorption spectra of PSFF remaining in the supernatant toluene

solution as compared to PSFF in the original toluene solution prior to the surface

functionalization of the Nanoparticles. The mass ratios of loaded PSFF and silica

Nps are 51:1000, 35:1000 and 18:1000, respectively, for PSFF, silane-PSFF, and

PSFF coated C_{18} modified silica Nps, respectively.

Table **1** shows the sizing and zeta potentials of the coated Nanoparticles.

	Plain NPs	C_{18} NPs	PSFF C_{18} NPs	PSFF coated NPs	Silane- PSFF NPs
Size/nm	185 ± 45	220 ± 65	255 ± 45	290 ± 50	275 ± 60
Zeta-potential /mV	-25.0	-15.0	-1.0	-1.5	-5.5

The PSFF has a relatively high average molecular weight of 26,000 Da

(GPC analysis vs. polystyrene standards). In the first coating method, it is likely

that the PSFF chains are physisorbed from solution and trapped in the porous

structure of the naked silica NPs. It is also probable that some polymers are able

to penetrate the porous wall and adsorb to the inner surface.   When

trimethoxysilane capped PSFF was coated onto silica Nanoparticles the reaction

with surface Si-OH groups occurs simultaneously with any adsorption, and

appears to limit the amount of polymer taken up by the porous Nanoparticles.

Furthermore, the covalent surface attachment of PSFF appears to decrease the

porosity of the silica shell and partially impede the absorption of additional

polymer within the pores and core of the Nanoparticles. Similarly, the covalently

anchored C_{18} layer also decreases the effective pore size and available surface area of the silica shell, which also explains why less PSFF could be physisorbed on the hydrophobic C_{18} modified Nanoparticles. The zeta potential of C_{18} modified NPs decreases dramatically from-25 mV to -15 mV. This is a result of the covalent attachment of the PSFF onto the surface hydroxide groups, which impart the Nanoparticles with a reduced negative zeta potential. The reduction of the zeta potential of C_{18} Nanoparticles after PSFF coating suggests that a relatively large amount of adsorbed PSFF further shields the surface charge. In Fig. **2** SEM
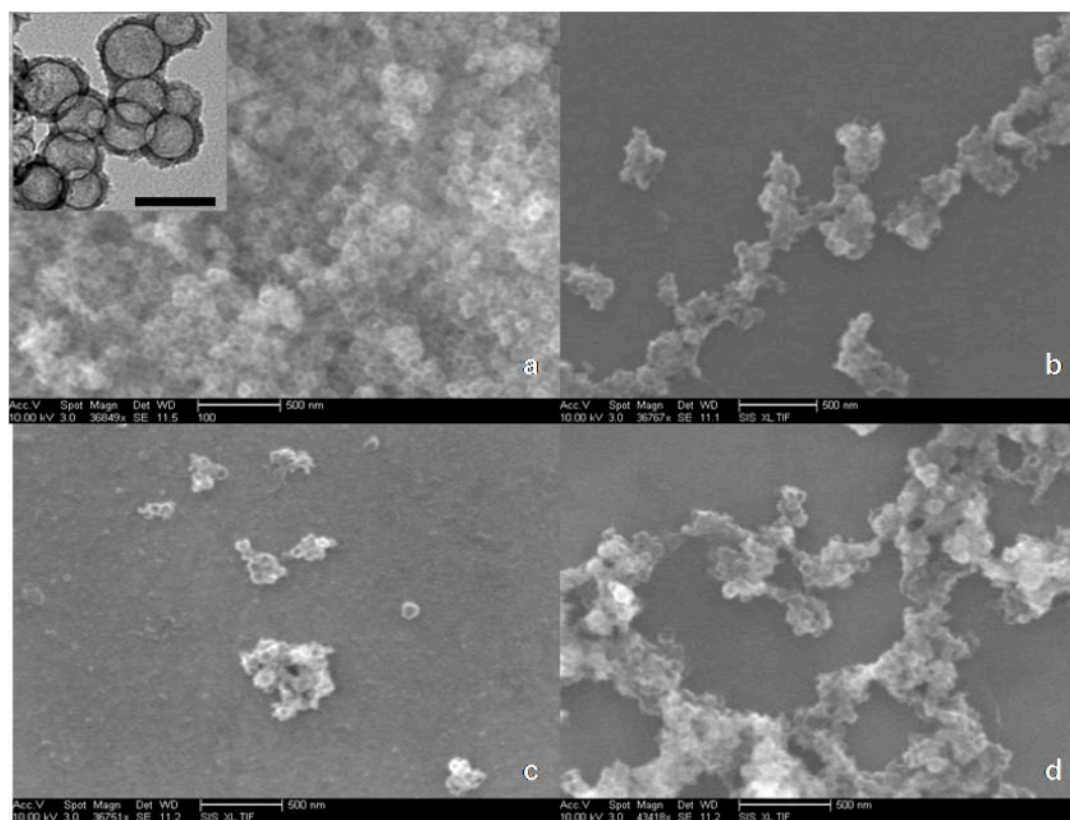
Figure **2** shows SEM images of silica NPs (**a**), PSFF coated NPs (**b**), PSFF coated C_{18} modified NPs (**c**) and silane-PSFF coated NPs (**d**). All scale bars in SEM pictures are 500 nm. Inserted figure in **a** is TEM image of hollow silica NPs, scale bar is 100 nm.

images of unfunctionalized particles (**2a**) and the surface functionalized particles

are shown (**2c-d**). In Fig. **2b** PSFF is adsorbed to the surface and a TEM insert of

the same particles. In Fig. **2c** the particles have had C_{18} covalently anchored to

the surface and PSFF adsorbed. In Fig. **2d** PSFF has been covalently anchored to

the surface, using the trimethoxysilane capped PSFF.

Hollow silica Nanoparticles posses a negatively charged surface with a

zetapotential of -25 mV (Table **1**). These Nanoparticles can be resuspended in

a pH 7.4 PBS (phosphate buffered saline) and dynamic light scattering analysis

(DLS) shows their average size to be 185±45nm. After the C_{18} coating, their

size increases slightly (220±65nm) and the zeta potential decreases to -15 mV.

Increased aggregation of the silica Nanoparticles in solution is attributed to

the hydrophobic surface coating and the reduced zeta potential. Table **1** also

shows that the average diameter of PSFF coated Nanoparticles increases with

the addition of the hydrophobic polymer. The PSFF coated plain

Nanoparticles have a thicker hydrophobic polymer layer on the surface than

the other two polymer coated Nanoparticles. Their effective size from DLS

exceeds that of the naked silica Nanoparticles and C_{18} modified Nanoparticles.

Surface adsorption of the hydrophobic polymers should promote aggregation

of Nanoparticles in water. The near zero zeta potential will exacerbate the

tendency of the colloidal suspension to aggregate.

Fig. **3** shows the absorption and emission spectra of PSFF coated silica NPs

in a PBS suspension. Free PSFF in toluene solution has a maximal absorption at

341 nm[13] and a broad emission at 385 nm (Fig. **1**). PSFF coated silica NPs in PBS have a similar absorption wavelength, but there are some minor differences. The increased absorbance at higher energy (Fig. **3**) can be attributed to scattering by silica Nps. The emission of the Nps are red shifted and broader when compared to the free polymer in toluene; this resembles the PSFF in the solid state.[13] This could be due to the C_{18} creating a more hydrophobic environment, which may predispose the NP to adsorb longer polymer chains. Self-aggregation of PSFF could also occur on the silica Nps. Aggregation also causes the polymer emission to broaden from the various conformers present in the solid state as well as from excimer formation.[10]
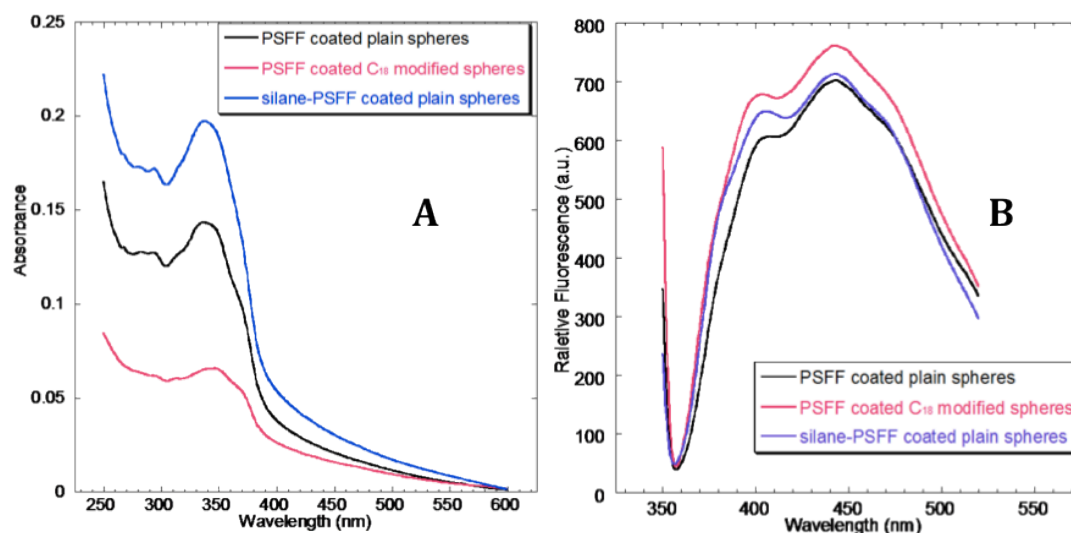
Figure **3** shows the absorption (**A**) and photoemission spectra (**B**) of PSFF coated silica Nps in a PBS suspension.

Table **2** is a summary of the optical properties and Stern-Volmer constants (Ksv) of toluene solution of PSFF and an aqueous PBS suspension of PSFF coated silica NPs

Entry	λ_{abs} /nm	ε_{max}/L mol^{-1} cm^{-1a}	λ_{flu}/nm	K_{SV}/ppm	Φ_{flu}/%
PSFF in toluene	341	18,000	385	0.0028[b]	22
PSFF	336	15,000	443	0.025[b]	4
PSFF C$_{18}$	340	23,700	442	0.10[b]	10
Silane-PSFF	336	46,100	443	0.11[b] 0.047[c]	13

[a] absorptivities are calculated per mole of silicon. [b] TNT detection. *Ksv* is calculated from the emission intensity at 443 nm except *Ksv* of PSFF in toluene, which is calculated from emission intensity at 385 nm. [c] RDX detection. *Ksv* is calculated from the emission intensity at 443 nm.

Relative quantum yields of PSFF coated silica Nps in PBS suspension were calculated using the equation[15] below:

$$\Phi_x = \frac{A_r}{A_x}\left(\frac{n_x^2}{n_r^2}\right)\Phi_r \int \frac{E_{mx}}{E_{mr}}$$

The fluorophore reference used was 9,10-diphenylanthracene. The emission and absorbance of 9,10-diphenylanthracene are similar to PSFF, thus making it a reasonable choice as a reference. In the equation, A_r is the absorption of the reference and A_x is the absorption for fluorophore. E_{mr} and E_{mx} are the total area under the emission plot of the reference(r) and fluorphore(x). n_x and n_r are the indices of refraction for the solvents being used.

Table **2** shows that the silane capped PSFF coated silica Nanoparticles exhibit the highest quantum yield of 0.13 and the coated plain NPs have a quantum yield as low as 0.044. The values inversely correlate with the amount of polymer loading. A close distance between polymer chains promotes excimer formation and emission quenching.   The data suggests that the covalently anchored PSFF coated NPs have the best balance of AIE due to restricted rotation in the surface constrained polymer, yet providing enough separation between the polymer chains to reduce self-quenching. All the PBS suspensions of PSFF coated silica Nanoparticles show stable optical properties. After 3 weeks of storage in the dark, no measurable decrease of fluorescence occurred.

TNT and RDX detection was quantified by adding a small aliquot of an acetone solution of TNT or an acetonitrile solution of RDX into a pH 7.4 PBS suspension of Nanoparticles while monitoring the fluorescence quenching. The Nanoparticles were made up at concentrations of: 0.1 mg/mL silica particles in PBS for PSFF coated plain spheres and PSFF coated C_{18} modified spheres and 0.02 mg/mL silica particles in PBS for silane-PSFF coated spheres. The quenching response was analyzed by fitting the data to the Stern-Volmer equation:[16]

$$I_0/I = K_{\mathrm{sv}}[Q] + 1$$
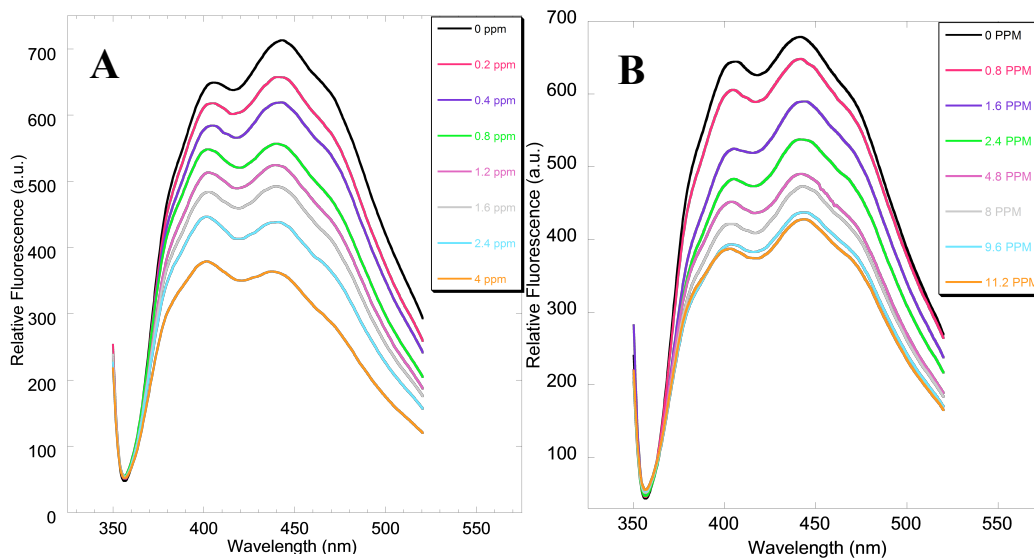
Figure **4** shows fluorescence quenching of a PBS suspension of silane-PSFF coated plain NPs in the presence of TNT (a) and RDX (b). Initial curves are baselines with no analyte added. In **3a** each aliquot corresponds to the addition of 0.2 ppm TNT and in **3b** each aliquot corresponds to the addition of 0.8PPM RDX. The mass concentration of Nanoparticles is 0.02 mg/mL.

Fluorescence quenching is dependent upon electron transfer from the excited state of the conjugated polymer to the lowest unoccupied molecular orbital of the explosive analyte. Figure **4** shows the decrease observed in fluorescence intensity of silane-PSFF coated silica Nanoparticles with the addition of TNT and RDX at low concentrations. In Fig. **4**, the quenching of PSFF fluorescence varied with the analyte used. Emission quenching by TNT led to a greater decrease at the low energy wavelength side of the emission band while emission quenching with RDX showed a greater decrease in the higher energy region of the emission band. This would suggest that the explosive analytes could be co-adsorbed onto the silica and in close enough proximity to the polymer thus, producing a better energy match between that of the fluorophore

and the LUMO of RDX or TNT. This yielded enhanced quenching for RDX on the

high-energy side of the emission and low energy quenching for TNT. The LUMO

of TNT is known to be significantly below that of RDX.[2]

The conservative detection limits reported are the first significant

observable fluorescence quenching caused by the addition of the explosive. This

can be seen in Fig. **4A**, for addition of a 200 ppb aliquot of TNT into silane-PSFF

coated NPs suspension. Since the concentrations of silica Nps in PBS buffer are

0.1 mg/mL and 0.02 mg/mL, respectively, the effective concentrations of the

active fluorophore PSFF on those two kinds of NPs are only 1.8 ug/mL and 0.7

ug/mL, respectively. Stern-Volmer constants in Table **2** show the PSFF coated

silica NPs to be 35 times more sensitive for aqueous TNT when compared with

TNT detection in toluene by soluble PSFF. A lower sensitivity was obtained with

PSFF adsorbed plain Nanoparticles, since the detection limit of TNT was 1 ppm

even though the concentration of PSFF in suspension is 5.1 ug/mL. In this case,

the high density of PSFF on the surface of silica NPs not only increases the

formation of excimers and decreases the quantum yield, as noted above, but it

also may hinder access of the TNT molecules to the polymer chains. The

detection limit of RDX by silane-PSFF coated spheres is 800 ppb. As seen in the

Stern-Volmer plots the Nanoparticles coated with a covalently attached PSFF
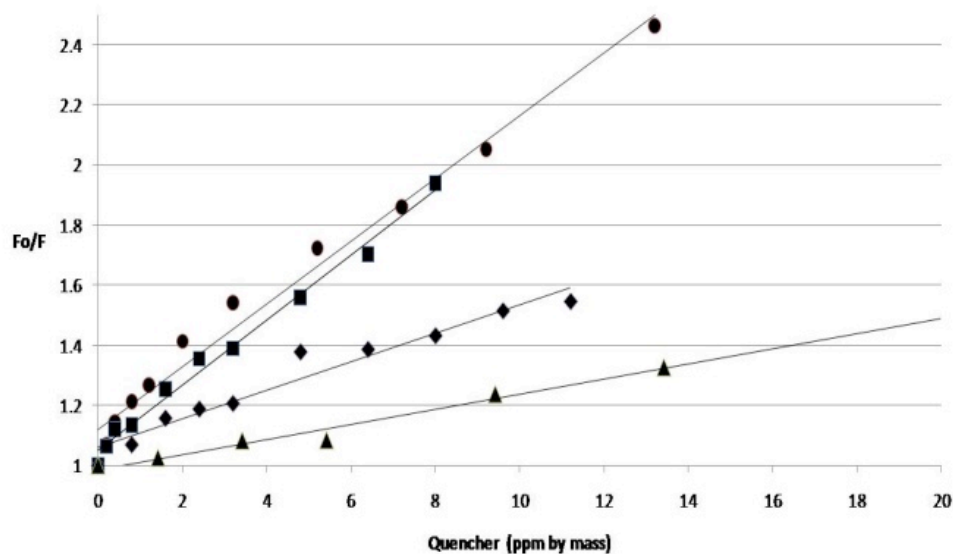
Figure **5** shows the Stern-Volmer plots of luminescence quenching of PSFF coated NPs suspended in water at varying percentages (ppm by weight) TNT and RDX. Legend: (PSFF adsorbed plain spheres with TNT▲, PSFF coated C_{18} modified spheres with TNT ●, silane-PSFF coated plain spheres with TNT ■, ◆.)

experience the most significant quenching, followed by are approximately linear as seen in Fig. **5**.   All of the plots are linear the Nanoparticles with only a PSFF coating underwent the largest quenching of all three surface treatments.

To our knowledge, this is the first example of the detection of aqueous RDX by fluorescence quenching with a luminescent polymer. Compared with other methods of detecting aqueous explosives, such as square-wave voltammetry sensing whose detection limit is as low as 20 ppb for TNT in seawater[12] and 120 ppb for RDX in extractions of soil samples,[17] fluorescence quenching of PSFF coated silica nanoparticles is a simple, fieldable sensor that has the potential to be a useful fluorescent assay for aqueous explosives. The

sensitivity obtained by supporting the fluorophore on an adsorptive silica nanoparticle exceeds that of cyclodextrin encapsulated fluorophores.[7a] The adsorptive nature of silica may assist in binding the explosive serving as a nano-extracting sensor.

Conclusions

The adsorptive properties of hollow silica Nanoparticles, in conjunction with fluorescent polymer coatings with or without surface modification have been shown to provide a new method for the detection of TNT and RDX in aqueous environments. This new method could be a useful orthogonal technique to work in parallel with the very successful electrochemical detection techniques.

Experimental

Coating of octadecyl group and PSFF polymers on hollow silica Nps:

Coating of PSFF on plain hollow silica Nps. 3 mg of silica Nps were suspended in 0.3 mL toluene and 0.3 mg of PSFF was added the suspension and mixture was stirred 4 hours before spinning down the Nps and washed by toluene, ethanol and water successively. The PSFF coated Nps were resuspended in 3 mL of pH7.4 PBS for explosive detection.

Coating of silane-PSFF. The procedure for coating silane-PSFF on plain silica Nps

was same as coating of PSFF except that absorption time was 8 hours.

Coating of octadecyl. Octadecyl groups coating on plain hollow silica Nps was accomplished by using 3 mg of silica Nps,suspended in 1 mL of toluene followed by the addition of 60 uL of octadecyl(triethoxy)silane the mixture was then let to stir overnight at room temperature. After washing with toluene the Nps were coated with PSFF with the same procedure of coating PSFF on plain silica Nps.

Much of the material in this chapter comes directly from a manuscript entitled "Hollow silica nanosheres containing a silafluorene-fluorene conjugated polymer for aqueous TNT and RDX detection," by Yang, J.; Ashmeyer, S.; Martinez, H.P.;Trogler, W.C. *Chem. Commun.,* **2010,** *46,* 6804-6804. *Reproduced by permission of The Royal Society of Chemistry*

References

1.   (a) Sohn, H.; Calhoun, R. M.; Sailor, M. J.; Trogler, W. C., Detection of TNT and Picric Acid on Surfaces and in Seawater by Using Photoluminescent Polysiloles. *Angewandte Chemie* **2001,** *113* (11), 2162-2163; (b) Sohn, H.; Sailor, M. J.; Magde, D.; Trogler, W. C., Detection of Nitroaromatic Explosives Based on Photoluminescent Polymers Containing Metalloles. *Journal of the American Chemical Society* **2003,** *125* (13), 3821-3830; (c) Toal, S. J.; Trogler, W. C., Polymer sensors for nitroaromatic explosives detection. *Journal of Materials Chemistry* **2006,** *16* (28), 2871-2883.

2.   Sanchez, J. C.; Urbas, S. A.; Toal, S. J.; DiPasquale, A. G.; Rheingold, A. L.; Trogler, W. C., Catalytic Hydrosilylation Routes to Divinylbenzene Bridged Silole and Silafluorene Polymers. Applications to Surface Imaging of Explosive Particulates. *Macromolecules* **2008,** *41* (4), 1237-1245.

3.   (a) Narayanan, A.; Varnavski, O. P.; Swager, T. M.; Goodson, T., Multiphoton Fluorescence Quenching of Conjugated Polymers for TNT Detection. *The Journal of Physical Chemistry C* **2008,** *112* (4), 881-884; (b) Yang, J.-S.; Swager, T. M., Fluorescent Porous Polymer Films as TNT Chemosensors:‚Äâ Electronic and Structural Effects. *Journal of the American Chemical Society* **1998,** *120* (46), 11864-11873.

4.   (a) Anderson, G. P.; Moreira, S. C.; Charles, P. T.; Medintz, I. L.; Goldman, E. R.; Zeinali, M.; Taitt, C. R., TNT Detection Using Multiplexed Liquid Array Displacement Immunoassays. *Analytical Chemistry* **2006,** *78* (7), 2279-2285; (b) Goldman, E. R.; Anderson, G. P.; Lebedev, N.; Lingerfelt, B. M.; Winter, P. T.; Patterson, J. C. H.; Mauro, J. M., Analysis of aqueous 2,4,6-trinitrotoluene (TNT) using a fluorescent displacement immunoassay. *Anal. Bioanal. Chem.* **2003,** *375* (4), 471-475.

5.   (a) Chen, J.; Law, C. C. W.; Lam, J. W. Y.; Dong, Y.; Lo, S. M. F.; Williams, I. D.; Zhu, D.; Tang, B. Z., Synthesis, Light Emission, Nanoaggregation, and Restricted Intramolecular Rotation of 1,1-Substituted 2,3,4,5-Tetraphenylsiloles. *Chemistry of Materials* **2003,** *15* (7), 1535-1546; (b) Hong, Y.; Lam, J. W. Y.; Tang, B. Z., Aggregation-induced emission: phenomenon, mechanism and applications. *Chem. Commun.* **2009,** (29), 4332-4353; (c) Luo, J.; Xie, Z.; Lam, J. W. Y.; Cheng, L.; Chen, H.; Qiu, C.; Kwok, H. S.; Zhan, X.; Liu, Y.; Zhu, D.; Tang, B. Z., Aggregation-induced emission of 1-methyl-1,2,3,4,5-pentaphenylsilole. *Chemical Communications* **2001,** (18), 1740-1741.

6.   Wang, M.; Zhang, G.; Zhang, D.; Zhu, D.; Tang, B. Z., Fluorescent

bio/chemosensors based on silole and tetraphenylethene luminogens with aggregation-induced emission feature. *Journal of Materials Chemistry* **2010,** *20* (10), 1858-1867.

7.   (a) Agency, U. E. P., Nitroaromatics and nitramines—HPLC-Method 8330. *Standard Analysis Methods* **2004**; (b) Agency, U. E. P., Nitroaromatics and nitramines by GC/ECD-Method 8095. *Standard Analysis Methods* **2004**; (c) Charles, P. T.; Gauger, P. R.; Patterson, C. H.; Kusterbeck, A. W., On-Site Immunoanalysis of Nitrate and Nitroaromatic Compounds in Groundwater. *Environmental Science & Technology* **2000,** *34* (21), 4641-4650; (d) Lu, J.; Zhang, Z., A reusable optical sensing layer for picric acid based on the luminescence quenching of the Eu--thenoyltrifluoroacetone complex. *Analytica Chimica Acta* **1996,** *318* (2), 175-179; (e) Shriver-Lake, L. C.; Donner, B. L.; Ligler, F. S., On-Site Detection of TNT with a Portable Fiber Optic Biosensor. *Environmental Science & Technology* **1997,** *31* (3), 837-841.

8.   Toal, S. J.; Magde, D.; Trogler, W. C., Luminescent oligo(tetraphenyl)silole nanoparticles as chemical sensors for aqueous TNT. *Chemical Communications* **2005,** (43), 5465-5467.

9.   Toal, S. J.; Jones, K. A.; Magde, D.; Trogler, W. C., Luminescent Silole Nanoparticles as Chemoselective Sensors for Cr(VI). *Journal of the American Chemical Society* **2005,** *127* (33), 11661-11665.

10.   Borisov, S. M.; Mayr, T.; Mistlberger, G. n.; Waich, K.; Koren, K.; Chojnacki, P.; Klimant, I., Precipitation as a simple and versatile method for preparation of optical nanochemosensors. *Talanta* **2009,** *79* (5), 1322-1330.

11.   Ponnu, A.; Anslyn, E. V., A fluorescence-based cyclodextrin sensor to detect nitroaromatic explosives. *Supramolecular Chemistry* **2010,** *22* (1), 65-71.

12.   Wang, J., Electrochemical Sensing of Explosives. *Electroanalysis* **2007,** *19* (4), 415-423.

13.   Sanchez, J. C.; Trogler, W. C., Efficient blue-emitting silafluorene-fluorene-conjugated copolymers: selective turn-off/turn-on detection of explosives. *Journal of Materials Chemistry* **2008,** *18* (26), 3143-3156.

14.   Yang, J.; Lind, J. U.; Trogler, W. C., Synthesis of Hollow Silica and Titania Nanospheres. *Chemistry of Materials* **2008,** *20* (9), 2875-2877.

15.   Morris, J. V.; Mahaney, M. A.; Huber, J. R., Fluorescence quantum yield determinations. 9,10-Diphenylanthracene as a reference standard in different solvents. *The Journal of Physical Chemistry* **1976,** *80* (9), 969-974.

16.   Lakowicz, J. R., *Principles of fluorescence spectroscopy*. Springer: New York, 2004.

17.   Ly, S.-Y.; Kim, D.-H.; Kim, M.-H., Square-wave cathodic stripping voltammetric analysis of RDX using mercury-film plated glassy carbon electrode. *Talanta* **2002,** *58* (5), 919-926.

Chapter 4

Emission Tuning of Functionalized Silafluroenes

Introduction

A fluorophore whose emission can be tuned can be a very desirable commodity; this is something very evident in biological and cellular research where the right combination of stains or fluorophores is vital to the success of a study. Shown in Fig. **1** was the combination of Hoechst stain (blue), a nuclear
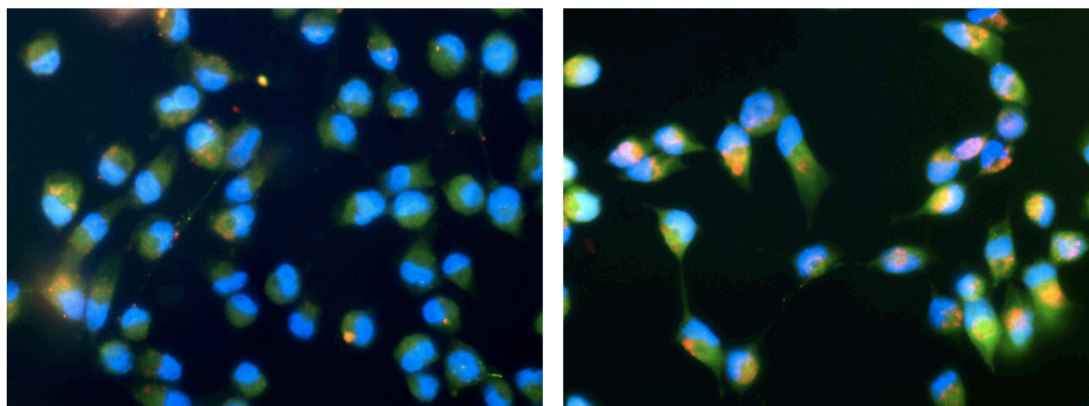
Figure **1** shows images of endocytosis of 100nm hollow silica (**A**) and 100nm Fe-doped, hollow silica (**B**) nanoshells. Samples (**A**) and (**B**) were coated with Alexa-647 and both were administered at 100 μg/mL to the MDA-MB-231 cell line (breast cancer). As can be seen above, uptake of the Fe-doped, hollow silica nanoshells appears to be favored. Images provided courtesy of Kristina K. Pohaku Mitchell.

stain, 5-chloromethylfluroscein diacetate (CMFDA-green), and alexafluro-647 (red). The dyes were used to outline the cell, the nucleus, and determine if any labeled nanoparticles had successfully entered the cell. This combination and many other combinations of fluorophores are a common occurrence in cellular biology research.[1]

In the sensor field, the emission wavelength has never been an issue. For sensor applications, while still very important, the emission choice has not always been a highly desirable option.[2] This is because most fluorescent based sensor platforms function by a "turn-off" mechanism, whereby the highest occupied molecular orbital (HOMO) must have the correct overlap with the
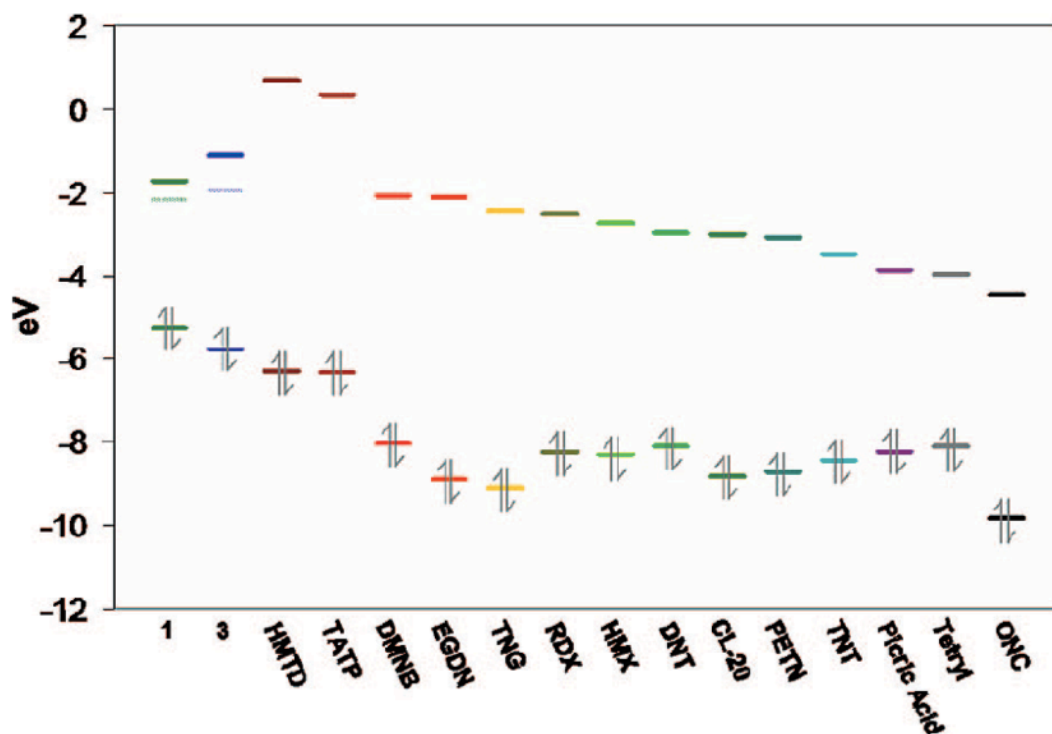
Figure **2** shows a DFT calculations of the HOMO-LUMO gap between the explosives listed and two polymeric sensory designed to detect these analytes[3]

lowest unoccupied molecular orbital (LUMO) in order for the sensor to function properly.[4] Emission tuning is usually done by the addition of an electron withdrawing or donating groups to obtain a bathochromic or hypsochromic shift of the emission. This inductive effect shifts the emission and also can affect the

HOMO-LUMO gap with the targeted analyte, thus possibly improving or worsening the detection limits.

As seen in Fig. **2** the balance necessary to achieve efficient fluorescent detection is small.[3] A closer look shows why triacetonetriperoxide (TATP) is not readily detected using this fluorescent platform. Therefore, it is easy to see why emission tuning is less of a luxury and more of a necessity when targeting specific analytes for fluorescent detection. The emission tuning for polymeric systems can be accomplished by utilizing different electron withdrawing or donating co-monomers.[5] A general effect of the polymerization of conjugated organic monomer is a highly conjugated polymeric system that due to an extended conjugated network the emission of the polymer is red shifted from that of the monomer.

While the emission wavelength may not be a significant concern for electronic sensors, where a photoavalanche device or photomultiplier tube determines the emission output, for field systems that rely on a human observer it can be the deciding factor.[6] For example, the prototype versions of the polysilole high explosive detection system rely on an observer distinguishing fluorescent emission from quenching.[7] For the polysilole and its co-polymer variants, emission is in the green region of the spectrum. The silafluorene and its co-polymer variants emit in the ultra violet-blue region of the spectrum.[8] This region can be difficult for the human eye to see and it is for this reason that the

functionalized silafluroenes were synthesized and studied. The functionalization of the fused-ring silole will allow for emission tuning.

Results and Discussion

Silafluorene is synthesized from 1,2-dibromobenzene, but in order to obtain a functionalized version, the starting materials would need to have the desired groups prior to the biphenyl formation.[9] This was done to minimize ring functionalization because it has been reported that functionalization of fused ring systems, such as 9,9'-spirobi[fluorene] functionalization, can lead to multiple isomers, which can make isolation of the desired product difficult. Using this strategy the synthesis of a 2,3,6,7-tetramethylsiliafluroene and 2,3,6,7-tetramethoxysilafluroene was accomplished by beginning with 1,2-dimethylbenzene(*o*-xylene) and 1,2-dimethoxybenzene (veratrole).[10] In order to obtain the desired biphenyl, the methyl and methoxy variants needed to be dibrominated at the 1,2 positions (as seen in Fig. **3**).
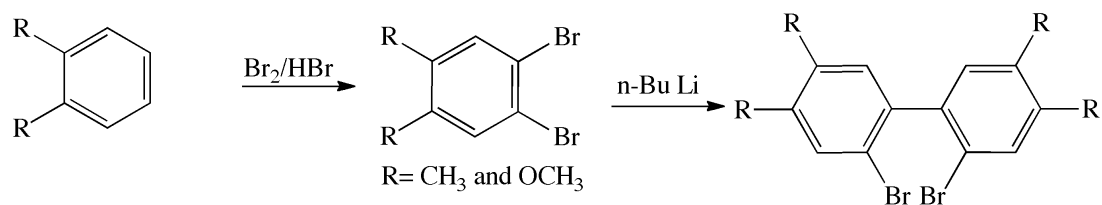
Figure **3** shows the synthetic scheme used to obtain a 1,2 –dibrominated benzene and the corresponding biphenyls.

Both brominations were carried out with a catalytic amount of iodine (I_2) and bromine in methylene chloride. The crude products were colored solids. 1,2-dibromo-4,5-dimethyoxybenzene was recrystallized from 2-propanol and 1,2-dibromo-4,5-dimethylbenzene was recrystallized from methanol. Both compounds were produced on the gram scale with a purified yield of 75-85%. A detailed account can be found in the experimental section. The biphenyl derivatives were prepared according to modified literature[3, 8-9, 11] procedures. The dibromophenyls were dissolved in freshly distilled THF and cooled to -72°C, at this time n-butyl-lithium was added dropwise using a pressure equalizing addition funnel. Once all of the base was added, the reaction mixtures were allowed to return to room temperature and stirred for an additional three hours. Following standard organic work up procedures, oils were obtained for both compounds. Both compounds were purified by column chromatography using a methylene chloride:hexanes gradient, the compounds were obtained in yields of 50-60%.

The dihydrosilafluorenes were prepared by treatment with two equivalents of n-butyl lithium at -72°C to the functionalized dibrombiphenyls in freshly distilled THF. After stirring for 2 hours at -72°C, two equivalents of dichlorosilane was slowly added to the reaction mixture. A summary of these reactions can be seen in Fig. **4** (note: dichlorosilane was purchased and used as a 25% (w/w) solution in xylenes).
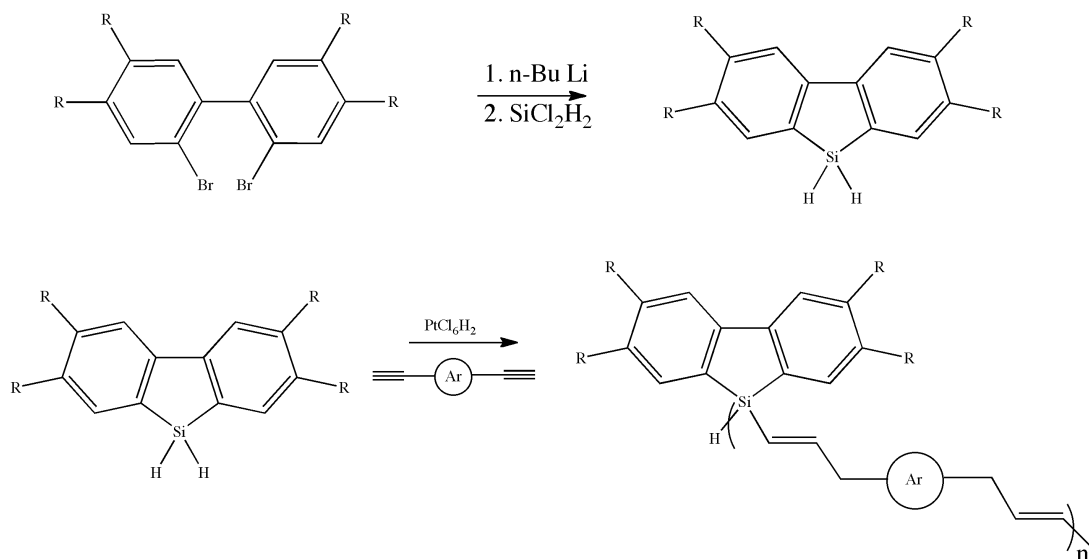
Figure **4** is a synthetic scheme for the preparation of dihydrosilafluroenes and their diethynyl co-polymers.

The polymerization was done, according to literature procedures[3, 8-9, 11], under argon and equal molar amounts of dihydrosilafluroene and diethynylaryl were added to a round bottom flask, along with a catalytic amount of chloroplatinic acid ($PtCl_6 \cdot H_2$). To this 1-2 ml of dry toluene was added, the reaction was heated to 60-70°C and let to stir under argon for 36 hours. After 36 hours, the heat was removed and when the reaction reached room temperature, dimethylphenylsilane was added to cap the co-polymer. The solvent was removed and the polymer precipitated by dissolving in THF and adding to a ten-fold volume of stirring methanol. The precipitation was done three times to remove shorter oligomers .
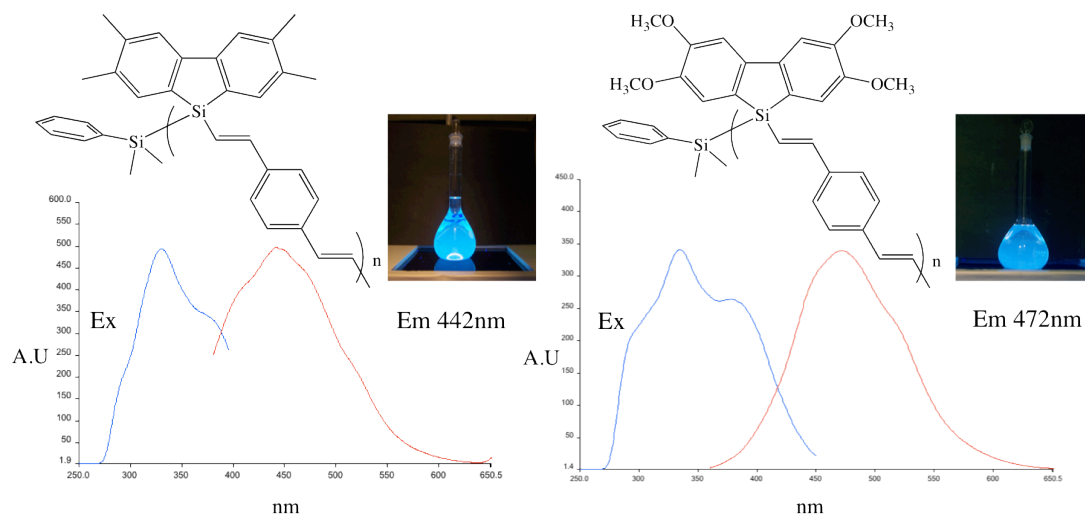
Figure **5** shows the excitation and emission curves for the tetramethyl and tetramethoxy diethynyl polymers, taken in toluene.

As seen in Fig. **5,** the emission curves for both tetramethyl and tetramethoxy substituted silafluroene polymers were red shifted 42 and 72 nm to that of the unfunctionalized corresponding polymer. The images of the solutions show both to be blue emitting polymers. The solution quantum yields were 3 and 1%,
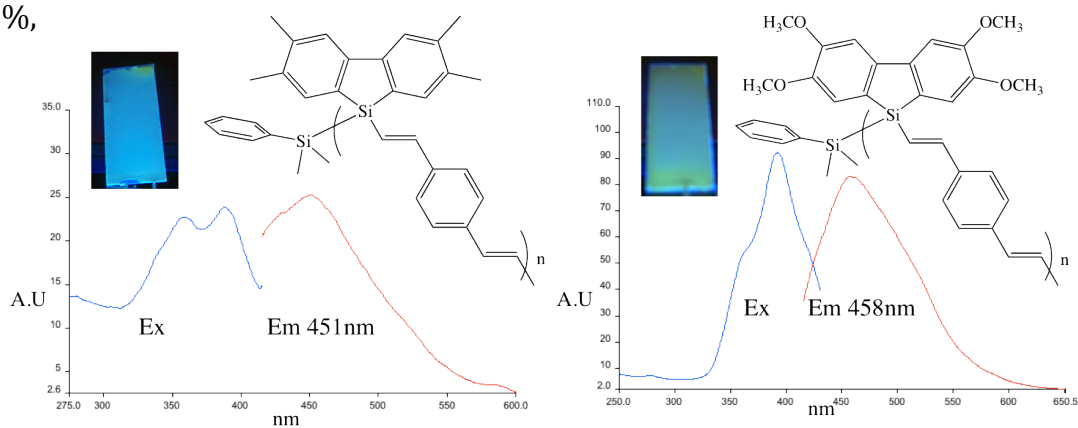
Figure **6** shows the solid-state excitation and emission curves for the tetramethyl (TMSF-DEB) and tetramethoxy (TMxSF-DEB) diethynyl polymer.

respectively; both significantly lower than the unfunctionalized silafluorene. The solid-state excitation and emission spectra were taken by coating the polymers onto non-fluorescent thin layer chromatography plates (as seen in Fig. **6**). The solid-state emission was slightly red shifted for both polymers; this is most likely due to the restriction of molecular motion. The blue-green solid-state emission did make the polymers easier to visualize, but their lower intensity was noticeable.

Using the dihydrotetramethylsilafluorene a second class of polymer was synthesized. The co-monomer chosen was a 3,6-diethynyl-9-methylcarbazole; this was done to mimic a reported macromolecule composed of carbazole which had an affinity for TNT (seen below in Fig. **7**). Following similar procedures as
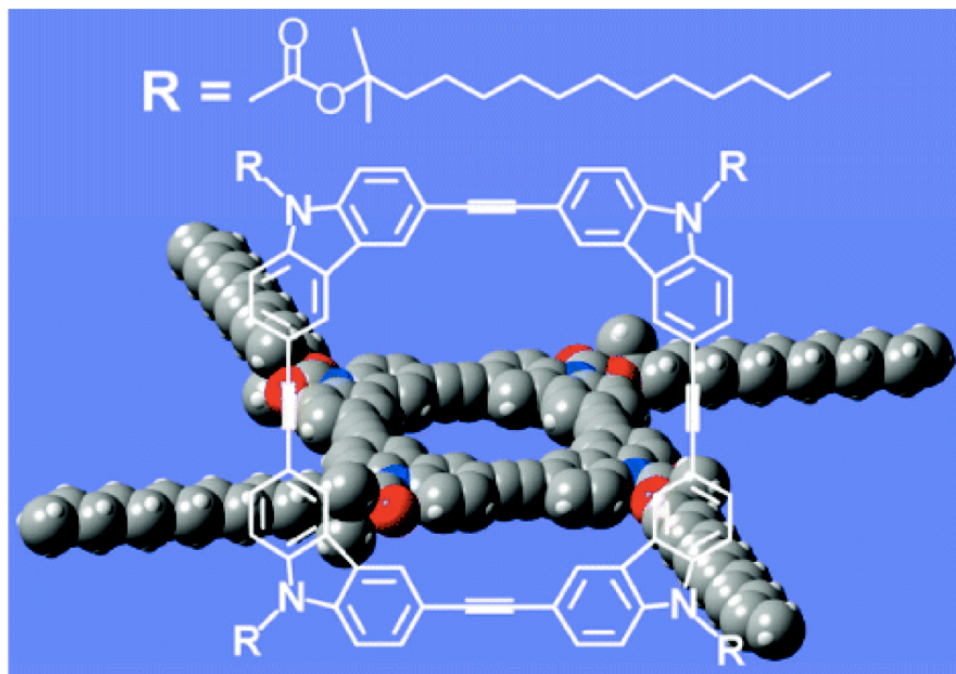
Figure **7** shows a macromolecule, which was reported to have a propensity for the detection of TNT.[12]

previously described a poly-tetramethylsilafluroenyl-diethynylcarbazole was prepared. Although the reported carbazole used was 2,7 functionalized, because it was not easily synthetically accessible, a 3,6 substituted variant was studied.[12]

Solution   Thin film
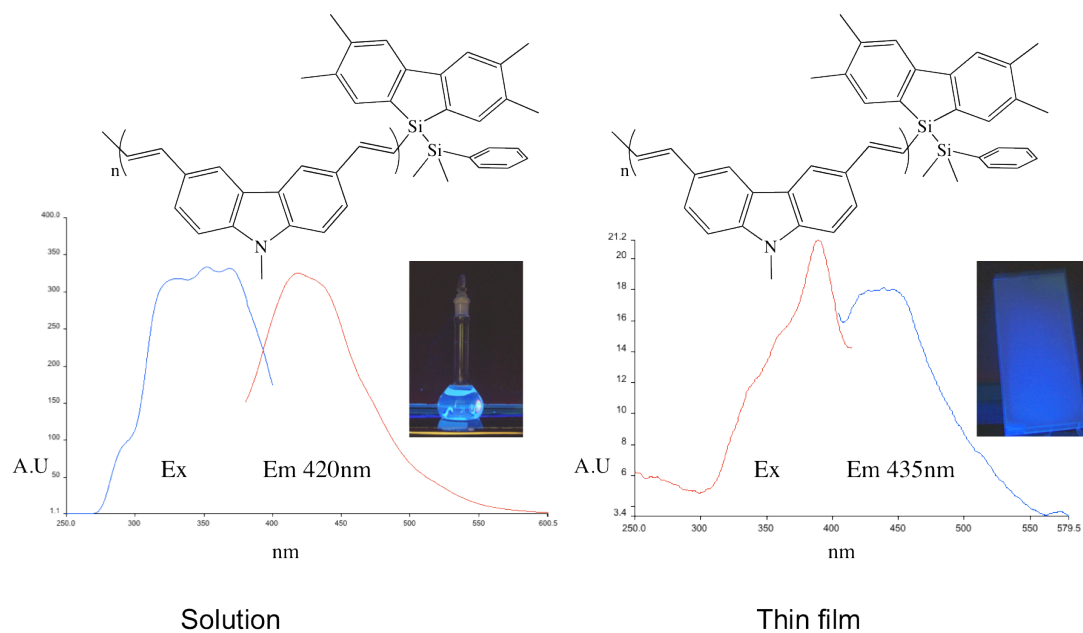
Figure **8** shows the solution and solid-state excitation and emission spectra for p-tetramethylsilafluroenyl-diethynylcarbazole.

As seen in Fig. **8,** the emission of the p-silafluorenyl-carbazole (TMSF-Car) was slightly blue shifted compared to the corresponding diethynylbenzene. The quantum yield was significantly lower still; all of the values are summarized in Table **1**.

Table **1** is a summary of the previously mentioned polymers.

	TMSF-DEB	TMxSF-DEB	TMSF-Car
Φ	3 %	1 %	0.1 %
M_w GPC data	4600	5100	8900
M_w/M_n GPC data	1.5	1.4	1.3
λ_{abs}	298 nm	305 nm	300 nm
$\lambda_{Fl\ Sol}$	442 nm	472 nm	420 nm
$\lambda_{Fl\ Thin\ Film}$	451 nm	458 nm	435 nm

All of the functionalized silafluorene polymers synthesized emitted within a 50nm range of each other. The two diethynylbenzene polymers exhibited quantum yields slightly lower than the unfunctionalized counterparts. This is attributed to the tetra-substitution. The added molecular motion directly affects the quantum efficiency. This is most likely why the poly-tetrmethoxysilafluorene exhibits an even lower quantum yield. An interesting observation to note about the poly-tetrmethoxysilafluorene is that when dissolved in chloroform, bromoform, or iodoform and exposed to ultraviolet excitation, the solution quickly becomes a bright pink color. This process is reversible and it takes approximately an hour or so to return to a clear, colorless solution. After several excitations, the solution becomes colored and the fluorescence intensity is

diminished. This is thought to be a charge transfer complex formed with the excited fluorophore and the haloform solvents. The colored solution was studied by NMR and fluorescence spectroscopy, but no significant data was produced. It was also hypothesized that the source of the yellow color in the solution and the weakened fluorescence intensity could be due to the degradation of the fluorophore due to photobleaching. The four methoxy groups make the ring system more electron rich and thus more susceptible to oxidation.

The application for all of the aforementioned polymers is particulate explosive detection. This is accomplished by depositing known amount of explosives to surfaces; filter paper, which is porous and absorbent, and ceramic wells, which are non-porous and have no substantial absorptive properties. The use of these two surfaces should encompass the two extremes for solid surface absorption. Once the deposited analyte's solvent has evaporated, a polymeric solution was applied as an aerosol. The aerosol application was done using a hobby airbrush. The amount of air pressure allowed the user to qualitatively control the amount or thickness of the film. Once the film was dry, an impartial observer viewed the surfaces under an ultraviolet lamp and determined where quenching was present. An example of what an observer would see is shown in Fig. **9**. These are images taken of Tetryl and trinitroglycerine (TNG) deposited onto filter paper and in ceramic wells. The images are not the best quality due to the low light needed to observe the fluorescence quenching.

TNG   Tetryl
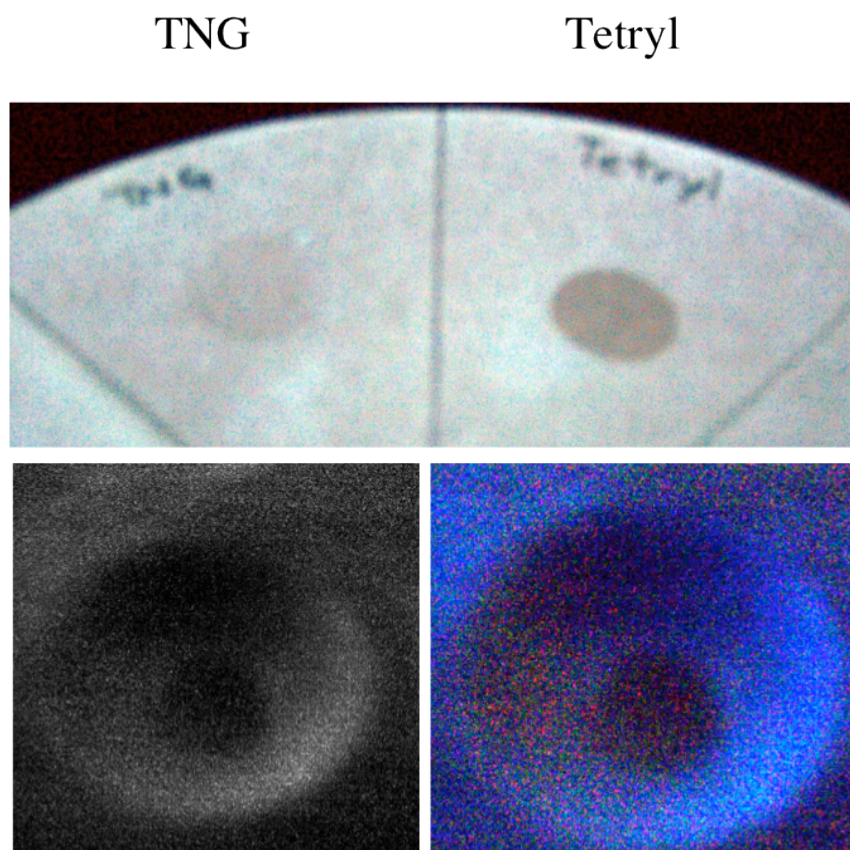
Figure **9** shows an example of the explosives particulate, (top) on filter paper and (bottom) in ceramic wells.

While the detection examples do not photograph well, the impartial observer had no trouble determining where quenching had occurred. The filter paper surface is always easier to determine, this is not solely due to its absorptive nature, but its lack of glare when viewed under the excitation of a UV lamp. A full summary of the detection limits can be seen in Table **2**. The detection limits achieved for these systems were similar to the unfunctionalized systems while

Table **2** is a summary of the detection limits achieved.

Filter Paper			
Explosive	TMSF-DEB (ng cm^{-2})	TMxSF-DEB (ng cm^{-2})	TMSF-Car (ng cm^{-2})
TNT	1	5	2.5
DNT	2	5	5
PA	2	5	10
Tetryl	10	5	2.5
HMX	20	20	5
TNG	10	10	5

Ceramic Plates			
Explosive	TMSF-DEB (ng cm^{-2})	TMxSF-DEB (ng cm^{-2})	TMSF-Car (ng cm^{-2})
TNT	2	5	2.5
DNT	4	5	5
PA	2	10	10
Tetryl	4	10	2.5
HMX	100	100	10
TNG	100	100	5

the p-TMSF-Car performed better than its diethynyl counterparts. Its lack of fluorescent efficiency impacted its detection limits.

Conclusions

While all of the substituted silafluorene polymers were no better than their unfunctionalized counterparts, the emission tuning was a success. The addition of varying degrees of electron donating group allowed the emission peak maximum to be shifted without greatly impacting the detection capabilities. The use of a carbazole co-monomer did seem to improve the detection. While the most significant issue is the diminished fluorescence intensity, there are still possible routes to overcome the shortcomings of this system. The use of more efficient fluorescent co-monomers would greatly aid the TMSF and TMxSF materials. The use of a fluorescent protecting group such as, fluorene or 9,9' spirobi[fluorene], for the amine of the carbazole would greatly bolster the

fluorescent intensity or the use of the 2,7-substituted carbazole, which is said to be more fluorescently efficient, improving the detection limits for this system.

Experimental

General. *Caution: TNT and picric acid are high explosives and should be handled only in small quantities. Picric acid also forms shock sensitive compounds with heavy metals. Purchased explosive standards were handled as dilute solutions to eliminate their explosion hazard.* All synthetic manipulations were carried out under an atmosphere of dry argon gas using standard Schlenk techniques. Dry solvents were purchased from Aldrich Chemical Co. Inc. and used after purification with an MBraun MB Auto Solvent Purification System. Spectroscopic grade THF and toluene from Fisher Scientific was used for the fluorescence measurements. All other reagents were purchased from Aldrich Chemical Co. and used as received. Picric acid and DNT were purchased from Aldrich Chemical Co. and recrystallized from ethanol and methanol, respectively. TNT was prepared from DNT[13] and recrystallized from toluene. RDX, HMX, Tetryl, TNG and PETN were purchased as 1 mg/mL analytical standards in acetonitrile from Cerilliant®.

NMR data were collected with a Varian Unity 400 or 500 MHz spectrometers (300.1 MHz for ^{1}H, 77.5 MHz for ^{13}C, and 99.4 MHz for ^{29}Si NMR). Infrared spectra were obtained with the use of a Nicolet Magna-IR™ Spectrometer 550. GPC-RI data were obtained with the use of a Viscotek GPCmax

VE 2001 GPC and a Viscotek VE 3580 refractive index detector calibrated with polystyrene standards. Fluorescence emission and excitation spectra were recorded with the use of a Perkin-Elmer Luminescence Spectrometer LS 45. UV-vis spectra were obtained with the use of a Perkin-Elmer Lamda35 UV/Vis spectrometer.

1,2-Dibromo-4,5-dimethoxybenzene. In a 500-ml three neck round bottom flask 15ml (117mmol) of veratrole (1,2-dimethoxybenzene) was added to 25ml of CH_2Cl_2. To this 0.65g (2.5mmol) of iodine (I_2) was added turning the solution a dark deep purple. The round bottom flask was now equipped with an addition funnel, into the addition funnel 20ml (388 mmol) of bromine (Br_2) was added. The Br_2 was slowly added to the stirring veratrole and I_2 solution. The addition was done over 1 hour, after stirring for 3 more hours all of the volatiles (I_2, Br_2, and CH_2Cl_2). This left an orange solid, which was dissolved, in hot isopropanol. Any insoluable material was filtered off. The solution was let to cool and the product crystallized out of this solution. This gave a slightly colored solid, which was recrystallized from hot isopropanol to yield white needles at 70-75% yield. ^{1}H NMR (400 MHz, CDCl3): δ7.86s (2H), δ3.86s.

2,2'-dibromo-4,4',5,5'-tetramethoxy-1,1'-biphenyl. In a 500-ml three neck round bottom flask 8.00g (27 mmol) 1,2-Dibromo-4,5-dimethoxybenzene was dissolved in 120ml of freshly distilled THF. This yielded a clear, colorless

solution. The solution was now cooled down to -75 C, using CO_2 and diethylether. Once cooled, 8.5ml (13.5mmol) of n-butyl lithium (1.6M in hexanes) was added drop-wise over an hour. Now the cooling bath was removed and the solution was let to stir another two hours at room temperature. The reaction was now quenched using 50ml of a 5%HCl solution. At this time the reaction mixture turned a faint yellow color. The THF was removed with the roto-evaporator, leaving behind the aqueous mixture. The aqueous mixture was extracted 3x with 15ml of diethylether. The organic solution was washed with a brine solution and dried over $MgSO_4$. The white solid was purified by column chromatography at 50-60% yield. ^{1}H NMR (400 MHz, CDCl3): δ7.11s (2H), δ6.77s (2H), δ3.91s (6H), δ3.86s (6H).

1,2-Dibromo-4,5-dimethylbenzene. In a 500-ml three neck round bottom flask 92ml (750mmol) of *o*-xylene(1,2-dimethylbenzene). To this 0.4g (2.5mmol) of iodine (I_2) was added turning the solution a lite purple. The round bottom flask was cooled in an ice bath and now equipped with an addition funnel, into the addition funnel 80ml (1533 mmol) of bromine (Br_2) was added. The Br_2 was slowly added to the stirring *o*-xylene and I_2 solution, making sure the temperature never rose above 0C. The addition was done over 1 hour, after stirring for overnight (12 hours). At time a large off-white solid was left behind, which was dissolved in diethylether. The organic solution was now washed with an 2N NaOH solution, washed with brine and dried over $MgSO_4$. The white solid

recovered was now recrstyallized from methanol to give white flakes at 70-75% yield. ^{1}H NMR (400 MHz, CDCl3): δ7.37s (2H), δ2.18s.

2,2'-dibromo-4,4',5,5'-tetramethyl-1,1'-biphenyl.   In a 500-ml three neck round bottom flask 10.00g (38 mmol) 1,2-Dibromo-4,5-dimethylbenzene was dissolved in 75ml of freshly distilled THF. This yielded a clear, colorless solution. The solution was now cooled down to -75 C, using CO_2 and diethylether. Once cooled, 12ml (19mmol) of n-butyl lithium (1.6M in hexanes) was added drop-wise over an hour. Now the cooling bath was removed and the solution was let to stir another two hours at room temperature. The reaction was now quenched using 50ml of a 5%HCl solution. At this time the reaction mixture turned a faint yellow color. The THF was removed with the roto-evaporator, leaving behind the aqueous mixture.   The aqueous mixture was extracted 3x with 15ml of diethylether. The organic solution was washed with a brine solution and dried over $MgSO_4$. The white solid was purified by column chromatography at 50-60% yield. ^{1}H NMR (400 MHz, CDCl3): δ7.42s (2H), δ6.99s (2H), δ2.88s (6H), δ2.24s (6H).

Synthesis of Polysilole-diethynylaryl co-polymers were prepared according to literature procedure-

Equal molar amount of   5*H*-dibenzo[*b,d*]silole   and   diethynylaryl compounds were put into a clean, dry round bottom flask equipped with a

condenser. To these solids a catalytic amount of $PtCl_6 \cdot H_2$ was added under Ar. To this mixture 1.5ml of dry toluene was add. The reaction was stirred under Ar at 60°C for 36hr. Then the temperature was reduced to 35°C and an excess (50 μL) of dimethylphenylsilane was added under Ar and stirring continued for 2hr. The $PtCl_6 \cdot H_2$ was removed by filtration using filter paper and the toluene was removed by vacuum. The yielded a brownish/yellow oil. The oil was taken up in 1ml of tetrahydrofuran and added to 10 ml of stirring methanol to precipitate polymer at 55-65% yield. This process was repeated two times and gave a faintly yellow solid. GPC: 13kDa, PDI 1.3.

References

1.   (a) Goldman, R. D.; Spector, D. L., *Live cell imaging : a laboratory manual*. Cold Spring Harbor Laboratory Press: Cold Spring Harbor, N.Y., 2005; (b) Shields, A.   F.   In   Vivo   Imaging   of   Cancer   Therapy. http://public.eblib.com/EBLPublic/PublicView.do?ptiID=338242.

2.   (a) Basabe-Desmonts, L.; Reinhoudt, D. N.; Crego-Calama, M., Design of fluorescent materials for chemical sensing. *Chem. Soc. Rev.* **2007,** *36* (6), 993-1017; (b) Kolla, P., The Application of Analytical Methods to the Detection of Hidden Explosives and Explosive Devices. *Angewandte Chemie International Edition in English* **1997,** *36* (8), 800-811; (c) Nambayah, M.; Quickenden, T. I., A quantitative assessment of chemical techniques for detecting traces of explosives at counter-terrorist portals. *Talanta* **2004,** *63* (2), 461-467.

3.   Sanchez, J. C.; DiPasquale, A. G.; Rheingold, A. L.; Trogler, W. C., Synthesis, Luminescence Properties, and Explosives Sensing with 1,1-Tetraphenylsilole- and 1,1-Silafluorene-vinylene Polymers. *Chemistry of Materials* **2007,** *19* (26), 6459-6470.

4.   (a) Albani, J. R., *Principles and applications of fluorescence spectroscopy*. Blackwell Science: Oxford; Ames, Iowa, 2007; (b) Lakowicz, J. R., *Principles of fluorescence spectroscopy*. Springer: New York, 2004.

5.   (a) Narayanan, A.; Varnavski, O. P.; Swager, T. M.; Goodson, T., Multiphoton Fluorescence Quenching of Conjugated Polymers for TNT Detection. *The Journal of Physical Chemistry C* **2008,** *112* (4), 881-884; (b) Yang, J.-S.; Swager, T. M., Fluorescent Porous Polymer Films as TNT Chemosensors:‚Äâ Electronic and Structural Effects. *Journal of the American Chemical Society* **1998,** *120* (46), 11864-11873.

6.   Swager, T. M. N., MA, US), Yang, Jye-shane (Ping-Chen, TW), Williams, Vance (Somerville, MA, US), Miao, Yi-jun (Chester, VA, US), Lugmair, Claus G. (San Jose, CA, US), Levitsky, Igor A. (Fall River, MA, US), Kim, Jinsang (Cambridge, MA, US), Deans, Robert (Cambridge, MA, US) Emissive polymers and devices incorporating these polymers. 2007.

7.   (a) Sohn, H.; Calhoun, R. M.; Sailor, M. J.; Trogler, W. C., Detection of TNT and Picric Acid on Surfaces and in Seawater by Using Photoluminescent Polysiloles. *Angewandte Chemie* **2001,** *113* (11), 2162-2163; (b) Sohn, H.; Sailor, M. J.; Magde, D.; Trogler, W. C., Detection of Nitroaromatic Explosives Based on Photoluminescent Polymers Containing Metalloles. *Journal of the American*

Chemical Society **2003,** *125* (13), 3821-3830; (c) Toal, S. J.; Magde, D.; Trogler, W. C., Luminescent oligo(tetraphenyl)silole nanoparticles as chemical sensors for aqueous TNT. *Chemical Communications* **2005,** (43), 5465-5467; (d) Toal, S. J.; Sanchez, J. C.; Dugan, R. E.; Trogler, W. C., Visual Detection of Trace Nitroaromatic Explosive Residue Using Photoluminescent Metallole-Containing Polymers. *Journal of Forensic Sciences* **2007,** *52* (1), 79-83; (e) Trogler, W. C. D. M., CA, US), Sanchez, Jason (San Diego, CA, US), Toal, Sara (Mission Viejo, CA, US), Wang, Zheng (La Jolla, CA, US), Dugan, Regina E. (Rockville, MD, US) DETECTION OF NITRO- AND NITRATE-CONTAINING COMPOUNDS. 2010; (f) Trogler, W. C. D. M., CA, US), Sanchez, Jason (San Diego, CA, US) FLUORESCENCE DETECTION OF NITROGEN-CONTAINING EXPLOSIVES AND BLUE ORGANIC LED. 2011.

8.   (a) Sanchez, J. C.; Toal, S. J.; Wang, Z.; Dugan, R. E.; Trogler, W. C., Selective Detection of Trace Nitroaromatic, Nitramine, and Nitrate Ester Explosive Residues Using a Three-Step Fluorimetric Sensing Process: A Tandem Turn-off, Turn-on Sensor*. *Journal of Forensic Sciences* **2007,** *52* (6), 1308-1313; (b) Sanchez, J. C.; Trogler, W. C., Efficient blue-emitting silafluorene-fluorene-conjugated copolymers: selective turn-off/turn-on detection of explosives. *Journal of Materials Chemistry* **2008,** *18* (26), 3143-3156.

9.   Sanchez, J. C.; Urbas, S. A.; Toal, S. J.; DiPasquale, A. G.; Rheingold, A. L.; Trogler, W. C., Catalytic Hydrosilylation Routes to Divinylbenzene Bridged Silole and Silafluorene Polymers. Applications to Surface Imaging of Explosive Particulates. *Macromolecules* **2008,** *41* (4), 1237-1245.

10.   (a) Duan, J.; Zhang, L. H.; Dolbier, Jr., A Convenient New Method for the Bromination of Deactivated Aromatic Compounds. *Synlett* **1999,** *1999* (8), 1245-1246; (b) Eguchi, H.; Kawaguchi, H.; Yoshinaga, S.; Nishida, A.; Nishiguchi, T.; Fujisaki, S., Halogenation Using N-Halogenocompounds. II. Acid Catalyzed Bromination of Aromatic Compounds with 1,3-Dibromo-5,5-dimethylhydantoin. *Bulletin of the Chemical Society of Japan* **1994,** *67* (7), 1918-1921.

11.   Sanchez, J. C.; Trogler, W. C., Hydrosilylation of Diynes as a Route to Functional Polymers Delocalized Through Silicon. *Macromolecular Chemistry and Physics* **2008,** *209* (15), 1527-1540.

12.   Naddo, T.; Che, Y.; Zhang, W.; Balakrishnan, K.; Yang, X.; Yen, M.; Zhao, J.; Moore, J. S.; Zang, L., Detection of Explosives with a Fluorescent Nanofibril Film. *Journal of the American Chemical Society* **2007,** *129* (22), 6978-6979.

13.   (a) Dennis, W. H.; Rosenblatt, D. H.; Blucher, W. G.; Coon, C. L., Improved synthesis of TNT isomers. *Journal of Chemical & Engineering Data* **1975,** *20* (2), 202-203; (b) Klap√∂tke, T. M. High energy density materials. http://www.myilibrary.com?id=93792.

Chapter 5

A Brief Introduction: Color Doppler Ultrasound Imaging

General Introduction

At present, the best chances for breast conservation therapy rely upon the early detection and removal of malignant tumors.[1] Once detected, tumors are imaged using computed tomography (CT) or positron emission tomography (PET). These imaging techniques are utilized for their high resolution and contrast. Once located, a tumor is then marked for removal using a guide wire and/or a radioactive seed. The guide wire is simply a large wire, which is inserted into the center of the tumor 18-24 hours prior to the procedure.[2] The
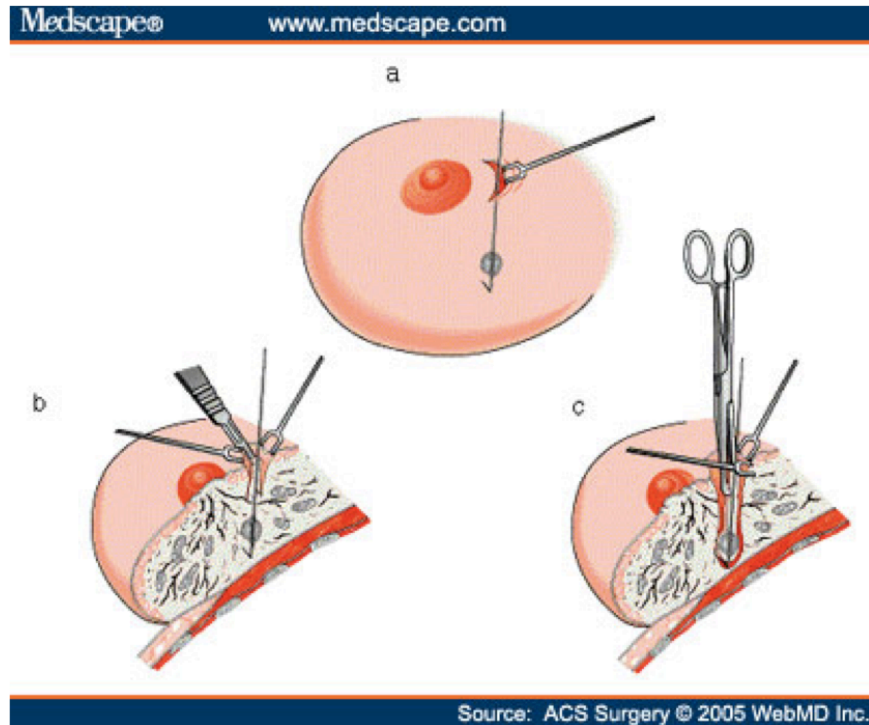
Figure **1** is a representation of the (a) insertion of the guide wires, and (b&c) the removal of the guide wire and the tumor whose location was marked by the wire.

wires, which protrude from the patient, are what the surgeon uses to locate and remove the tumor. The problem with this method is the pain it causes patients and the wires, which can move prior to surgery, do not allow surgeons to consistently achieve negative margins.[3] Negative margins are defined as containing no cancer cells present in the outer edge of the tissue and the rim of surrounding tissue that was removed, and a second surgical procedure must be performed when negative margins are not obtained. For these reasons, there is

Figure **2** shows the (left image) surgical guide wire tools used to mark tumors and (right image) a CT of a small tumor pre and post marking.

much interest in the development of improved tumor marking techniques. An excellent candidate for this would be ultrasound imaging; it is a non-invasive imaging technique that is the routine safest imaging technique available.[4]

When synthesizing new ultrasound contrast agents, one consideration to factor in is the echogenicity of the agent. Where the echogenicity is the ability of a material to create an echo, which is measured by calculating the backscattering and transmission coefficients as a function of frequency. The simplest factors contributing to the echogenicity are the density and compressibility of a material. For example, blood is 20 to 30 times less echogenic than tissue; this is due to the small impedance differences between red blood cells and plasma. Different types of tissue (i.e normal vs cancerous) can be difficult to distinguish by using ultrasound imaging. In order for ultrasound imaging to be a more widely used viable imaging technique, ultrasound contrast particles are used.[5] Ultrasound contrast particles are microbubbles that are encased in a variety of materials such as liposomes, polymers, proteins, or amorphous inorganics.[6] The contrast enhancement comes from the gases that are used to fill the particles. More specifically, the compressibility of air is 10^{-6} m^2/N while water is 10^{-11} m^2/N (same order of magnitude as tissue). This large difference allows contrast particles that contain gases to give a significant and easily detectible signal in ultrasound imaging. Therefore when designing an ultrasound contrast particle, there are many factors to consider such as size of the particle, material used for particle synthesis and the gas used to fill the particles. The size of the particles can be a concern for various reasons; the size of the particles can affect the efficiency of the interaction of the particles with the ultrasonic sound wave. Specifically a smaller internal gas payload yields a smaller compression or

rarefaction when compared to an equivalently larger particle, which leads to a smaller echogenic signal for a small particle. The reason that the gas payload is important is this directly correlates to the enhancement. The enhancement comes from the interaction of the particle with the pressure wave; the gas filled particles can undergo a compression, rarefaction or cavitation. The end result is
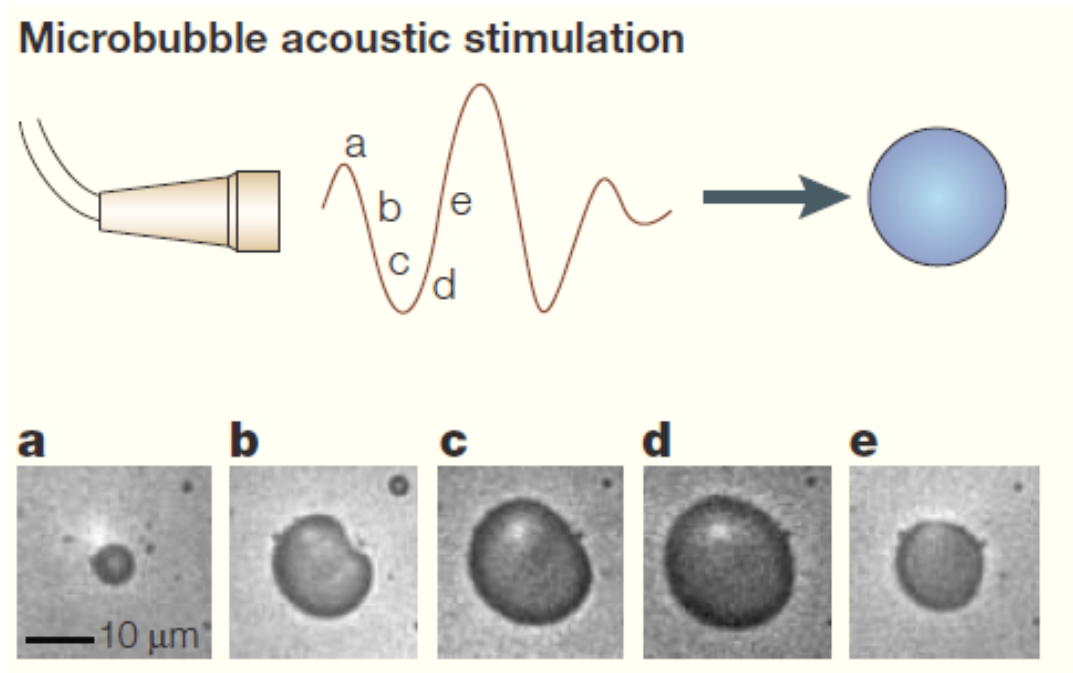
Figure **3** under compression (a), microbubbles shrink; under rarefaction (c and d), microbubbles expand. This strong physical responsiveness translates into strong and non-linear signal responsiveness. [6a, 7]

all of the physical responses seen above in Fig. **3**, which translate into nonlinear signal responses or detectable image enhancement.

Presently the only US FDA commercially approved ultrasound contrast particle is the Definity® microbubble, which is a soft-shelled liposome based

particle. When filled with decaflurobutane, it acts as an efficient contrast particle for determining blood flow in the vasculature system. Definity® ultrasound contrast particles were designed to be injected into the vasculature system, specifically to determine the amount of blood flow.[8] They have a total lifetime of approximately 1 hour and an effective imaging time of only 5-8 minutes. Due to the life threatening dangers of embolisms, it is understandable why the particles must have short lifetimes. Unfortunately, these types of contrast agents would not function well as an ultrasound tumor marker, because the material needed to replace or work in conjunction with guide needles would ideally need to have a lifetime of 24-48 hours, be robust enough to undergo several imaging session and must also be immobile once injected.

The ultrasound technique most receptive is the color flow or color Doppler imaging (CDI). In this technique, a sound or pressure wave generated from the ultrasound transducer is sent to some region and depth set by the sonographer. The interaction with the material in the region of interest depends on the material's echogenicity. Contrast particles are quite echogenic and their interaction with pressure wave creates a return echo or sound wave that the same transducer receives. The return signal is then processed into an image. For color Doppler imaging there is one more component (this process is shown in Fig. **4**). Since there is a time delay from the initial sent and the received sound wave
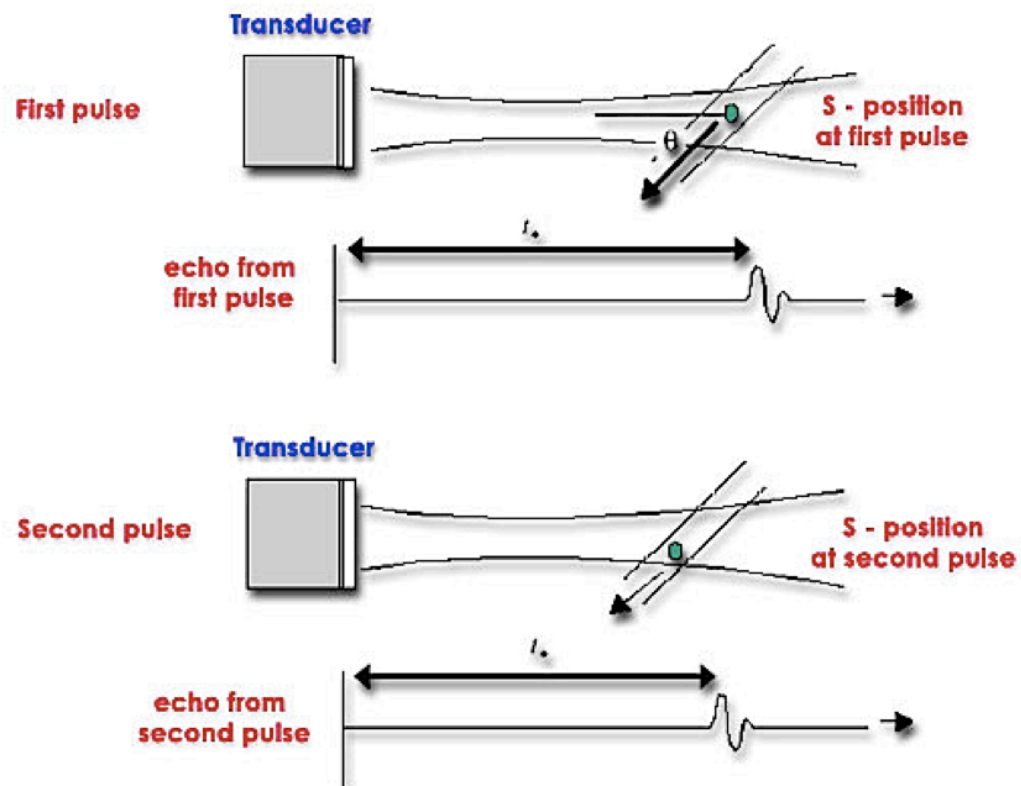
Figure **4** shows that in pulsed wave Doppler ultrasound, a series of pulses are transmitted, and phase changes in the response signal are detected between sequential pulses. Scatterers moving toward or away from the transducer induce detectable phase shifts in their response signals. Microbubble destruction, results in a loss of signal in the second pulse, which is detected as a strong signal. Image above from C. Deane <u>Doppler ultrasound: principles and practice</u>.[9]

the Doppler frequency can be calculated. This is then converted into a velocity by the instrument, which is assigned to pixels when the echoes returning from a voxel are non-correlated following the transmission of multiple ultrasound pulses. A voxel is an element representing a value on a regular grid in three-dimensional space. The processed voxel is converted from a frequency shift into a velocity, which is displayed on the ultrasound a display as different colors. The

colors correspond to signals that are moving towards or away from the transducer. This mode when used in conjunction with a contrast agent is quite useful in determining blood flow and ascertaining whether there are obstructions in the vasculature system. It also offers s a method for imaging rigid shell gas bubbles that are not compressible, but may leak gas or break to release gas.

References

1.   (a) Folkman, J., Tumor angiogenesis: therapeutic implications. *N Engl J Med* **1971,** *285* (21), 1182-6; (b) Folkman, J., Tumor angiogenesis. *Adv Cancer Res* **1985,** *43*, 175-203; (c) Folkman, J., Role of angiogenesis in tumor growth and metastasis. *Semin Oncol* **2002,** *29* (6 Suppl 16), 15-8.

2.   (a) Cox, C.; Furman, B.; Stowell, N.; Ebert, M.; Clark, J.; Dupont, E.; Shons, A.; Berman, C.; Beauchamp, J.; Gardner, M.; Hersch, M.; Venugopal, P.; Szabunio, M.; Cressman, J.; Diaz, N.; Vrcel, V.; Fairclough, R., Radioactive Seed Localization Breast Biopsy and Lumpectomy: Can Specimen Radiographs Be Eliminated? *Annals of Surgical Oncology* **2003,** *10* (9), 1039-1047; (b) Gray, R. J.; Pockaj, B. A.; Karstaedt, P. J.; Roarke, M. C., Radioactive seed localization of nonpalpable breast lesions is better than wire localization. *Am J Surg* **2004,** *188* (4), 377-80; (c) Pavlicek, W.; Walton, H. A.; Karstaedt, P. J.; Gray, R. J., Radiation safety with use of I-125 seeds for localization of nonpalpable breast lesions. *Acad Radiol* **2006,** *13* (7), 909-15; (d) Richard, J. G.; Barbara, A. P.; Patricia, J. K.; Michael, C. R., Radioactive seed localization of nonpalpable breast lesions is better than wire localization. *American journal of surgery* **2004,** *188* (4), 377-380.

3.   Blair, S. L.; Thompson, K.; Rococco, J.; Malcarne, V.; Beitsch, P. D.; Ollila, D. W., Attaining Negative Margins in Breast-Conservation Operations: Is There a Consensus among Breast Surgeons? *Journal of the American College of Surgeons* **2009,** *209* (5), 608-613.

4.   (a) American Institute of Ultrasound in, M., *Medical ultrasound safety*. American Institute of Ultrasound in Medicine: Laurel, MD (14750 Sweitzer Lane, Laurel 29707-5906), 1994; (b) Gibbs, V.; Cole, D.; Sassano, A., *Ultrasound physics and technology : how, why and when*. Churchill Livingstone/Elsevier: Edinburgh; New York, 2009; (c) Harris, G. R.; Center for, D.; Radiological, H., *Ultrasound safety*

standards. Center for Devices and Radiological Health, US Food and Drug Administration: Rockville, MD, 1992.

5.   (a) de Kerviler, E.; Gossot, D.; Celerier, M.; Frija, J., Limitations of intraoperative sonography for the localization of pulmonary nodules during thoracoscopy. *Am. J. Roentgenol.* **1998,** *170* (1), 214-215; (b) De Schepper, A. M.; Vanhoenacker,   F.   Imaging   of   Soft   Tissue   Tumors. http://public.eblib.com/EBLPublic/PublicView.do?ptiID=264847.

6.   (a) Calliada, F.; Campani, R.; Bottinelli, O.; Bozzini, A.; Sommaruga, M. G., Ultrasound contrast agents: basic principles. *European journal of radiology* **1998,** *27*, 157-60; (b) Glajch, J. L.; Carpenter, A. P., Jr.; Cheesman, E. H. Porous inorganic targeted ultrasound contrast agents. 2001; (c) Glajch, J. L.; Loomis, G. L.; Mahler, W. Porous inorganic ultrasound contrast agents. 1992.

7.   Chomas, J. E.; Dayton, P.; Allen, J.; Morgan, K.; Ferrara, K. W., Mechanisms of contrast agent destruction. *IEEE transactions on ultrasonics, ferroelectrics, and frequency control* **2001,** *48* (1), 232-48.

8.   (a) Liu, J.; Levine, A. L.; Mattoon, J. S.; Yamaguchi, M.; Lee, R. J.; Pan, X.; Rosol, T. J., Nanoparticles as image enhancing agents for ultrasonography. *Phys. Med. Biol.* **2006,** *51* (9), 2179-2189; (b) Liu, J.; Levine, A. L.; Mattoon, J. S.; Yamaguchi, M.; Lee, R. J.; Pan, X. L.; Rosol, T. J., Nanoparticles as image enhancing agents for ultrasonography. *Physics in Medicine and Biology* **2006,** *51* (9), 2179-2189.

9.   (a) Schwartz, R. L. P. a. R. A., *Practical Doppler ultrasound for the clinician*. Urban & Schwarzenberg: Baltimore 1991; (b) Woodcock, P. A. a. J. P., *Doppler ultrasound and its use in clinical measurement*. Academic Press: New York, 1982.

Chapter 6

Hard Shell Gas-Filled Contrast Enhancement Particles for Color Doppler
Ultrasound Imaging of Tumors

Introduction

Ultrasound imaging is used frequently for medical diagnosis because it is safe, fast, and noninvasive. Ultrasound's major shortcoming is its image contrast when compared to techniques such as magnetic resonance imaging (MRI). Therefore, methods to improve ultrasound image contrast and quality are crucial to its new applications. Microbubbles generated by agitating saline have been used as a contrast agent for ultrasound since the 1960's. These are free bubble and limited to right heart imaging, as they do not survive pulmonary capillary circulation. More stable microbubbles have been commercialized, three of which are currently FDA approved in the U.S. (Albunex®, Optison®, and Definity®). The FDA approved ultrasound image contrast particles previously mentioned, are gas bubbles entrained within soft-shells made of proteins, such as albumin, or lipids. Soft shell ultrasonic contrast particles, specifically proteins, polysaccharides, and lipid-based particles, have not been extended to sizes below 400nm. This is due to the high surface tension of water, which prevents air filled nanobubbles from forming at atmospheric pressure for the time needed for imaging. The polymeric make up of a microbubble greatly influences its properties. For example microbubbles made of phospholipids are considered soft-shell particles and are much more sensitive to pressure changes. Microbubbles made of polycyanoacrylate are hard-shell and thus produce a more robust and stable particle.[1] Furthermore, polymeric microbubbles have been shown in animal studies to be a viable tool for renal imaging by way of

intravenous injection.[2] Ultrasound contrast particles have not been limited to polymeric materials, as many inorganic particles have also been shown to possess promising echogenic properties.[3] Air filled porous silica coated gold, porous silica encapsulated ferrite, and porous borate and aluminate particles, which are considered a hard shell particles have been shown to have favorable ultrasound enhancement capabilities.[3-4] Uncalcined hollow silica-gel particles have been shown to behave as soft-shelled particles that also exhibit ultrasound contrast properties.[5] The only nanoscale bubbles observed to date have been adsorbed on surfaces of single crystal silicon. [6] To our knowledge, there are no rigid or hard shell hollow, inorganic hybrid particles being used as ultrasound contrast agents. Hollow silica shells can be synthesized with a large range of particle sizes down to 100nm diameter. [7] Besides access to smaller uniform sizes and low toxicity,[8] there are other advantages of using nanoporous silica shells to contain a micro- or nanobubble (a) silica facilitates adhesion to tissue and cells thereby making the particles immobile; (b) silica can be doped to modify its strength, (c) nanoporous shells can be chemically modified with fluorophores, (d) the silica surface can also be covalently conjugated to cell receptor targeting agents or to small molecules in order to adjust the surface charge and polarity.

In this report, the first three properties are exploited to demonstrate the potential utility of gas filled silica micro- and nanoshells particles for ultrasound-enhanced imaging. Perfluorcarbon (PFC) vapor filled hollow silica nano- and microshells can be effectively utilized as immobile, rigid ultrasound image

contrast particles (UICP) when injected subcutaneously. The reason that this platform could be advantageous over some commercially available UICPs is the highly adsorptive nature of silica gel. The immobility of the uncoated silica shells in tissue makes this platform amenable to be used as an adjunct or as a possible replacement to needle localization of nonpalpable tumors to mark tumors for surgical removal. For the past fifteen years, surgeons have removed early stage breast cancers by placing a wire in the breast tumor under X-ray or ultrasound guidance to mark the detected abnormality for removal by the surgeon.[9] However, this procedure is associated with a 20-50% rate of positive margins necessitating a second operation. In the past few years, some surgeons have reduced the number of second surgeries needed in breast conservation therapy by injecting radioactive seeds under image guidance in and around the tumor preoperatively to better localize the entire tumor to achieve negative surgical margins.[9-10] The disadvantages of using radioactive seeds include: (a) the half-life of the seed being only a few hours, thereby requiring the seeds to be implanted on the day of surgery, (b) difficulty marking multiple tumor foci or fields of cancer cells, which is common in ductile in-situ carcinoma (DCIS), (c) exposure of the patient and surgeon to ionizing radiation (d) the need for trained radiation personnel, (e) the need for a large bore needle to inject the seed which is painful for the patient, (f) the lack of 3D imaging tools for radioactive seeds in the operating room, and (g) the seeds are expensive to purchase and dispose safely.

The use of ultrasound for the location and removal of tumors has already been shown to be a useful intraoperative technique; however, the limited imaging contrast of tumorsreduces the effectiveness of this method. In this report,the gas filled silica micro and nanoshells injected directly in tissue are shown to persist for several days and can be readily imaged in human breast tissue in three dimensions after injection.

Results and Discussion

Synthesis

Initial attempts to synthesize 2.0 micron (μm) hollow silica particles were done using the same sol gel procedure as the one used to produce hollow silica nanoshells.[11] This procedure utilizes a polystyrene bead as a template that is coated with a polyamine to facilitate the sol gel reaction (shown in Fig. **1**). Once the sol gel reaction is completed, the organic core is calcined to give
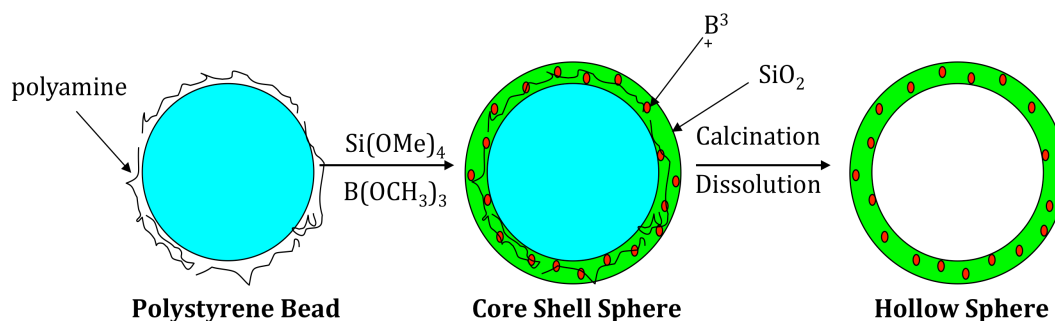
Figure **1** shows a general scheme for the sol-gel synthesis of hollow shells.

a hollow particle.[12] When extended to the microscale, this process yielded

hollow microshells that were very fragile. These particles would fracture and

eventually break completely after 1-2 hr of bath sonication or centrifugation

above 1.7 RFG (Fig. **2**).   In order to prepare a more robust microshell, another

component needed to be incorporated into the silica matrix to strengthen it;
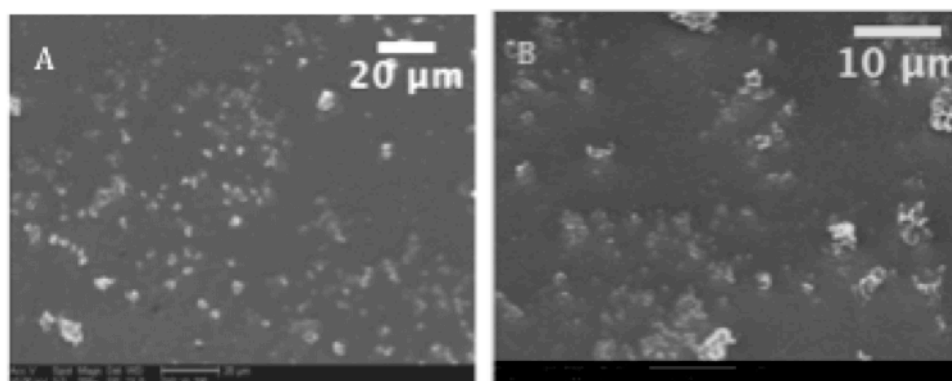
Figure **2** shows two SEM images of material recovered after calcination using the
standard procedure for particle synthesis, without boron doping.   As seen above
A (758x mag.) and **B** (2300x mag.) there are very few well-formed, unbroken
particles produced using the standard procedure.

therefore, boron was doped into the silica matrix during the sol-gel reaction

by addition of trimethoxyboron.   Due to the difference in reactivity of

tetramethylorthosilicate and trimethoxyboron, the former reagent was

allowed to react for 2 hr before addition of trimethoxyboron. This allowed the

slower reacting silane to begin the template formation of the silica microshell,

before allowing the boron to be incorporated into the nascent silica matrix.

The particles were washed with water and ethanol to remove unreacted

starting materials.   The 2 μM polystyrene bead core was subsequently

removed by calcination at 550 °C for 18 hr. This yielded a hollow porous silica gel particle with a relatively uniform wall thickness, approximately 10 nm, and possessing greater structural strength compared to the corresponding hollow silica particles. The boron-doped microshells can withstand 12 hr of bath sonication with little to no visible breakage; although only 10 minutes of sonication is required for complete dispersal of the 2 µM boron-doped silica shells in aqueous solutions.

Figure **3** shows three SEM images are of the boron-doped 2µm shells with increasing magnification (9342x, 9354x, and 18708x). Microshells are well formed and virtually no broken shells are observed.

These sonicated 2 µm silica shells remain dispersed in solution for at least several days, requiring only minor agitation to regain suspension weeks later. Scanning electron microscopy (SEM) showed (Fig. **3**) well-formed monodisperse spheres and the measured zeta potential (ZP) was -39mV (seen below in Fig. **4**). Fig. **3** Three SEM images are of the boron-doped 2µm shells
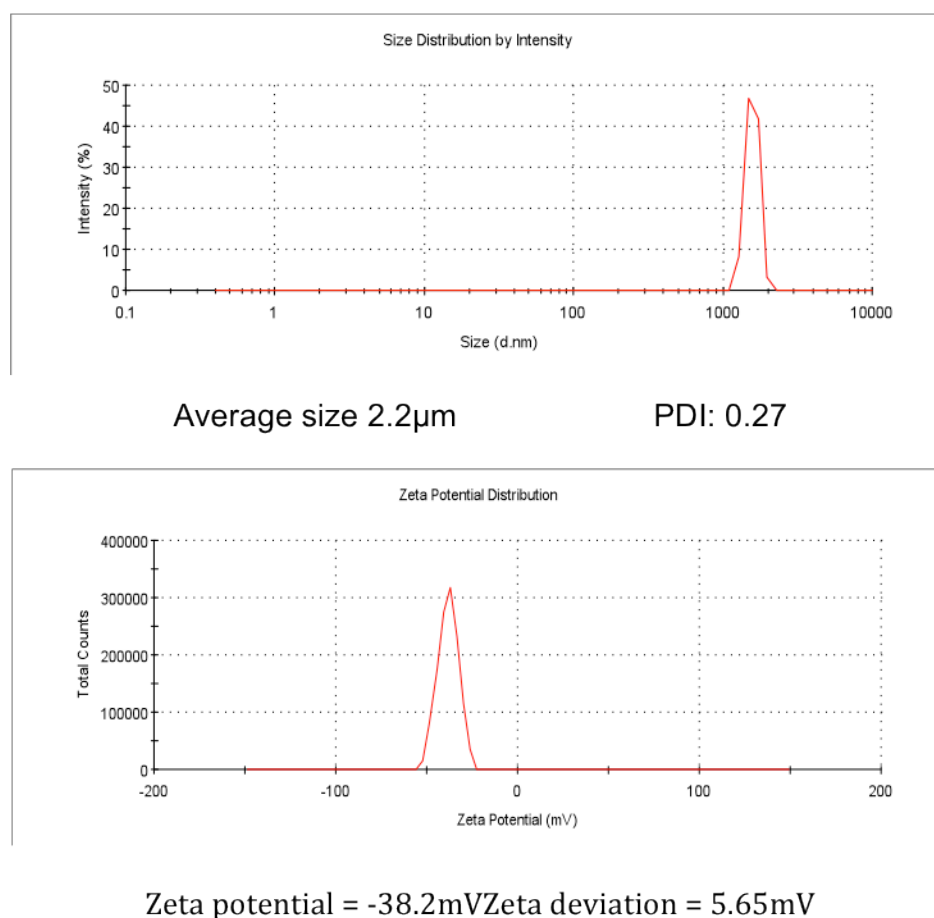
Figure **4** (top) shows the DLS data, the partilcle average size is 2.2μm and (bottom) graph shows the zeta potential recorded -38.2mV.

with increasing magnification (9342x, 9354x, and 18708x). Microshells are well formed and virtually no broken shells are observed. The 200 nm silica shells were synthesized using a similar technique; however, boron doping is not required since the smaller nanoshells are sufficiently robust to withstand ultrasound dispersal. The increased strength of the nanoshells may be attributed to the similar wall thickness found in both the small and large

shells. The 200nm silica shells can withstand 24 hr of bath sonication with little to no visible breakage; however, only 60 minutes of sonication is required for complete dispersal of the 200 nm silica shells, as shown by dynamic light scattering. The sonicated 200 nm silica shells remain dispersed in solution for at least several weeks. Scanning electron microscopy (SEM) showed well formed, monodisperse spheres and a measured zeta potential of −32mV confirmed sufficient surface charge for a stable dispersion. The particles were filled with perfluropentane (PFP) in order to test whether the particles could effectively contain perflurocarbon (PFC) vapors for a significant period of time. PFP was used because of its insolubility in water. The difference in index of refraction between PFP vapor and that of the aqueous surroundings made it an excellent candidate for the gaseous portion of an UICP.   Vapor-filling was accomplished by first evacuating the hollow particles ($\sim$10^{-3}torr) for approximately 30 min. Using a gas syringe, the PFP vapors in the headspace above the liquid PFP were injected into the vessel containing the particles. This was repeated three times, followed by the addition of degassed water to trap the PFP vapors inside the nano and microshells.   The gas filled nano and microshells were sonicated just enough to create a uniform suspension: approximately 30 sec for 2 μm and 200 nm shells. To confirm that the particles contained PFP, the silica shells were visualized using a standard light microscope approximately 1 hr after filling

Solvent Filled   Gas Filled
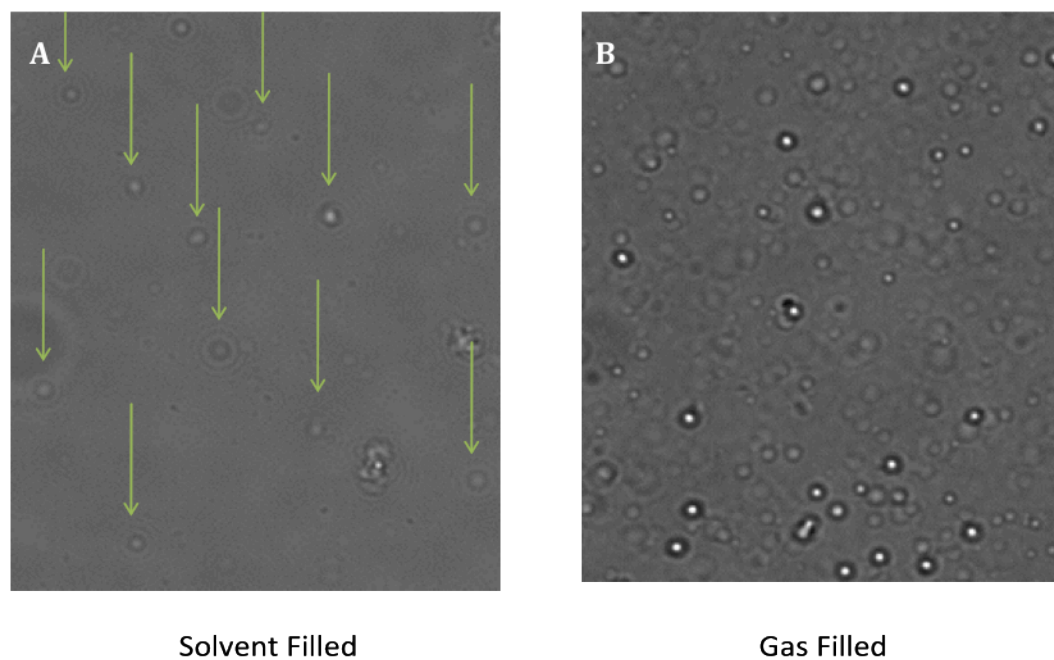
Figure **5** shows light microscope images of 2μM silica shells at 40x magnification. (**A)** Solvent filled microshells are difficult to visualize, while (**B**) PFC vapor filled microshells appear bright in the image

with gas (Fig. **5**). The difference in the indices of refraction between liquid media and gas caused the particles to appear brighter than the background, as seen in the brightfield microscope images. The gas-filled particles are easily identifiable, whereas the solvent filled particles are difficult to locate (seen in Fig. **5**).

Table **1** Particle Summary

	200nm Silica Particles	**2.0mM Silica Particles**
Internal Volume (One particle)	$0.028mm^3$	$28.74\ mm^3$
50 μL Injection		
Number of particles	1.1×10^{10}	3.95×10^8
Mass	100μg	100μg
Area of CDI signal	$23.7mm^2$	$47.1mm^2$
100μL Injection		
Number of particles	2.2×10^{10}	7.9×10^8
Mass	200μg	200μg
Area of CDI signal	$43.4mm^2$	$95.5mm^2$

Ultrasound Imaging

In order to determine if the vapor-filled particles would produce an ultrasound signal, the vapor-filled particles were injected into agar. The mode that was most responsive was color Doppler imaging (CDI). In CDI, color is assigned to pixels when echoes returning from a voxel are non-correlated following the transmission of multiple ultrasound pulses. Gas bubbles can generate a CDI signal either by moving or if the first pulse of a multi-pulse sequence destroys the bubble that has been termed "stimulated acoustic emission."[13] These differences can be measured directly or as a phase shift from which the Doppler frequency is obtained.[14] For 100uL of a 2mg/ml suspension injected into an agar phantom, the CDI signal persisted for 75 min of continuous

imaging. This means in a clinical setting the particle could be imaged multiple times since the ultrasound is only applied periodically. While, conventional ultrasound microbubble imaging agents which use soft shells, such as albumin or lecithin, have only been shown to persist for 15 minutes in tissues.

To determine whether the vapor remained in the 2.0 μm particles or dissolved into fat tissue, the particles were injected into chicken livers and imaged every 24hr. As shown in Fig. **6**, there was a strong signal post injection and after 24 hr. The imaging time used for each observation was approximately 5 min. The relative area of observable signal of the 72 hr study implies a half-life of approximately 24 hr (Fig. **5**). The signal begins to degrade after 48 hr and is barely distinguishable after 72 hr. After 24 hr, there is some degradation of the CDI in both nano and microshells, but this could be due to migration of the injected sample within the excised tissue or the diffusion of PFP from the microbubble core (ultrasound instrument details and parameters are provided in experimental section).

Post-injection   48 Hrs

24 Hrs
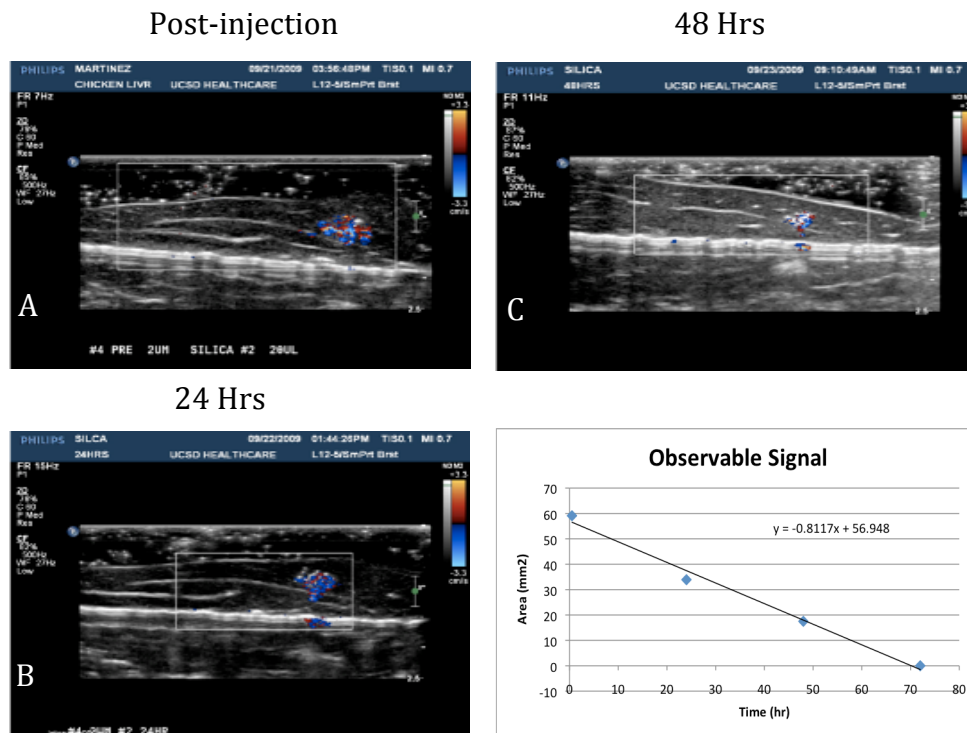
Figure **6** CDI sonograms of 100μg of PFC-filled microshells injected in a tissue phantom imaged at 24hr (A) 24h, (B), 48h, and (C) 72hr. The signal decreases over time, but is still easily visible after 48h.   (D) CDI observable signal vs imaging delay time. A fit of the data shows that the microshells

The weight factor equation (Eq. **1**) allows for estimation of the number of particles for a given mass of silica shells, thereby providing an estimate of the total gas payload for a specific mass of nano or micro shells. The 2μm and 200 nm nanoshells differ in internal volume by 1000x, but as shown in Table 1 they differ in mass by only 100x. Consequently, the microshells have 37 times more gas storage for a similar mass injection. However, the CDI signal observed is only twice as large for the microshells when compared to the nanoshells. A summary

Calculation of Weight factor

$$V = \frac{4}{3}\pi r^3$$

$$V = \frac{4}{3}\pi r_{solid}^3 - V = \frac{4}{3}\pi r_{shell}^3$$

$$\frac{V_{shell}}{V_{soild}} = Weight\,fraction$$

$$WF = \left(\frac{r_{solid}^3 - r_{Shell}^3}{r_{solid}^3}\right)$$

2.0 µM Particles

$$WF = \left(\frac{1\mu M^3 - 0.990\mu M_{Shell}^3}{1\mu M^3}\right) = 0.0297$$

200 nm Particles

$$WF = \left(\frac{100nm^3 - 90\mu M_{Shell}^3}{100nm^3}\right) = 0.297$$

Mass per particles

2.0 µM Particles

$$1.183 \times 10^{8\,Beads}/_{mg} \rightarrow \frac{1}{x} = 8.453 \times 10^{-9\,mg}/_{Beads}$$

$$8.453 \times 10^{-9\,mg}/_{Beads} \times 0.0297 = 2.51 \times 10^{-10\,mg}/_{Beads}$$

200 nm Particles

$$1.19 \times 10^{11\,Beads}/_{mg} \rightarrow \frac{1}{x} = 8.40 \times 10^{-12\,mg}/_{Beads}$$

$$8.40 \times 10^{-12\,mg}/_{Beads} \times 0.297 = 2.49 \times 10^{-12\,mg}/_{Beads}$$

Equation **1** This equation is based on the known weights and number of particles for a given mass of solid silica microparticles, as obtained from Polysciences Inc. The weight factor equation allows for a reasonable mass estimation of a hollow particle. This was done bye the determination of a weight factor expression that estimates the percentage of the mass that the shell accounts for by subtraction of the internal volume using the inner and outer radii from TEM images. This ratio allows for an estimate of the number of particles for a given size and mass.

of injection volumes, number of particles and corresponding masses can be seen in Table **1**. To determine if the particles would perform similarly in human tissue, breast tissue from a prophylactic mastectomy was tested. In order to have a proper histological analysis of the tissue, India ink was also added to the particle suspension to locate and track the injection.

As seen in Fig. **7,** the vapor filled particles can be identified just as well in the breast tissue as in the chicken liver tissue using CDI ultrasound. For the 100uL injection of both the nano- and micro-gasfilled shells there is a clear CDI signal.   Although the nanoshell injection contained 100 times more particles than that of the microshells, the microshells show a CDI observable signal that is 2.3 times larger based on the area of observable signal. This could be a result of

2 uM particles   200 nm particles

100uL injection 7.9 x 10^8 100μL injection ~4.0 x
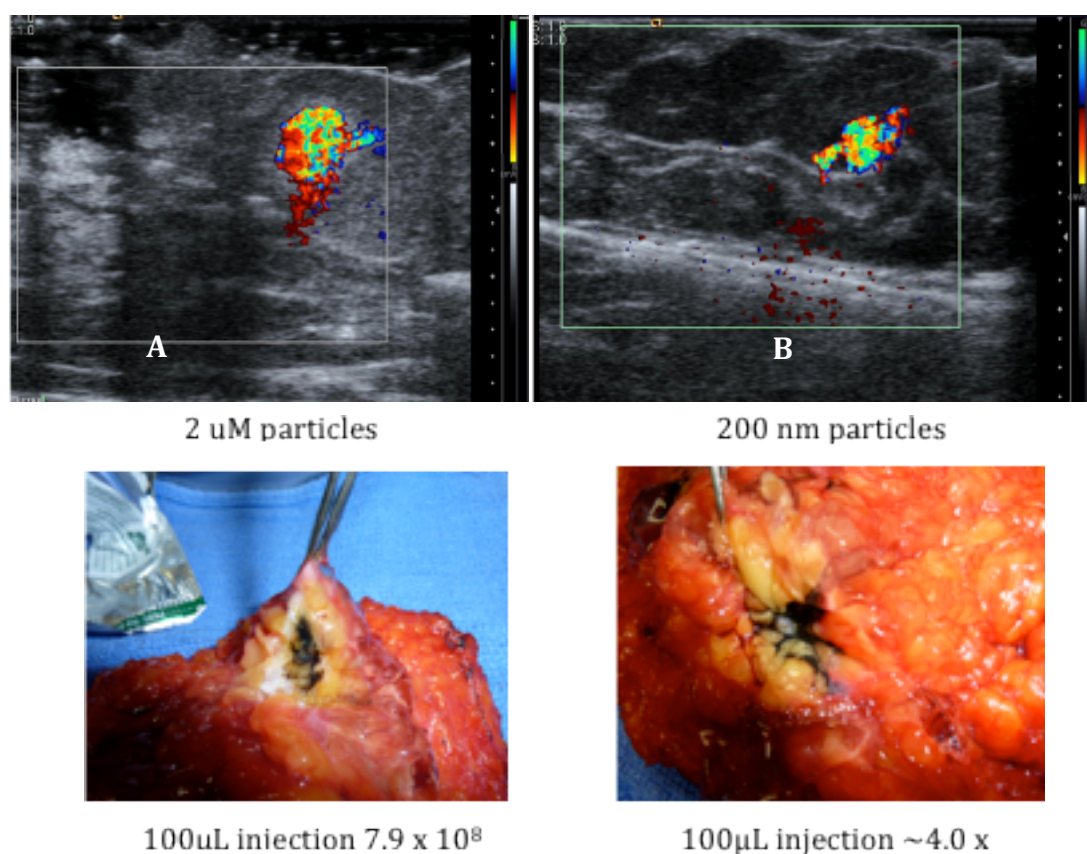
Figure **7** (top) CDI images of 100μL of PFC filled Nano and MicroShells in Human Mastectomy Tissue: (a) After injection of 4 x 10^{10} nanoshells. (b) After injection 8 x 10^8 microshells The nanoshells image (A) is magnified ~2.5x and thus in this comparison appears to be larger. An accurate measure the DCI area can be found in Table 1. (bottom) images of the tissue injected, stained with India ink in order to locate the injection site.

several factors: first, while there are 100 times more nanoshells (for a 100μg injection), each microshell has a gas volume 1000 times greater. For equal mass injections this translates to 37 times greater payload of gas for a 100μg injection of microshells. Second, due to the microshells larger size and payload, it is probable that a more favorable interaction with the sound wave occurs with microshells, thereby producing a larger observable signal. Even on a weight basis, the nanoshells are less efficient contrast agents than the microshells. They are however, more efficient on a volume basis; this is unexpected since bubbles which are smaller than a micron cannot normally exist due to their instability and would be expected to have a weak interaction with ultrasound radiation.
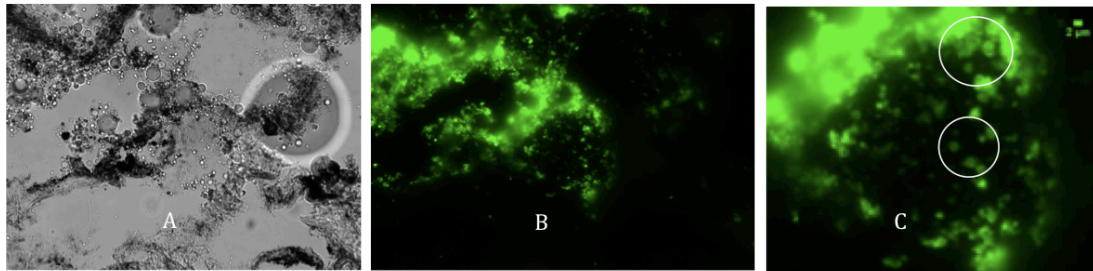
Figure **8** shows optical Imaging of 100μL of Microshells Injected into Mastectomy Tissue, (**A**) Bright field image of embedded breast tissue. Black regions on image are traces of india ink, (40x Mag). **(B)** Green fluorescent image of 2um microshells in embedded breast tissue. **(C)** Zoom in region of green fluorescent image using Image J. White circles identify regions where 2 μm microshells can be observed. Scale upper left is 2 μm.

Fluorescence microscopy was performed on breast tissue in order to determine if the microshells remained at the injection site after ultrasound imaging (Fig. **8**). The injection solution used consisted of PFP gas filled, Alexafluor-488 covalently linked microshells, along with 10μL/ml India ink. The

resulting solution was injected into excised prophylactic mastectomy breast tissue. After the tissue was imaged by ultrasound, a small piece of the breast tissue was resected and placed into a histology cassette for tissue fixation. ‡Images were taken of different areas where India ink was visible under bright field conditions, fluorescent examination confirmed the presence of the microshells at the injection site. The microshells presence provided further evidence that the CDI signal did originate from the PFC 2μm fluorescently labeled microshells. The paraffin embedded tissue block was sliced until India ink was visible and sectioned in 5 micron slices, with two consecutive slices per slide, and spaced at 100 microns before the next slide. Paraffin was removed from slides by soaking for 30 minutes in xylene at room temperature and sealed with Cytoseal prior to visualization. The paraffin embedded tissue slides were analyzed using a Nikon Eclipse E600 upright fluorescent microscope fitted with a 40_ objective (Nikon Plan Apo, 0.95NA) and with a triple band pass filter (DAPI/FITC/Texas Red w/Single-Band Exciters, Chroma Technology Corp). Areas of interest were first identified by the location of India ink with bright field imaging; afterwards, a fluorescent image was captured using a Spot camera. The images were processed for background level and mean fluorescent signals using ImageJ software (National Institutes of Health)

Conclusions

A new hybrid inorganic rigid platform for an ultrasound image contrast particle has been successfully synthesized and tested. Gas filled hollow porous silica microshells possess properties that cannot be duplicated by soft shell counterparts (a) synthesis of a wide range of specific sizes, (b) covalent functionalization of the shell surface, (c) long term suspension in solution, (d) adhesion to cells and tissue, and (e) long imaging lifetime in tissue. The PFP vapor filled micro- and nanoshells are a promising complement to the other ultrasound contrast agents currently being used. They also represent a promising replacement to the radioactive seeds currently employed to improve breast tumor localization for several reasons: (a) they have a longer lifetime than that of the several minute lifetime of commercially available UICPs, (b) several foci can be marked using very fine gauge needles, (c) they can be imaged in 3D, and (d) no specialized radiation safety is required. There is little risk to the patient due to the small injected dose needed, known nominal cellular toxicity of silica, and their removal during surgery. The ability to make bubbles that can be imaged in the nanometer size regime also raises the possibility of new applications, such as imaging microcapilliaries in tumors and sentinel lymph nodes near tumors.

Experimental

Materials: Tetramethoxysilane and 0.1% wt poly-L-lysine solution were obtained from Aldrich-Sigma Ltd. All chemicals were used as received. Polystyrene beads were purchased from Polyscience Ltd. Fluorophore were purchased functionalized from Invitrogen Ltd.

Preparation of hollow silica nanospheres: To a 15ml plastic corning conical vial 10ml of phosphate buffer solution, 2ml of poly-L-lysine, and 500μL of 200nm polystyrene microspheres were added. This mixture was mixed using a vortex mixer for 10 min. To this 250μL of silicic acid was added and mixed for 15 min. At this time the reaction mixture was pelleted down using a centrifuge. The liquid was removed and the pellet was 2x with 5ml of H_2O and 1x with absolute ethanol. The coreshells were dried overnight to yield a white powder. The coreshells were now put into a muffle furnace to be calcined at 550°C using an 18 Hr gradient ramp. This yielded a white powder. Average zeta potential measurement was -35mV. Sizing from dynamic light scattering after 2hr of bath sonication was 260nm with a poly dispersity index of 0.29. The SEM measurements were conducted on a FEI/Philips XL30 FEG ESEM microscope with an accelerating voltage of 10 kV.

Preparation of hollow silica microspheres: To a 2 ml plastic conical vial 1ml of phosphate buffer solution, 130μL of poly-L-lysine, and 50μL of 2.0μm polystyrene microspheres were added. This mixture was mixed using a vortex mixer for 10 min. To this 3.1μL of tetramethylorthosilicate was added and mixed for 2.5 hrs. After 2.3

hrs of mixing 50μL of 5% trimethoxyborate solution was added and the mixture was let to mix for 4.5 hrs. At this time the reaction mixture was pelleted down using a centrifuge. The liquid was removed and the pellet was 1x with 1ml of H_2O and 2x with absolute ethanol. The coreshells were dried overnight to yield a white powder. The coreshells were now put into a muffle furnace to be calcined at 550°C using an 18 Hr gradient ramp. This yielded a white powder. Average zeta potential measurement was -35mV. Sizing from dynamic light scattering after 1hr of bath sonication was 2.1μm with a poly dispersity index of 0.23. The SEM measurements were conducted on a FEI/Philips XL30 FEG ESEM microscope with an accelerating voltage of 10 kV.

Preparation of 5% trimethoxy borate solution: To a 2 ml plastic conical vial 1ml of absolute ethanol, to this 2.5μL of trimethoxy borate was added. This was let to mix for 5 minutes and only prepared as needed for reactions, and never stored.

Characterization: The samples were prepared as KBr pellets. The SEM measurements were conducted on a FEI/Philips XL30 FEG ESEM microscope with an accelerating voltage of 10 kV. The average diameter of the nanospheres was determined by SEM images. The TEM image was JEO-2000EX (200kV) CryoElectro Microscope with an accelerating voltage of 200 kV. Zeta potentials and size distributions by DLS were measured using a Malvern Zetasizer Nano series instrument. Zeta potentials were measured using a Malvern disposable zeta potential cuvette with ethanol as a dispersant. DLS sizing was done using Malvern disposable sizing cuvettes and phosphate buffered saline solutions

(PBS). Samples were sonicated in their respective solvents for 30 mins prior to measurements.

Much of the material in this chapter comes directly from a manuscript entitled "Hard shell gas-filled contrast enhancement particles for colour Doppler ultrasound imaging of tumors," by Martinez, H.P.; Kono,Y.;Blair,S.L.; Sandoval,S.; Wang-Rodriguez,J.; Mattrey, R.F.; Kummel, A.C.; and Trogler, W.C. *Med. Chem. Commun.*, **2010**, 1, 266–270. *Reproduced by permission of The Royal Society of Chemistry*

References

1.   Kiessling, F.; Huppert, J.; Palmowski, M., Functional and molecular ultrasound imaging: concepts and contrast agents. *Curr. Med. Chem.* **2009,** *16* (5), 627-642.

2.   Zhanwen, X.; et al., The fabrication of novel nanobubble ultrasound contrast agent for potential tumor imaging. *Nanotechnology* **2010,** *21* (14), 145607.

3.   (a) Glajch, J. L.; Carpenter, A. P., Jr.; Cheesman, E. H. Porous inorganic targeted ultrasound contrast agents. 2001; (b) Glajch, J. L.; Loomis, G. L.; Mahler, W. Porous inorganic ultrasound contrast agents. 1992.

4.   (a) Chen, Y.-S.; Kruizinga, P.; Joshi, P. P.; Kim, S.; Homan, K.; Sokolov, K.; Frey, W.; Emelianov, S.; Oraevsky, A. A.; Wang, L. V., On stability of molecular therapeutic agents for noninvasive photoacoustic and ultrasound image-guided photothermal therapy. *Proc. SPIE* **2010,** *7564* (Photons Plus Ultrasound: Imaging and Sensing 2010), 75641Q/1-75641Q/8; (b) Zhang, M.; Kitamoto, Y.; Abe, M., Ferrite-capsulated porous silica microspheres for ultrasonic contrast agents. *J. Phys. IV* **1997,** *7* (C1, 7th International Conference on Ferrites, 1996), C1/669-C1/670.

5.   Lin, P.-L.; Eckersley, R. J.; Hall, E. A. H., Ultrabubble: A Laminated Ultrasound Contrast Agent with Narrow Size Range. *Advanced Materials* **2009,** *21* (38-39), 3949-3952.

6.   Main, M. L.; Goldman, J. H.; Grayburn, P. A., Thinking Outside the "Box" The Ultrasound Contrast Controversy. *J Am Coll Cardiol* **2007,** *50* (25), 2434-2437.

7.   (a) Kirkhorn, J., . Frinking,Peter J.A., de Jon,Nico and Torp,Hans In *1999 IEEE Ultrasonics Symposium Proceedings*, Ultrasonics Symposium, 1999. Proceedings. 1999 IEEE, 1999; 1999; pp 0_2-0_22; (b) Nico de Jong, A. B., and Peter Frinking, Basic Acoustic Properties of Microbubbles. *Echocardiography 2013 Jnl Cardiovascular Ultrasound & Allied Techniques* **2002,** *19* (3), 229-240.

8.   Brunner, T. J.; Wick, P.; Manser, P.; Spohn, P.; Grass, R. N.; Limbach, L. K.; Bruinink, A.; Stark, W. J., In Vitro Cytotoxicity of Oxide Nanoparticles:‚Äâ Comparison to Asbestos, Silica, and the Effect of Particle Solubility‚Ä†. *Environmental Science & Technology* **2006,** *40* (14), 4374-4381.

9.   (a) Cox, C.; Furman, B.; Stowell, N.; Ebert, M.; Clark, J.; Dupont, E.; Shons, A.; Berman, C.; Beauchamp, J.; Gardner, M.; Hersch, M.; Venugopal, P.; Szabunio, M.; Cressman, J.; Diaz, N.; Vrcel, V.; Fairclough, R., Radioactive Seed Localization Breast Biopsy and Lumpectomy: Can Specimen Radiographs Be Eliminated? *Annals of Surgical Oncology* **2003,** *10* (9), 1039-1047; (b) Richard, J. G.; Barbara, A. P.; Patricia, J. K.; Michael, C. R., Radioactive seed localization of nonpalpable breast lesions is better than wire localization. *American journal of surgery* **2004,** *188* (4), 377-380.

10.   (a) Blair, S. L.; Thompson, K.; Rococco, J.; Malcarne, V.; Beitsch, P. D.; Ollila, D. W., Attaining Negative Margins in Breast-Conservation Operations: Is There a Consensus among Breast Surgeons? *Journal of the American College of Surgeons* **2009,** *209* (5), 608-613; (b) Gray, R.; Salud, C.; Nguyen, K.; Dauway, E.; Friedland, J.; Berman, C.; Peltz, E.; Whitehead, G.; Cox, C., Randomized Prospective Evaluation of a Novel Technique for Biopsy or Lumpectomy of Nonpalpable Breast Lesions: Radioactive Seed Versus Wire Localization. *Annals of Surgical Oncology* **2001,** *8* (9), 711-715.

11.   Yang, J.; Lind, J. U.; Trogler, W. C., Synthesis of hollow silica and titania nanospheres. *Chemistry of Materials* **2008,** *20* (9), 2875-2877.

12.   (a) Ding, X.; Yu, K.; Jiang, Y.; Hari, B.; Zhang, H.; Wang, Z., A novel approach to the synthesis of hollow silica nanoparticles. *Materials Letters* **2004,** *58* (27-28), 3618-3621; (b) Wu, W.; Caruntu, D.; Martin, A.; Yu, M. H.; O'Connor, C. J.; Zhou, W. L.; Chen, J. F., Synthesis of magnetic hollow silica using polystyrene bead as a template. *Journal of Magnetism and Magnetic Materials* **2007,** *311* (2), 578-582.

13.   (a) Blomley, M. J. K.; Albrecht, T.; Cosgrove, D. O.; Patel, N.; Jayaram, V.; Butler-Barnes, J.; Eckersley, R. J.; Bauer, A.; Schlief, R., Improved Imaging of Liver Metastases with Stimulated Acoustic Emission in the Late Phase of Enhancement with the US Contrast Agent SH U 508A: Early Experience. *Radiology* **1999,** *210* (2), 409-416; (b) Hadinoto, K.; Cheow, W. S., Hollow spherical nanoparticulate aggregates as potential ultrasound contrast agent: shell thickness characterization. *Drug Dev. Ind. Pharm.* **2009,** *35* (10), 1167-1179; (c) Tiemann, K.; Becker, H.; Bimmel, D.; Schlief, R.; Nanda, N. C., Stimulated Acoustic Emission: Nonbackscatter Contrast Effect of Microbubbles Seen with Harmonic Power Doppler Imaging. *Echocardiography* **1997,** *14* (1), 65-69.

14.   (a) Schwartz, R. L. P. a. R. A., *Practical Doppler ultrasound for the clinician*. Urban & Schwarzenberg: Baltimore 1991; (b) Woodcock, P. A. a. J. P., *Doppler ultrasound and its use in clinical measurement*. Academic Press: New York, 1982.

Chapter 7

A Mechanistic Study of Ultrasound Contrast Particles for Color Doppler
Ultrasound Imaging

Introduction

The importance of the determination of a mechanism of the imaging ultrasound contrast agent allows insight into the acoustical properties of the material.[1] This determination is extremely important for many reasons. An intimate understanding of the mechanism of contrast allows for the system, material, stimulation frequency or pulse sequence to be optimized for specific tasks. For example, if longevity were a necessary property then a robust material would be desired, but since this material is ultimately being used within a living organism, there are other considerations. An extremely robust material may never clear the host and present a problem with bioaccumulation.[2] Furthermore, if the dominant mechanism is cavitation, which destroys the particle, then concern must be paid to the size and composition of the fragments left behind. If the fragments are still relatively large, they could present a problem if they enter the vasculature system. A material that is not easily cleared could present problems for the kidneys or liver. All of these considerations must be taken into account when designing and developing a new ultrasound contrast agent.

There are many ways to study the mechanical properties of an acoustic material. One method is to use a custom aqua-acoustic isolation apparatus where single pulses can be generated and the interaction of single particles or a single flow of particles can be studied. This technique can yield large amounts of acoustical response data, but the majority of these systems are custom built for

specific questions to probe (an example can be see in Fig. **1**. The drawbacks are that particles must be large enough to be view by the optics, must be stable, and
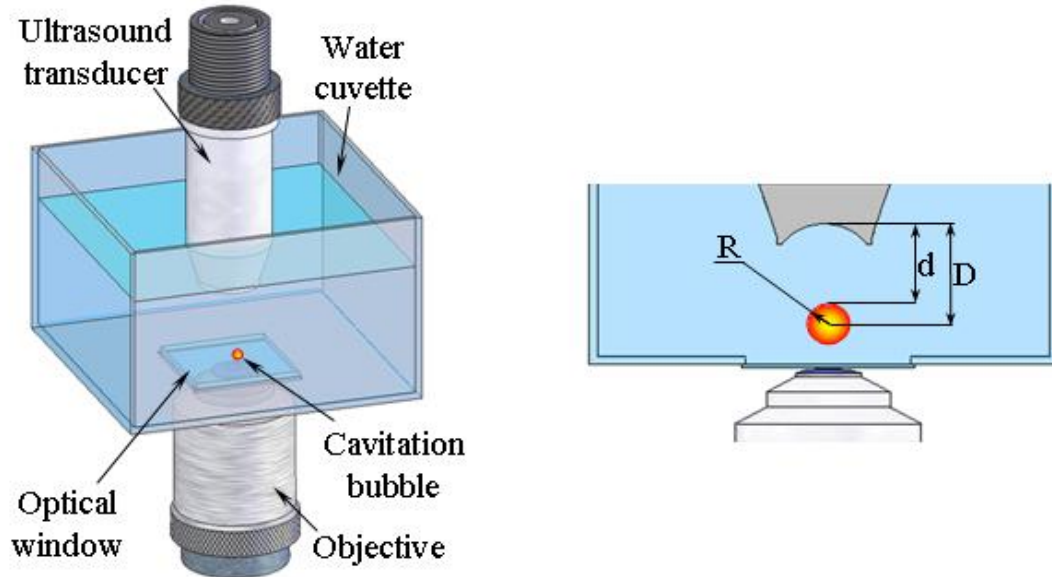

Figure **1** shows a custom optical aqua apparatus designed to study cavitation of microbubbles.[3]

must be immune to aggregation to optimize single particle analysis. In addition, it can be difficult to draw comparisons to a diagnostic medical imaging device. The reason that direct comparisons are not always relevant is that aqua-acoustic isolation systems are setup to produce 1-10 pulses per minute where medical imaging devices typically produce thousands of pulses per minute. This difference in the number of pluses that a material is subjected to can have enormous implications on the longevity and the mechanistic properties for events such as cavitation or deformation.

Using the instrument that the material is meant to be imaged with is not without its challenges. The majority of medical diagnostic imaging ultrasounds are designed for use by sonographers and radiologists whose primary purpose is the patients' diagnostic exam. Because of this it is difficult to gain access to the raw, unprocessed data. Furthermore, imaging in gel phantoms work very well to mimic tissue, but unless a liquid is used as the phantom it can be arduous to recover the imaged particle without damage during the isolation process.

For our studies, we have tried a number of techniques to gain a better understanding of the physical events that allow a rigid particle such as the boron doped silica micro or nanoshell to function as an ultrasound contrast agent. For soft shell contrast particles, such as the commercially available Definity®, the source of the contrast comes from the ability of the decaflurobutane filled liposome to oscillate, compress, expand, and cavitate. All these physical deformations produced by interaction with an ultrasound wave translate to an echogenic signal. Conversely, the rigidity and robustness needed to increase the lifetime of the ultrasound contrast agent also eliminates many of these physical deformations caused by the sound wave.[4] Because the boron doped silica particles are composed of a rigid and durable shells we have concluded that there are three probable mechanisms, that would allow the sound wave to interact with the gas filled particles: (1) The sound wave simply uses the path of least
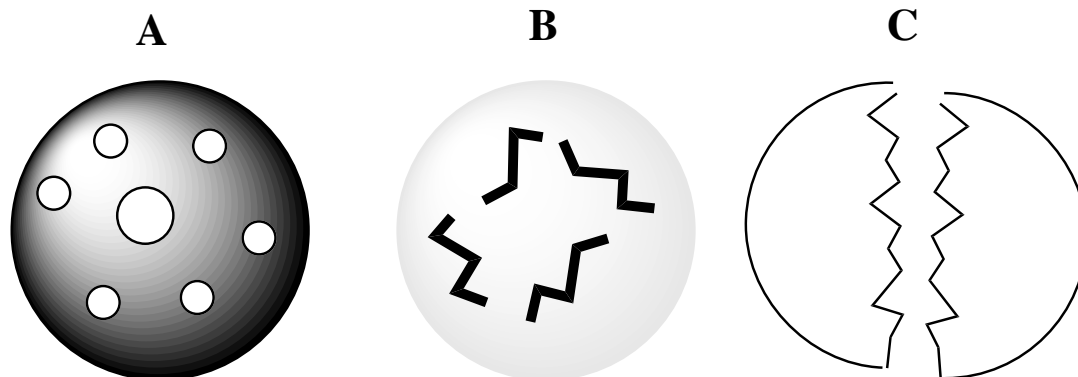
Figure **2** (A) shows the intact state of a particle as described in scenario 1. (B) Shows the cracks created by a sound wave described in scenario 2. (C) Shows a destroyed particle, a result of its interaction with a sound wave as described in scenario 3.

resistance and forces the perflurocarbon gas out of the porous particle. For this to occur the sound wave would have to force out the perflurocarbon vapor through the shell nanopores, to create some sort of free-formed exterior gas bubble. (2) The sound wave can cause micro fractures in the walls of the particles.   It is conceivable that with enough large crevices that the perflurocarbon gas could then be forced out. (3) The sound wave could cause enough pressure to fracture the structure into multiple fragments. One would have to assume that a resonant frequency to cause massive cavitations would be possible at specific frequencies. In all likelihood all three of these events are taking place, but one should be dominant. This study will focus on gaining a better understanding of the mechanism by which a color Doppler signal is

generated. This will be done in a variety of ways, first to examine the relationship of the size of the particle compared to the signal. Second, the stimulation frequency will be varied to see how the output signal is affected. Third, gas filled particles will be imaged until they are no longer produce a color Doppler image followed by directly examining their physical state. Lastly, pulse wave ultrasound, a technique that allows the area imaged to be focused to a very small area where the sound, time, intensity and the number of events taking place can be qualitatively recorded.

Results and Discussion

First, in order to determine the extent of the effect of the size of the particle, several size nanoshells were prepared, filled with dodecafluropentane (PFC) vapor and their color Doppler intensities measured in two different phantoms. The phantoms chosen were beefsteak and chicken livers. These phantoms have direct comparisons to human tissue, and offer a baseline for the performance the particles in tissue with varying amounts of fats. The 200nm and 500 nm particles were prepared according to the literature procedure described by Yang et al.[5] The larger particles, 1, 2, and 3 microns were prepared utilizing the new boron doping technique described in the previous chapter. The boron is required for the larger particles stability since undoped particles lack the strength to support the structure. The addition of boron gives the particles the
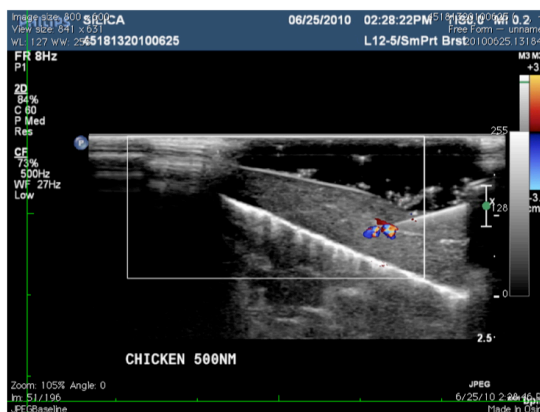
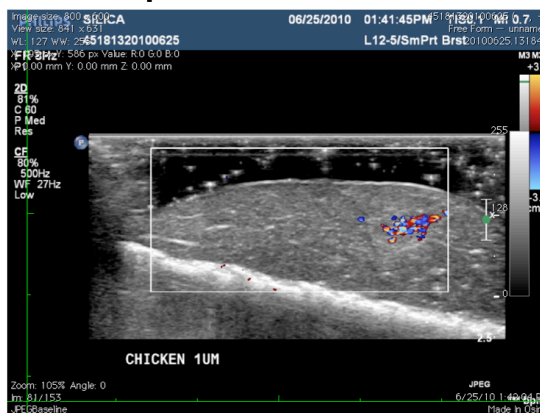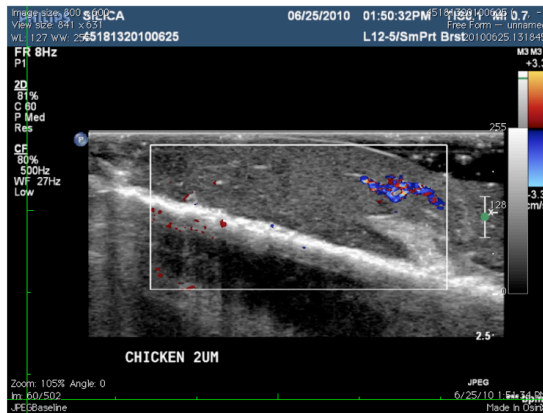## 200 nm Chicken
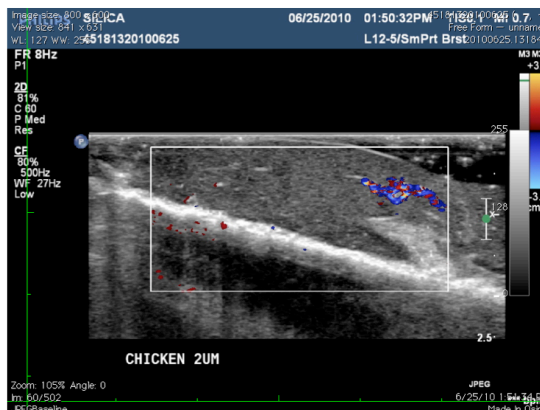
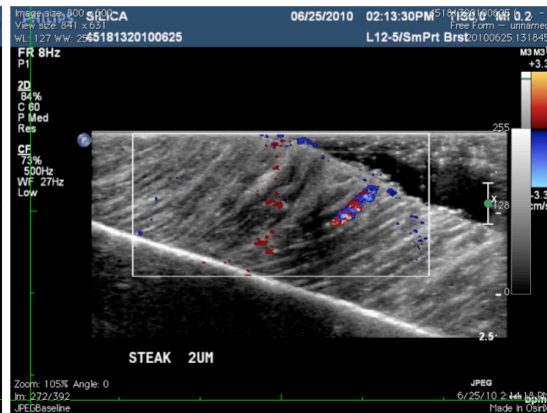## 200 nm Steak
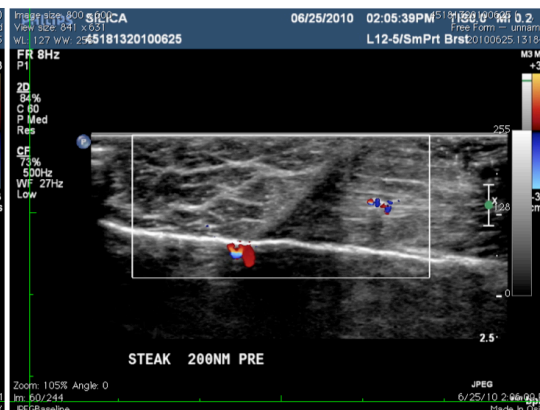
500 nm Chicken

500 nm Steak

1µm Chicken

1µm Steak

Figure **3** has five two-pane images corresponding to 200nm, 500nm, 1µm, 2µm, and 3µm particles injected into a chicken liver and steak phantom.

2μm Chicken

2μm Steak

3μm Chicken
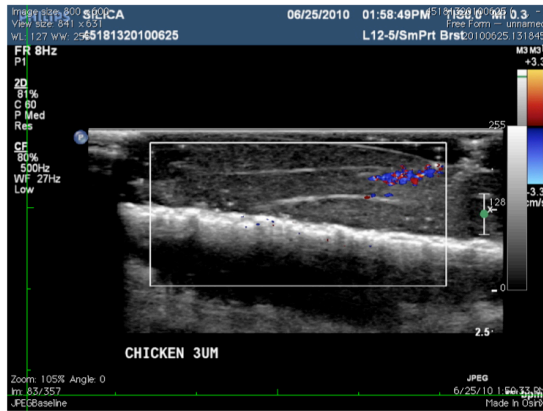
3μm Steak
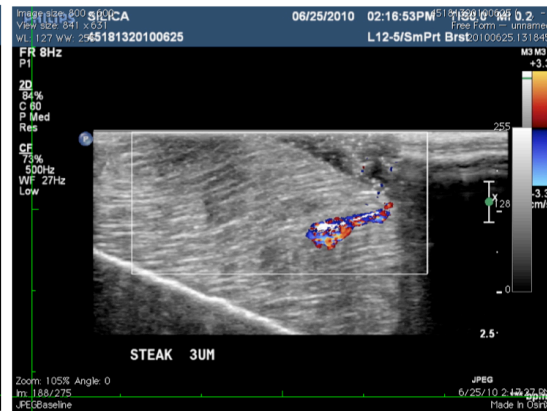
Figure **3** continued.

necessary mixture of rigidity and elasticity to with stand the workup and calcination procedures.

As seen in Fig. **3** the area of the color Doppler signal increases as the diameter of the particle increases. This is to be expected since the larger the particle the larger the cross section that will interact with the sound wave. The larger the diameter the larger the payload of perflurocarbon gas, for example the

2µm particle has an internal volume of 28.74µm^3 while the 200m particle has an internal volume of 0.028µm^3, this is a factor of a 1000 difference. When the number of particles is taken into account for a 50µl injection of a 2mg/ml suspension the 2µm shells still have a 37x greater internal payload. This signal seen is clearly not 37x greater, so there must be other factors besides the size of the particle that affect the color Doppler signal intensity.[6]

Since it was apparent that the size of the particle did have an affect on the amount of color Doppler signal recorded. It is probable that holding the frequency constant and varying the size of the particle slowly shifts away from the resonant frequency, thus causing a decrease in echogenic signal returned. In order to study this behavior, perflurocarbon gas filled 2µm particles were injected into a chicken phantom and the frequency was shifted from 7 to 14MHz in increments of approximately 2MHz. The increments were not exactly 2MHz because the instrument had preprogrammed allowable frequencies. The color Doppler images shown in Fig. **3** were collected after cycling to higher frequencies and back to lower frequencies before recording the images.
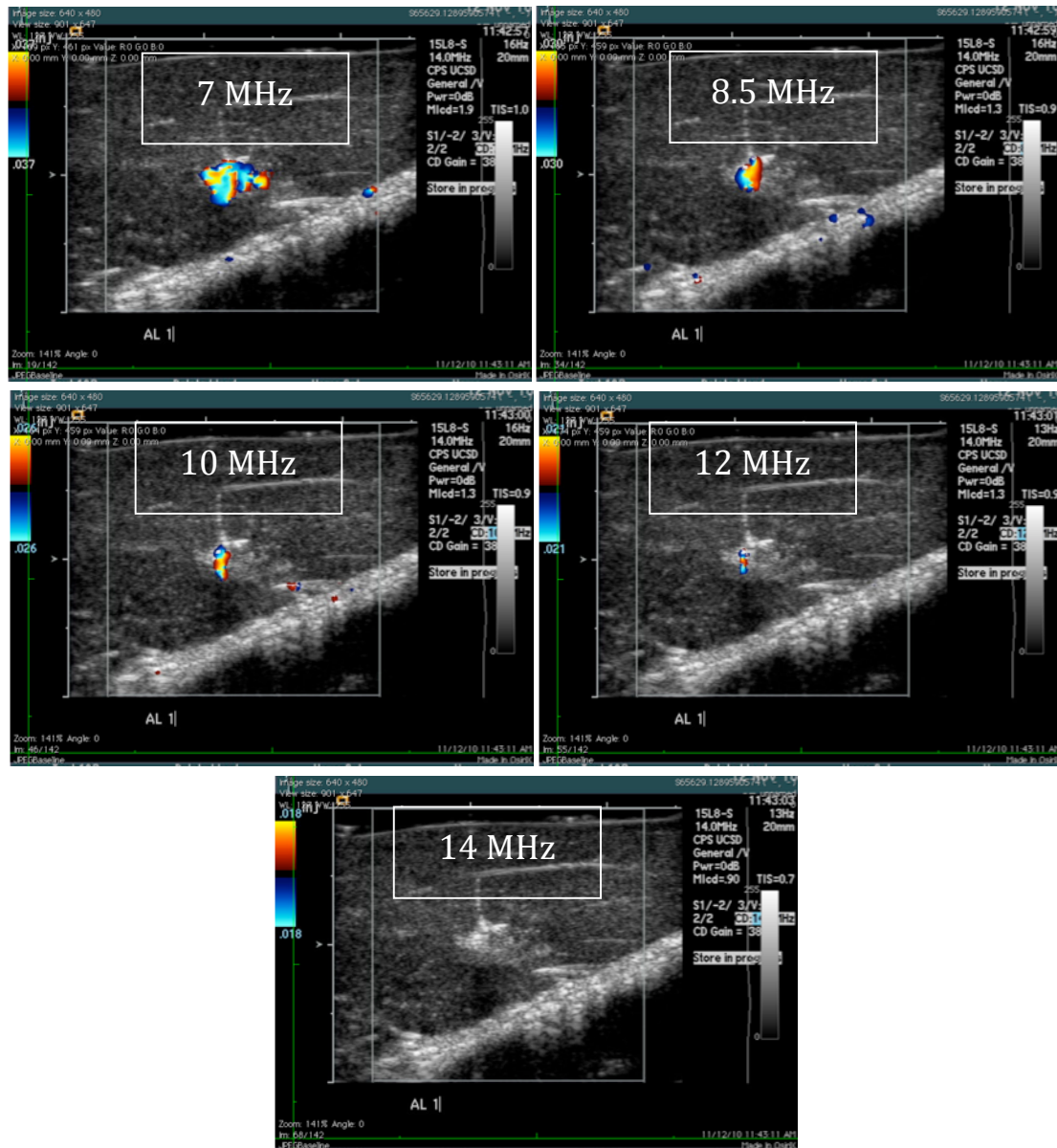
Figure **4** is color Doppler images taken at various frequencies for 50 µl injections of PFC filled 2µm particles.

As seen in Fig. **4** the largest signal seen is at 7MHz and as the frequency is increase the signal decreases completely in the image take at 14 MHz. in order to see if there were any specific trends the areas of each image were measure and
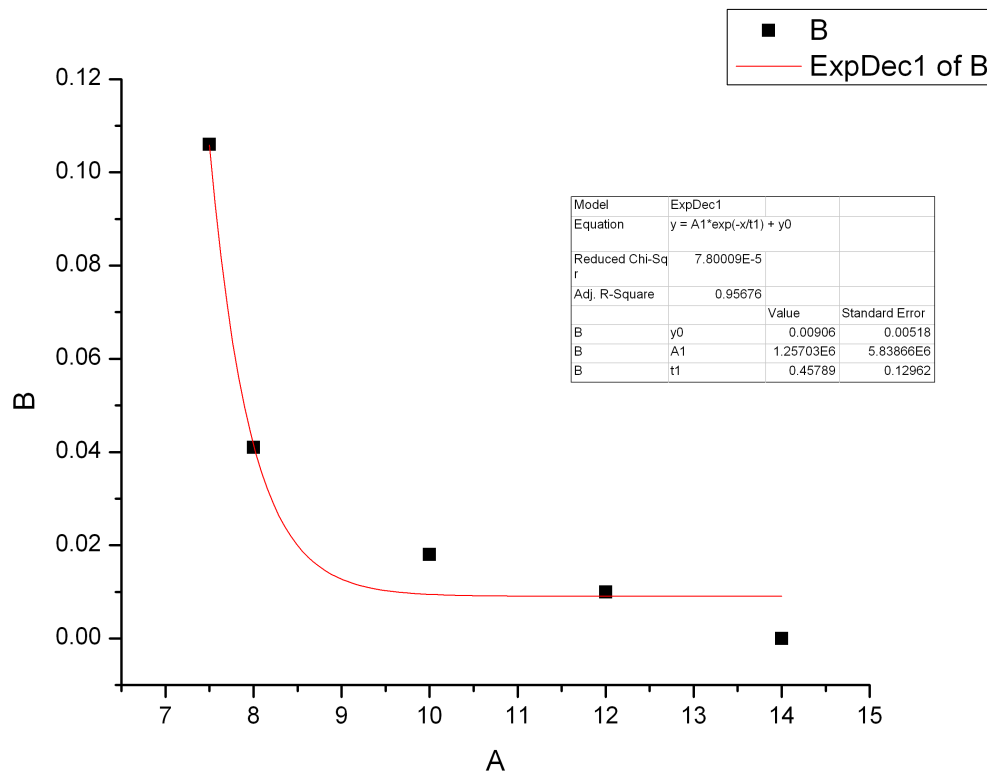
Figure **5** is a graph of the areas of the images seen in Fig. **4** plotted versus the frequency that they were collected at and fit to an exponential curve.

plotted versus the frequency this plot is shown below in Fig. **5**. It would appear

that the frequency response decreases at an exponential rate, but these results

are counter intuitive. In ultrasound imaging, the higher the frequency the greater

is the resolution obtained.[7] There are several possible explanations for this data,

first it is possible that by moving to a highly resolved frequency that particles are

no longer in a active spectral window of the ultrasound. This seems unlikely

since the higher resolution is a product of higher frequency sound waves, which

have smaller wavelength and thus are being capable of reflecting or scattering

more efficiently from smaller structures. Higher frequency sound waves also

have a larger attenuation and are more readily absorbed in tissue. Another possibility is that as the frequency is increased we are slowly moving away from the optimal, available resonant frequency. This explanation seems a little more plausible, since as stated above a higher frequency sound wave equates to a shorter wavelength which may no longer have the ability to resonate the particle in a manner to generate enough pressure to cause fracturing and or cavitations needed to an echogenic signal.

In a more qualitative study, the perflurocarbon gas filled 2µm particles were imaged in two different phantoms, ultrasound gel and normal saline until there was no longer a detectable signal. Ultrasound gel is composed of polypropylene glycol and water. It a similar density to water and allows for a more immobile matrix. Normal saline is sterile solution of water with 0.9% NaCl and its density is approximately equal to that of water, which is very close to the density of tissue. Both phantoms have positive and negative attributes. The ultrasound gel could be considered more similar to a tissue, since it has roughly the same density. Although it is not fibrous like tissue it does have good retention properties, so injected solutions stay immobile for some time. A problem with the ultrasound gel is that samples injected into the gel can be extremely difficult to recover. This is due to the gel make-up being quite durable. The regent that gave the best results for breaking up the gel to free the imaged particles was sodium dodecasulfate. The detergent breaks up the gel, allowing it to be solublized and the particles were recovered with minimal residue left

behind. The problem with this that the process is time consuming and the recovery yields is small, 1-5% of the injection mass used. The use of aqueous solutions as phantoms works very well for particle recovery, but since the particles are free to move throughout the solution their motion can absorb some of the sound wave's energy. This is evident when comparing the longevity or lifetime for the same particle in the two phantom mediums, the signal lifetime is 75-85 minutes in a aqueous solution, but only 45-55 minutes in ultrasound gel at the highest mechanical index (MI). The mechanical index is defined as the peak rarefractional pressure (negative pressure) divided by the square root of the ultrasound frequency.[8] Shown below, in Fig. **6** are images taken using scattering electron microscopy (SEM). 50μl of a 2mg/ml suspension of perflurocarbon gas filled particles, which were injected into 5cc of saline and approximately 500cc of ultrasound gel. Although the gel's volume was 100x larger, only 10cc of gel was removed to extract the particles.
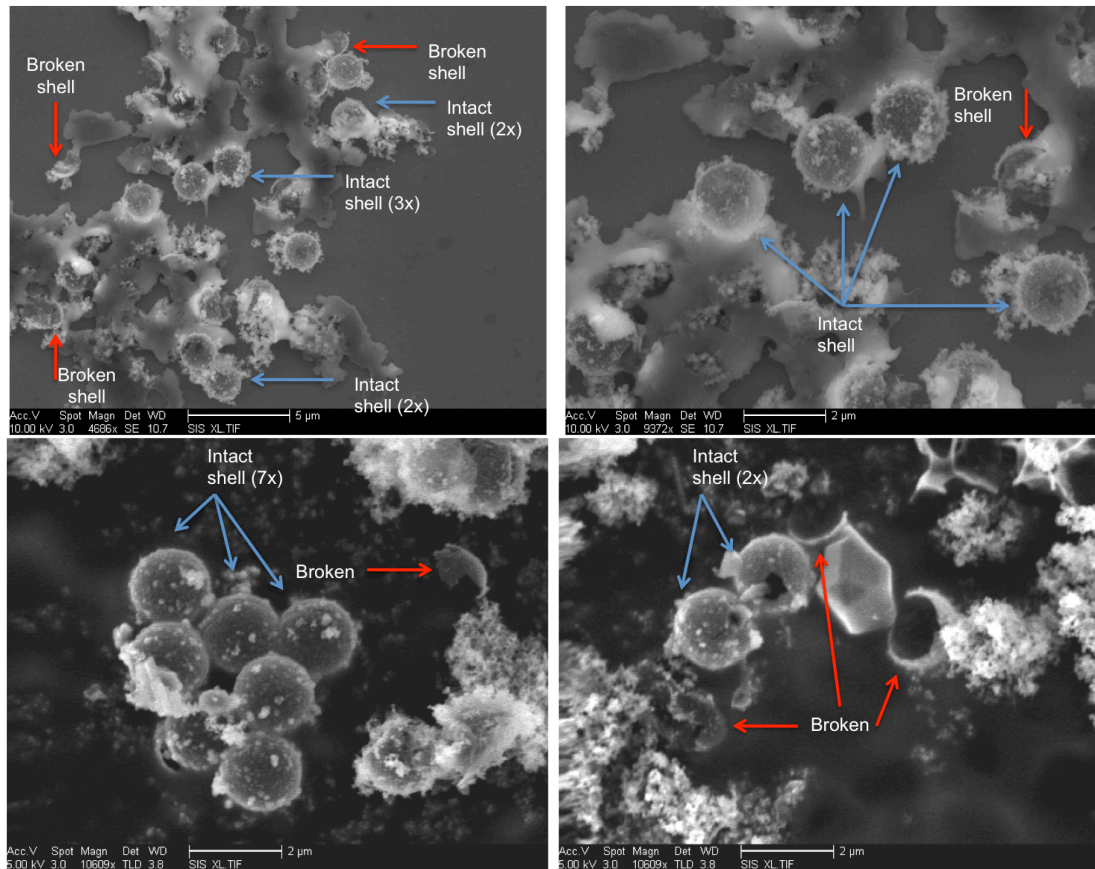
Figure **6** (top panel) shows a sample of the particles recovered after imaging in a saline phantom. Bottom panel show a sample of particles recovered after imaging in an ultrasound gel phantom.

The images in Fig. **6** are just a small portion of the total sample, but the trend throughout all of the areas view was approximately 25% of the shells were broken or fractured as observed at resolution of the SEM. Allowing for an error of 10%, this still would indicate that more than 70% of the particles remained intact, after a complete imaging sequence where the particles were imaged until distinguishable signal was no longer visible. The results are consistent between the two different phantom mediums. The one difference to note was that the

particles in the aqueous medium persisted nearly twice as long, but this is due to

the particle being able to dissipate the energy impacted in them through motion

with in the saline solution.

The last technique used to investigate the mechanism of imaging the

boron doped silica microparticles is pulse wave (PW) Doppler ultrasound. In

pulse wave Doppler ultrasound the system sends a signal that alternates between

transmission and reception. This allows the Doppler shift data for selectively
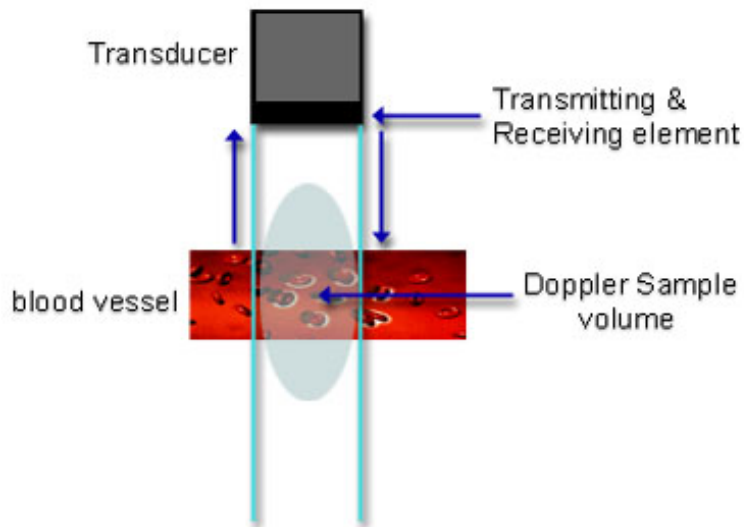
Figure **7** shows an example of a pulse wave Doppler ultrasound system in this
instance being used to scan the sample volume of a blood vessel.[7a, 8a, b, 8d, 9]

smaller areas or segments along the ultrasound wave, referred to as the "sample

volume" or cursor area to be recorded. The user can set the cursor size and

location easily. The main advantage of pulse wave technique is it's enhance

sensitivity; this is due to a continuous, pulsed high frequency wave which is more

gentle on the imaged area.
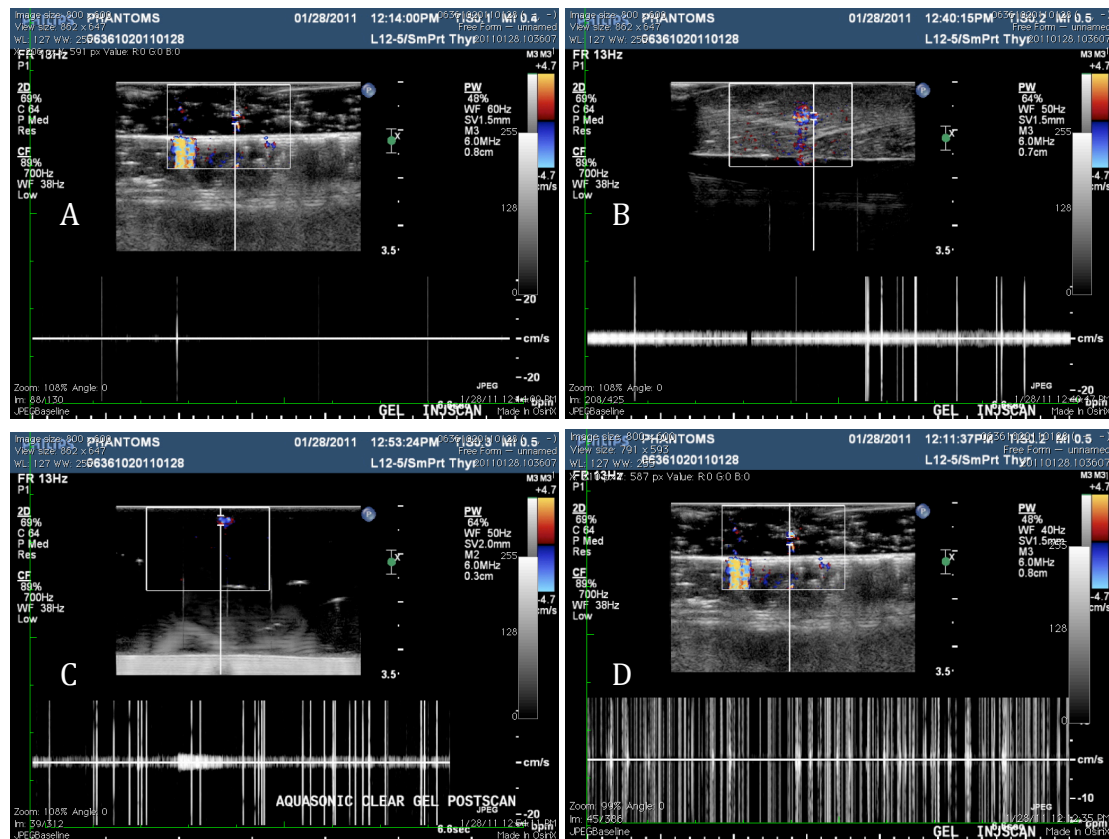
Figure **8** shows four pulse wave (PW) Doppler ultrasound sonograms. The color image above is the color Doppler image; the graph below is the pulse wave data collected for the selected sample volume.

Fig. **8** shows four pulse wave (PW) Doppler sonograms take in different location throughout the same sample. The top portion of the image is the color Doppler image that is taken in a color flow mode. The cursor is the vertical lines intersecting the sonogram; the size can be widened to study a larger area if needed. In Fig. **8A** the cursor is over an area where the color signal is very weak and show in the pulse wave section there are only two sharp peaks with a velocity of approximately 20cm/s. Moving from **8B**, to **8C**, and lastly **8D** the

number of peaks present in the pulse wave section increases. This occurs for two reason, first the cursor or region of interest was moved each time to an area where the color Doppler signal was stronger or a great local population of ultrasound contrast particles and second, is the in the last sonogram the cursor was made smaller to study a smaller sample volume. A trend throughout all of the pulse wave data is the intensity and interval of the signals or events taking place. This would indicate that whatever physical events taking place that allow the particles to produce a color Doppler ultrasound signal are an events that are the norm and not anomalies. The width of the peaks indicates the timescale of the event and its height corresponds to the strength or intensity. A sharp peak would be indicative of a rapid event such as cracking of the particle and conversely a broad peak would be a slower event such as a gas bubble oscillating. In Fig. **8C** there are other smaller, possibly broader peaks, below the major sharp peaks. This could indicate a secondary, less dominant event-taking place. This is important to see since it shows that there are multiple types of interactions occurring simultaneously, but that the majority of events recorded are occurring on faster time scale and are more intense.

Conclusion

Initial results would suggest that whether due to size and efficiency of interaction with the sound wave or internal payload the micro sized particles perform better. It would seem that the 2μm shells have the right mixture of strength and payload capacity, which allow them to outperform both the 1μm and 3μm particles. From the frequency data it would appear the there is definitely an improved signal output at approximately 7MHz, but until the lower range of frequencies can be sufficiently studied we cannot state the particles true resonant frequency. The recovery data supports a less destructive mechanism since the majority of particles post imaging remain intact. The pulse wave sonograms show that an overwhelming majority of the peaks are sharp and narrow, which would indicate that a fast process was taking place. The sum of all of this data would suggest that the mechanism is consistent with some sort of cracking or microfracturing of the particles which produces enough echogenicity to sustain a constant color Doppler ultrasound signal.

Experimental

Materials: Tetramethoxysilane and 0.1% wt poly-L-lysine solution were obtained from Aldrich-Sigma Ltd. All chemicals were used as received. Polystyrene beads were purchased from Polyscience Ltd. Fluorophore were purchased functionalized from Invitrogen Ltd.

Preparation of hollow silica nanospheres: To a 15ml plastic corning conical vial 10ml of phosphate buffer solution, 2ml of poly-L-lysine, and 500µL of 200nm polystyrene microspheres were added. This mixture was mixed using a vortex mixer for 10 min. To this 250µL of silicic acid was added and mixed for 15 min. At this time the reaction mixture was pelleted down using a centrifuge. The liquid was removed and the pellet was 2x with 5ml of H_2O and 1x with absolute ethanol. The coreshells were dried overnight to yield a white powder. The coreshells were now put into a muffle furnace to be calcined at 550°C using an 18 Hr gradient ramp. This yielded a white powder. Average zeta potential measurement was -35mV. Sizing from dynamic light scattering after 2hr of bath sonication was 260nm with a poly dispersity index of 0.29. The SEM measurements were conducted on a FEI/Philips XL30 FEG ESEM microscope with an accelerating voltage of 10 kV.

Preparation of hollow silica microspheres: To a 2 ml plastic conical vial 1ml of phosphate buffer solution, 130µL of poly-L-lysine, and 50µL of 2.0µm polystyrene microspheres were added. This mixture was mixed using a vortex mixer for 10 min. To this 3.1µL of tetramethylorthosilicate was added and mixed for 2.5 hrs. After 2.3 hrs of mixing 50µL of 5% trimethoxyborate solution was added and the mixture was let to mix for 4.5 hrs. At this time the reaction mixture was pelleted down using a centrifuge. The liquid was removed and the pellet was 1x with 1ml of H_2O and 2x with absolute ethanol. The coreshells were dried overnight to

yield a white powder. The coreshells were now put into a muffle furnace to be calcined at 550°C using an 18 Hr gradient ramp. This yielded a white powder. Average zeta potential measurement was -35mV. Sizing from dynamic light scattering after 1hr of bath sonication was 2.1μm with a poly dispersity index of 0.23. The SEM measurements were conducted on a FEI/Philips XL30 FEG ESEM microscope with an accelerating voltage of 10 kV.

Preparation of 5% trimethoxy borate solution: To a 2 ml plastic conical vial 1ml of absolute ethanol, to this 2.5μL of trimethoxy borate was added. This was let to mix for 5 minutes and only prepared as needed for reactions, and never stored.

Characterization: The SEM measurements were conducted on a FEI/Philips XL30 FEG ESEM microscope with an accelerating voltage of 10 kV. The average diameter of the nanospheres was determined by SEM images. The TEM image was JEO-2000EX (200kV) CryoElectro Microscope with an accelerating voltage of 200 kV. Zeta potentials and size distributions by DLS were measured using a Malvern Zetasizer Nano series instrument. Zeta potentials were measured using a Malvern disposable zeta potential cuvette with ethanol as a dispersant. DLS sizing was done using Malvern disposable sizing cuvettes and phosphate buffered saline solutions (PBS). Samples were sonicated in their respective solvents for 30 mins prior to measurements.

References

1. (a) Chomas, J. E.; Dayton, P.; Allen, J.; Morgan, K.; Ferrara, K. W., Mechanisms of contrast agent destruction. *IEEE transactions on ultrasonics, ferroelectrics, and frequency control* **2001,** *48* (1), 232-48; (b) Perez, E. A., Impact, mechanisms, and novel chemotherapy strategies for overcoming resistance to anthracyclines and taxanes in metastatic breast cancer. *Breast Cancer Res Treat* **2009,** *114*, 195-201.

2. (a) Baun, A.; Sorensen, S. N.; Rasmussen, R. F.; Hartmann, N. B.; Koch, C. B., Toxicity and bioaccumulation of xenobiotic organic compounds in the presence of aqueous suspensions of aggregates of nano-C60. *Aquatic Toxicol. Aquatic Toxicology* **2008,** *86* (3), 379-387; (b) Chapman, P., Environmental Risks of Inorganic Metals and Metalloids: A Continuing, Evolving Scientific Odyssey. *Human and Ecological Risk Assessment* **2008,** *14* (1), 5-40; (c) O'Brien, N.; Cummins, E., Ranking initial environmental and human health risk resulting from environmentally relevant nanomaterials. *Journal of Environmental Science and Health, Part A* **2010,** *45* (8), 992-1007; (d) Singh, K.; Arora, S., Removal of Synthetic Textile Dyes From Wastewaters: A Critical Review on Present Treatment Technologies. *Critical Reviews in Environmental Science and Technology* **2011,** *41* (9), 807-878; (e) Zhu, X.; Chen, Y.; Chang, Y., Toxicity and bioaccumulation of TiO2 nanoparticle aggregates in Daphnia magna. *Chemosphere Chemosphere* **2010,** *78* (3), 209-215.

3. Aglyamov, S. R.; Karpiouk, A. B.; Bourgeois, F.; Ben-Yakar, A.; Emelianov, S. Y., Ultrasound measurements of cavitation bubble radius for femtosecond laser-induced breakdown in water. *Opt. Lett.* **2008,** *33* (12), 1357-1359.

4. Calliada, F.; Campani, R.; Bottinelli, O.; Bozzini, A.; Sommaruga, M. G., Ultrasound contrast agents: basic principles. *European journal of radiology* **1998,** *27*, 157-60.

5. Yang, J.; Lind, J. U.; Trogler, W. C., Synthesis of hollow silica and titania nanospheres. *Chemistry of Materials* **2008,** *20* (9), 2875-2877.

6. Martinez, H. P.; Kono, Y.; Blair, S. L.; Sandoval, S.; Wang-Rodriguez, J.; Mattrey, R. F.; Kummel, A. C.; Trogler, W. C., Hard shell gas-filled contrast enhancement particles for colour Doppler ultrasound imaging of tumors. *Med. Chem. Commun.* **2010,** *1* (4), 266-270.

7.   (a) Kremkau, F. W., *Diagnostic ultrasound : principles and instruments*. W.B. Saunders: Philadelphia, 2002; (b) Woodcock, P. A. a. J. P., *Doppler ultrasound and its use in clinical measurement*. Academic Press: New York, 1982.

8.   (a) Barry B. Goldberg, D. A. M., Colin R. Deane, *An Atlas of Ultrasound Color Flow Imaging* Informa Healthcare: January 1997; (b) Evans, D. H., *Doppler ultrasound physics instrumentation and clinical applications*. J. Wiley: Chichester, 1991; (c) Gibbs, V.; Cole, D.; Sassano, A., *Ultrasound physics and technology : how, why and when*. Churchill Livingstone/Elsevier: Edinburgh; New York, 2009; (d) Goldberg, B. B.; Merton, D. A.; Deane, C. R., *An atlas of ultrasound color flow imaging*. Martin Dunitz ; Distributed by Mosby-Year Book: London; St. Louis, 1997.

9.   (a) Schwartz, R. L. P. a. R. A., *Practical Doppler ultrasound for the clinician*. Urban & Schwarzenberg: Baltimore 1991; (b) Shung, K. K., *Diagnostic ultrasound : imaging and blood flow measurements*. Taylor&Francis: Boca Raton, FL, 2006; (c) Thrush, A.; Hartshorne, T., *Vascular ultrasound : how, why, and when*. Churchill Livingstone: Edinburgh; New York, 2010.